



Norwegian University of
Science and Technology

Quantitative Analysis of Vascular Function in Malignant Tumours

A thesis presented for the degree of
Master of Science in Physics

Vidar Hemmingsen

December 2018

Supervisor: Kathrine Røe Redalen

Department of Physics
Norwegian University of Science and Technology

Preface

This thesis was written as a part of the two year master's degree programme in physics at the Norwegian University of Science and Technology (NTNU). The work was carried out at the Institute of Physics at NTNU. The work was carried out during the year of 2018. This thesis is has been a part of the bigger OxyTarget stud. Results from this thesis has also been shared with other projects to help further the scientific work in the field of cancer research.

I would like to thank Lars Tore Gyland Mikaelson for supplying me with the main framework for the Matlab program used in the analysis of the immunohistochemical images and for answering my many questions about it and the field of biophysics. I would also like to thank Ingrid Framås Syversen for providing me with her code and sharing the experience she had in studying the MRI parameters we both worked with. Next i would like to thank Tengzhi Liu for his help in making the tumour masks for the histological images. Finally i would like to express my sincerest gratitude to Kathrine Røe Redalen for suggesting this wonderful thesis to me and for guiding me through the process. It has been a great experience

NTNU, Trondheim, December 2018

Vidar Hemmingsen

Abstract

The purpose of this thesis was to investigate the vascular function of malignant tumours using histological and immunohistochemical (IHC) sections and look for associations with magnetic resonance imaging (MRI) and clinicopathological parameters. The vascular function of malignant tumours is known to have a strong influence on the tumours response to chemoradiotherapy (CRT) and much of this is attributed to tumour hypoxia and its reduction of radiation effectiveness through the oxygen effect. There is currently no methods applicable in the clinical setting to assess tumour hypoxia. MRI has been proposed as a potential non-invasive imaging modality that could assess tumour hypoxia and MRI machines are already in widespread clinical use. To study the validity of the data from an MRI the study of IHC images could be used. Images from histological and IHC sections have been used to study tumour vasculature for some time, but the varying methods used by different research groups make the results hard to compare. As a result of these problems automated computer programs have been developed.

103 patients with rectal cancer underwent static T_2^* -weighted MRI and dynamic susceptibility contrast (DSC) MRI before CRT and surgery. The static R_2^* (the reciprocal of T_2^*) was calculated from the T_2^* -weighted images. Dynamic R_2^* time curves were derived from the DSC data, before the peak value (R_2^* -peak_{enh}) and the area under the curve (R_2^* -AUC) were calculated. The MRI data was then correlated with clinicopathological parameters. The study for the IHC parameters focused on digitized images of histological and IHC samples. The investigated parameters are obtained through an automated computer program developed in Matlab. The IHC analysis was performed on a substudy of 39 of the patients in the total cohort, the images were analysed and parameters were generated. The results from the IHC images were correlated with the MRI data and clinicopathological parameters.

In the analysis of the MRI data, significant results were found for R_2^* -peak_{enh} and R_2^* -AUC. Four significant results were found for the parameter R_2^* -AUC ($p = 0.008 - 0.047$). High time intervals had higher amounts of significant results than the lower ones. R_2^* -peak_{enh} was found to correlate with nodal metastasis ($p = 0.024$). From the correlation between IHC data and MRI data, the parameters microvessel density (MVD) ($p = 0.037$), inter capillary distance (ICD) ($p = 0.004$) and vessel size ($p = 0.008$) were found to be significantly correlated with R_2^* . Vessel size was also correlated with R_2^* -peak_{enh} ($p = 0.034$) and several strong trends for other parameters were also found. Many of the parameters that have been suggested as prognostic factors in the literature showed good trends towards significance in the analysis or were significant.

In conclusion this thesis found a handful of significant results and most seem to be in line with what is indicated in the literature. However the small number of patients makes it difficult to draw any clear conclusions based on the results. Studies with larger patient groups should be done to verify that the results are indeed correct and a larger quantity of significant results, is then likely to be found. Finally, this thesis has demonstrated the use of an automated computer program in the analysis of IHC images. This should be the main method for studying IHC images for the future to ensure that similar methods were used when researchers want to compare results. Additionally the automated system removes any subjective bias from the process and enables larger amounts of data to be analysed.

Sammendrag

Formålet med denne avhandlingen var å undersøke den vaskulære funksjonen i ondartede svulster ved hjelp av histologiske og immunohistokjemiske (IHC) snitt og se etter assosiasjoner med magnetresonanstomografi (MR) og klinisk-patologiske parametere. Den vaskulære funksjonen av ondartede svulster er kjent for å ha en sterk innflytelse over kreft sin respons på kjemoterapi (CRT), og mye av dette tilskrives tumorhypoksi og reduksjon av strålingseffektivitet gjennom oksygeneffekten. Det finnes for øyeblikket ingen metoder som er anvendelige i klinisk praksis for å vurdere tumorhypoksi. MR har blitt foreslått som en potensiell ikke-invasiv avbildningsmodalitet som kan vurdere tumorhypoksi og MR-maskiner er allerede i omfattende klinisk bruk. For å studere validiteten av dataene fra en MR kan man bruke IHC-bilder. Bilder fra histologiske- og IHC-snitt har vært brukt til å studere svulster i en hvis tid, men de ulike metodene som brukes av ulike forskningsgrupper gjør at resultatene er vanskelige å sammenligne. Som et resultat av disse problemene har det blitt utviklet automatiserte dataprogrammer.

103 pasienter med endetarmskreft gjennomgikk statistisk T_2^* -vektede MR og dynamisk sensitivitetskontrast (DSC) MR før de fikk CRT og kirurgi. Statisk R_2^* (den resiproke av T_2^*) ble kalkulert fra de T_2^* -vektede bildene. Tidskurver for dynamisk R_2^* ble funnet fra DSC-dataene, før toppverdi (R_2^* -peak_{enh}) og arealet under kurven (R_2^* -AUC) ble kalkulert. MR-dataene ble deretter korrelert med klinisk-patologiske parametere. Studien av IHC parameterne fokuserte på digitaliserte bilder av histologiske og IHC prøver. De undersøkte parameterne ble generert gjennom et automatisert dataprogram utviklet i Matlab. Bildene fra 39 pasienter ble analysert and parametere ble generert. Resultatet fra IHC bildene ble korrelert med MR-dataene og de klinisk-patologiske parametere.

I analysen av MR-dataene ble det funnet signifikante resultater for R_2^* -peak_{enh} og R_2^* -AUC. Fire signifikante resultater ble funnet for parameteren R_2^* -AUC (0.008 – 0.047). Intervaller med høyere tider hadde flere signifikante resultater enn de lavere tidsintervallene. R_2^* -peak_{enh} ble funnet til å korrelere med pN ($p = 0.024$). Fra korrelasjonen mellom IHC data og MR data, ble det funnet at microåre tettheten (MVD) ($p = 0.037$), interkapilær distanse (ICD) ($p = 0.004$) og årestørrelse ($p = 0.008$) hadde signifikante korrelasjoner med R_2^* . Årestørrelsen ble også korrelert med R_2^* -peak_{enh} ($p = 0.034$) og mange sterke trender ble funnet for andre parametere. Mange av parameterne som har blitt foreslått som prognostiske faktorer i litteraturen viste gode trender mot signifikans eller var signifikante.

For å konkludere, så fant denne avhandlingen en håndfull med signifikante resultater og de fleste synes å være i tråd med hva som har blitt indikert i litteraturen. Allikevel, det lave antallet av pasienter gjør det vanskelig å trekke noen klare konklusjoner basert på resultatene. Studier med større pasientgrupper burde gjennomføres for å verifisere at resultatene i denne avhandlingen er korrekte og en større mengde signifikante resultater burde bli funnet da. Til slutt, denne avhandlingen har demonstrert bruken av automatiserte dataprogrammer i analysen av IHC bilde. Dette burde være hoved metoden for å studere IHC bilder i framtiden for å forsikre at like metoder blir brukt når forskere vil sammenligne resultater. I tillegg, fjerner det automatiserte systemet subjektiv subjektiv vurdering fra prosessen og gjør at større mengder data kan bli analysert.

Contents

| | | |
|----------|---|-----------|
| 1 | Introduction | 10 |
| 2 | Theory | 12 |
| 2.1 | Cancer | 12 |
| 2.2 | The Hallmarks Of Cancer | 12 |
| 2.2.1 | Tumour Node Metastasis System | 15 |
| 2.3 | Vascularization | 16 |
| 2.4 | Tumour Vascularization | 17 |
| 2.4.1 | General Tumour Vasculature Characteristics | 19 |
| 2.5 | Hypoxia | 21 |
| 2.5.1 | Consequences of Tumour Hypoxia | 21 |
| 2.6 | Magnetic Resonance Imaging | 23 |
| 2.6.1 | History | 23 |
| 2.6.2 | Working Principle | 24 |
| 2.6.3 | Pulse Sequences | 26 |
| 2.6.4 | Dynamic Susceptibility Contrast MRI | 27 |
| 2.7 | Histology and Immunohistochemistry | 28 |
| 2.7.1 | Fixation, Embedding, Sectioning, Staining and Mounting | 28 |
| 2.7.2 | Immunohistochemistry | 28 |
| 2.7.3 | Histological and Immunohistological Markers Used in This Study | 30 |
| 2.7.4 | Automated Image Analysis | 30 |
| 3 | Method | 31 |
| 3.1 | R_2^* MRI Study | 31 |
| 3.2 | Patients | 31 |
| 3.3 | MRI | 31 |
| 3.3.1 | Image Analysis | 32 |
| 3.3.2 | Statistics | 34 |
| 3.4 | Histology and Immunohistochemistry | 35 |
| 3.4.1 | Staining | 36 |
| 3.4.2 | Scanning of Images | 36 |
| 3.4.3 | Tumour Mask creation | 36 |
| 3.4.4 | Image Analysis | 37 |
| 3.4.5 | Statistics | 41 |
| 4 | Results | 42 |
| 4.1 | MRI Results | 42 |
| 4.1.1 | Results for Static R_2^* | 42 |
| 4.1.2 | Results for Dynamic R_2^* -peak _{enh} | 43 |
| 4.1.3 | Results for Dynamic R_2^* -AUC | 43 |
| 4.2 | Results from the immunohistochemical analysis | 43 |
| 4.2.1 | CD34 Results | 43 |
| 4.2.2 | CAIX Results | 45 |
| 4.2.3 | HIF1- α results | 45 |
| 4.2.4 | Results for the Correlation Between MRI Parameters and IHC Features | 46 |

| | |
|--|-----------|
| 5 Discussion | 48 |
| 5.1 Discussion of MRI | 49 |
| 5.1.1 Discussion of Materials | 49 |
| 5.1.2 Discussion of Methods | 51 |
| 5.1.3 Additional Methodological Factors | 52 |
| 5.1.4 Discussion of Results | 52 |
| 5.2 Discussion of Quantitative Immunohistochemistry | 54 |
| 5.2.1 Discussion of Materials | 54 |
| 5.2.2 Discussion of Methods | 56 |
| 5.2.3 Discussion of Histology Results | 56 |
| 5.2.4 Discussion of Correlation between MRI and Quantitative Immunohisto- chemistry | 59 |
| 5.3 Suggestions for Further Work | 60 |
| 6 Conclusion | 61 |
| A Appendix | 65 |
| B Matlab Code | 65 |
| B.1 Code for MRI Analysis | 65 |
| B.2 Code for the IHC Analysis | 87 |

List of Figures

| | | |
|----|---|----|
| 1 | Illustration of sprouting angiogenesis in the vicinity of tumour cells. Recreated with permission from [7]. | 17 |
| 2 | Illustration showing (a) Vasculogenesis (b) Angiogenic remodelling (c) Maturation (d) Destabilization (e) Regression and (f) sprouting angiogenesis. The roles different signalling molecules and proteins is shown for each process. Recreated with permission from [49]. | 18 |
| 3 | Illustration of normal (left) and cancerous (right) vasculature. In normal tissues, red vessels indicate oxygen-rich feeding arteries and arterioles, blue vessels are veins carrying deoxygenated blood and the connecting regions are the capillary stage with mixed colour. In cancerous tissues, slow blood flow is indicated by reduced colour intensity. Recreated with permission from [12]. | 20 |
| 4 | Illustration showing the blood vessels from normal (left) and tumour (right) vasculature. It also shows defects in the endothelial layer of tumour vessels. In a normal vessels endothelial cells for a tight grid. In tumour vessels the endothelial cells sprout and branch uncontrolled leading to a defective endothelial layer. The poor structure leads to gaps that can cause leakage. Recreated with permission from [10]. | 20 |
| 5 | Illustration of chronic and acute tumour hypoxia. In the figure on the left we can see how chronic tumour hypoxia is limited by the diffusion distance of the blood. As a consequence the oxygen concentration decreases with distance from the vessel. On the right we can see all tumour cells surrounding the vessel are in a temporary state of hypoxia. The graph illustrates how the blood flow, or blood perfusion, can vary over time and therefore leave the cells without oxygen for short periods. Recreated with permission from [17]. | 22 |
| 6 | Illustration of the indirect and direct effects of radiation on DNA. In the direct effect the radiation interacts with an electron which damages the DNA. In the indirect effect the radiation strikes an electron which creates a free radical by interacting with a water molecule. The free radical goes on to fixate the damage of the DNA. Recreated with permission from [36]. | 23 |
| 7 | Image of an H&E image. The structure of the tissue is well resolved thanks to the H&E stain. | 29 |
| 8 | MRI pictures from the different sequences in the same patient. | 33 |
| 9 | Curve of the signal averaged over all pixels in the mask. The gray area is the area under the curve (AUC) and the top of the initial curve is the peak. The baseline in this image was set according to the process explained in section 3.3.1. | 34 |
| 10 | Tumour mask and H&E image. | 36 |
| 11 | Images from different parts of the image registration. The first figure (a) shows how the mask should fit on the image based on how it was drawn on the H&E image. The second figure (b) shows how the initial registration fails to align the mask and image correctly compared to the first figure. In this example it is caused by a mixture of rotation, contraction. In the third figure (c) we see that the image from the second figure (b) is now aligned with the H&E image. When the mask is applied in the last figure (d) it now fits a lot better. | 38 |
| 12 | Image of an tumour mask that has been scaled/eroded. The coloured part has been removed from the mask to make sure the mask stays within the tumour area. | 39 |
| 13 | CD34 image after segmentation and post-processing. The green pixels are stains of CD34, vessels. | 40 |
| 14 | CAIX image after segmentation and post-processing | 40 |

| | | |
|----|---|-----|
| 15 | HIF1- α image after segmentation and post-processing | 41 |
| 16 | Correlation matrix for IHC features and TRG. Entries above and below the diagonal are identical. The number in each window represents the correlation between the two parameters and the scatter-plot is shown in the same window. Values in red reflects Spearman correlations were the correlation value is > 0.50 or < 0.50 | 48 |
| 17 | Correlation matrix for MR and IHC data. Entries above and below the diagonal are identical. R2 is the paramter R_2^* , R2pk is R_2^* -peak _{enh} and R2AUC is R_2^* -AUC for the time point 525second. The number in each window represents the correlation between the two parameters and the scatter-plot is shown in the same window. Values in red reflects Spearman correlations were the correlation value is > 0.50 or < 0.50 | 50 |
| 19 | Kaplan-Meier plot for stained fraction of CD34 | 65 |
| 20 | Kaplan-Meier plot for the vessel size | 65 |
| 21 | Kaplan-Meier plot for the solidity | 118 |
| 22 | Kaplan-Meier plot vessel radius | 118 |
| 23 | Kaplan-Meier plot for the number of vessels | 118 |
| 24 | Kaplan-Meier plot for MVD | 119 |
| 25 | Kaplan-Meier plot for ICD | 119 |
| 26 | Kaplan-Meier plot | 120 |
| 27 | Kaplan-Meier plot for the stained fraction of HIF-1 α | 120 |
| 28 | Kaplan-Meier plot for the stain size of HIF-1 α | 121 |
| 29 | Kaplan-Meier plot for the stain size of CAIX | 121 |
| 30 | Kaplan-Meier plot for the stained fraction of CAIX | 122 |

List of Tables

| | | |
|----|---|----|
| 1 | Table explaining the different stages of tumour regression grading | 16 |
| 2 | Patients divided into groups according to what was collected and what treatments they received. | 31 |
| 3 | Patients included or excluded from results in the MR analysis. | 33 |
| 4 | Grouping info showing number of patients in each group. | 35 |
| 5 | Parameters used for staging and evaluation of response. | 35 |
| 6 | Grouping info for the pathological data. Notice that there are no patients in Δ T2-4 or Δ T3-4 | 42 |
| 7 | Results from the statistical analysis of the static R_2^* -values of different endpoints. The Results are given as median values and the range given in parenthesis. The full dataset can be found in the appendix 192021 | 42 |
| 8 | Results from the statistical analysis of the dynamic $R_2^* - peak_{enh}$ -values of different endpoints. The Results are given as median values and the range given in parenthesis. The full dataset can be found in the appendix 192021. | 43 |
| 9 | Results from the statistical analysis of the dynamic $R_2^* - AUC$ -values of different endpoints. The Results are given as median values and the range given in parenthesis. The full dataset can be found in the appendix 192021. | 44 |
| 10 | Results from the statistical analysis of the dynamic $R_2^* - AUC$ -values of different endpoints. The Results are given as median values and the range given in parenthesis. The full dataset can be found in the appendix 192021. | 44 |
| 11 | Results from the statistical analysis of the dynamic $R_2^* - AUC$ -values of different endpoints. The results are given as median values and the range given in parenthesis. The full dataset can be found in the appendix 192021. | 45 |
| 12 | Results from the statistical analysis of the dynamic $R_2^* - AUC$ -values of different endpoints. The Results are given as median values and the range given in parenthesis. The full dataset can be found in the appendix 192021. | 45 |
| 13 | Results from the quantitative IHC analysis of the features: vessels, vessel size, vessel radius and MVD from pathological CD34-images. The Results are given as median values and the range (min-max) given in parenthesis. The full dataset can be found in the appendix 24 and 25 | 46 |
| 14 | Results from the quantitative IHC analysis of the features: ICD, solidity and stained fraction from the CD34-images. The Results are given as median values and the range (min-max) given in parenthesis. The full dataset can be found in the appendix 24 and 24 | 47 |
| 15 | Results from the quantitative IHC analysis of the CAIX-images. Stain fraction is the fraction of coloured pixels versus number of pixels in the tumour mask. Median number of pixels for each vessel in the tumour mask. The Results are given as median values and the range (min-max) given in parenthesis. The full dataset can be found in the appendix 26 | 47 |
| 16 | Results from the quantitative IHC analysis of the HIF-1 α -images. Stain fraction is the fraction of coloured pixels versus number of pixels in the tumour mask. Median number of pixels for each vessel in the tumour mask. The Results are given as median values and the range (min-max) given in parenthesis. The full dataset can be found in the appendix 26 | 49 |
| 17 | P-value for the pathological data. The p-value for the correlation of each feature with all other features as well as TRG. Each side of the diagonal, represented by the ones, are identical. Values in bold are significant values, as long as they do not represent the same thing (like CAIX and HIF-1 α). | 49 |

| | | |
|----|---|-----|
| 18 | P-value matrix for MR and Histological data. The p-value for the correlation of each feature with all other features as well as TRG. Each side of the diagonal, represented by the ones, are identical. R_2 is the parameter R_2^* , R_{2pk} is R_2^* - $peak_{enh}$ and R_{2AUC} is R_2^* -AUC for the time point 525second. Values in bold are significant values, as long as they do not represent the same thing (like CAIX and HIF-1 α). | 51 |
| 19 | MR values for all patients. Part 1/5. | 123 |
| 20 | MR values for all patients. Part 2/5. | 124 |
| 21 | MR values for all patients. Part 3/5. | 125 |
| 22 | MR values for all patients. Part 4/5. | 126 |
| 23 | MR values for all patients. Part 5/5. | 127 |
| 24 | Results from quantitative immunohistochemisrty of $CD34$ stain. Part 1/2. . . . | 128 |
| 25 | Results from quantitative immunohistochemisrty of $CD34$ stain. Part 2/2. . . . | 129 |
| 26 | Results from quantitative immunohistochemisrty of CAIX and HIF1- α stains. . . | 130 |

1 Introduction

GLOBOCAN, Global Cancer observatory, a project of the International Agency for Research on Cancer (IARC), estimates that in 2018: "There will be an estimated 18.1 million new cancer cases (17.0 million excluding non-melanoma skin cancer) and 9.6 million cancer deaths (9.5 million excluding nonmelanoma skin cancer) in 2018" [13]. Specifically it estimates that 1.8 million new colorectal cancer cases and 881,000 deaths from colorectal cancer in 2018. This accounts for 10% of cancer cases and deaths. Colorectal cancer is the third most common cancer, but has the second most mortalities. Norway has the 4th highest rate of colorectal cancer rates per 100,000. When adjusted for sexes, Norwegian men had the 10th highest rate with 46.9 per 100,000, while Norwegian women had the highest rate of all women with 39.3 per 100,000 [13]. This puts the estimate number of new cases of colorectal cancer for males at around 1600 and 1500 for females, in 2018.

Rectal cancer is a subgroup of colorectal cancer and is cancer of the lower part of the large intestine. In an adult human the rectum is approximate 12 cm. In 2017 there were 1325 cases of rectal cancer in Norway. The mortality rate was in 2016 6.1 for women and 9.9 for men per 100,000 persons per year and the survival in the period 2013-2017 was 69.4% for women and 68.9% for men [19]. The frequency of local recurrence has been greatly reduced after the introduction of total mesorectal excision (TME) surgery for rectal cancer patients. However, still about 10% of the patients experience a local recurrence [47].

The main treatment of rectal cancer is surgery, but neoadjuvant chemoradiotherapy (CRT) is added for patients with locally advanced disease [39] [46]. There is however large individual variation in the response to treatment. Today treatment is individually adapted, but further adaptation would be hugely beneficial. One of the major obstacles in successfully treatment is the development of metastasis. A well known contributor to metastasis is the presence of hypoxia (oxygen deficiency) [44]. However, a remaining challenge is that there exist no clinically useful tools for reliable cancer-hypoxia detection at the time of diagnosis. If the presence and extent of hypoxia could be measured before treatment, different actions could be taken to combat hypoxia, reduce the probability of metastatic development and thereby improve the treatment outcome and increase survival. Currently there are no proven and reliable methods of doing this in clinical practice, but there is a lot of research being done within this field.

One method being researched for hypoxia assessment is functional magnetic resonance imaging (fMRI) [20]. The field of MRI has made large technological advances in the last decades and imaging the functions of tissue environments is now a possibility. Blood with low oxygen concentration is more sensitive to magnetism than blood with higher oxygen concentration. Due to this effect it is possible to visualize the distribution of blood with different oxygen concentrations, this is known as BOLD (blood oxygenation level dependent) signal. In hypoxic regions this should generate signal differences when imaging normally oxygenated and hypoxic tissue and enable fMRI to visualize the hypoxia. This has been shown in some cancer types, mainly brain cancer, but not in rectal cancer [40] [21].

Tumour hypoxia is a consequence of the underlying vascular system and its shortcomings. By studying the vascular system and its properties more information about the tumour can be gained and further help investigate the conditions and triggers for tumour hypoxia. This is often done through histology, where the tumour is studied in a microscope after it has been surgically removed, sectioned into slices and prepared for imaging in the microscope. In what is called immunohistochemistry (IHC), the tissue can be stained with dyes attached to proteins

and antibodies to visualize the presence and locations of different proteins, cells and enzymes within the tissue. This can be done to study the vascular system of the tumour as well as hypoxia. This provides a way to compare the physical tumour with the images created in the MRI.

In this thesis IHC-analysis of tumour tissue sections was compared with functional MR images from the same tumours, in order to investigate whether MRI non-invasively and quantitatively could assess the vascular function of the tumours. The study was conducted in 113 rectal cancer patients; where 52 were referred to surgery alone whereas 61 patients underwent neoadjuvant CRT. The objectives were:

- To calculate MRI parameters from hypoxia-related dynamic contrast-based MRI.
- To look for association between the MRI parameters and clinicopathological parameters.
- To identify and extract tumour regions from histological images.
- To estimate vascular parameters of the tumour regions based on IHC.
- To look for associations between vascular parameters from IHC and clinicopathological parameters.
- To look for associations between vascular parameters from IHC and MRI.

The thesis will continue with relevant theory, this includes MRI and histology theory as well as cancer biology. Thereafter an overview of the methods and materials are given before the results are presented along with a discussion of the strengths and weaknesses as well as relevance to other research. There will also be suggestions on how this research can be continued and expanded upon and in the appendix the Matlab scripts used and the full result tables are attached.

2 Theory

2.1 Cancer

Cancer is a group of related diseases with the common property that cells of some part of the body divide without stopping and spreads to surrounding parts of the body. Under normal circumstances cells grow and divide to generate new cells when the body needs them, for instance when cells grow old or when they are damaged, they die and new cells can take their place. Cancer disrupts some of these processes and therefore affected cells do not die when they are supposed to, and create new cells although they are not needed. The creation of new cells can cause uncontrolled growth and may form solid tumours which are masses of tissue.

Tumours are classified into two groups: Malignant and benign. **Malignant tumours** can spread into surrounding tissue thereby increasing the area affected. They can also spread to other parts of the body, this is known as metastasis and happens if a part of the tumour breaks off and is caught up in the blood or lymph system and is transported to a different part of the body. **Benign tumours** do not spread; this makes them somewhat less dangerous as long as they are not located near a vital organ, for instance a brain tumour is life threatening, but a tumour in foot is not directly life-threatening. When a benign tumour is removed it will usually not return, as long as the entire tumour is removed.

Cancer is caused by changes in the genetic information that controls the cells function. This can arise for example through a fault in DNA replication during the cell cycle or by environmental exposure such as ionizing radiation or chemicals.

2.2 The Hallmarks Of Cancer

In 2000, Douglas Hanahan and Robert A. Weinberg 2.2. released a review article explaining what they thought to be the six hallmarks of cancer. In the discussion it is implied that as normal cells evolve progressively towards a neoplastic state they acquire these hallmarks in one order or another. In 2011, they published an expanded version of their framework for understanding neoplastic disease where new hallmarks are included as well as their enabling characteristics. They also suggest that the biology of tumours can only be understood by studying and understanding the specialized cell types within tumours as well as the tumour micro-environment.

The hallmarks of cancer are:

Sustaining Proliferative Signalling. One of the fundamental properties of cancer is the ability to sustain chronic proliferation. In normal tissue the release of growth signals determines the proliferation of cells and is very carefully controlled. When growth signals are exposed to a cell culture, proliferation is observed. In contrast, tumour cells in culture show a largely decreased dependence on this external growth stimulation for proliferation. This indicates that tumour cells may generate their own growth signals. Although relatively little is known about how proliferative signals operate in healthy tissue, we do know quite a bit about how they operate in cancer cells. Cancer cells can acquire proliferative signalling in a few alternative ways: They can produce growth signalling molecules themselves, which reacts with their related receptors. They can send signals to normal cells to stimulate them to supply growth signals. Or by increasing receptor proteins at the cancer cell surface, this has the effect of increasing the sensitivity of

of the cell to growth signals, and therefore very small amounts would be needed for proliferation.

Evading Growth Suppressors. In healthy tissue there are also systems that help control proliferation by inhibiting growth. These systems are often controlled by tumour suppressor genes, which encode special proteins (TP53- and Retinoblastoma-related (RB)-protein). These proteins control cells progression to growth and division phases, as well as checking the cells micro-environment and genome damage. If the micro-environment is suboptimal or there is genome damage the proteins halt the cell-cycle progression until the conditions improve. If there is extensive damage to the the genome, programmed cell-death, called apoptosis, is triggered by the proteins. If there are defects in the functions of these proteins or they are circumvented cancer cells will not be stopped from proliferating. It is not stated how or why cancer cells evade these systems. However the signalling molecule tumour growth factor beta, (TGF- β), which is known for its anti-proliferative effects, has been seen to be redirected away from suppressing cell proliferation to activate a cellular program termed epithelial-to-mesenchymal-transition (EMT), in late stage tumours. In this program epithelial cells lose their cell polarity and cell-cell-adhesion to gain mobility.

Resisting Cell Death. Cell population is determined not only by cell proliferation but also cell attrition. One major source of cell attrition comes from apoptosis, programmed cell death. Apoptosis is a latent program that is present in virtually all cell types of the body. Once triggered a series of steps takes place, the cell membrane is disrupted, the cytoplasm and nuclear skeleton is broken down, the intracellular fluid is fragmented and in the end the cell remnants are consumed by nearby cells. too. Tumour cells have many different strategies to circumvent apoptosis. Most common is the loss of protein tumour suppressing functions that monitor critical damage in the cell. Other means are to increase the expression of anti-apoptotic regulators or of survival signals, by down regulating pro-apoptotic factors, or by short-circuiting the signalling-molecule-induced death pathway.

Necrosis is a another form of cell death and in contrast to apoptosis, were the cell dissolves and disappears calmly, necrotic cells become bloated and explode spreading their contents into the local micro-environment. Necrosis releases pro-inflammatory signals into the micro-environment, and as such can recruit inflammatory cells of the immune system. The function of these immune cells is to survey the tissue damage and clear necrotic debris. However in cancer cells, immune inflammatory cells can be actively tumour promoting as they encourage angiogenesis and cell proliferation.

Enabling Replicative Immortality. In most normal tissue, cells are only capable of passing through a limited number of successive cell cycles. Once beyond this number the cells end up in one of two states, senescence, a non-proliferative state and crisis which ends in cell death. Sometimes cells can pass through the state of crisis without dying, this has been termed immortalization, it is indicated that the protection of the chromosome ends, the telomeres, is involved in this process. The length of the telomeric DNA in a cell dictates how many successive cell generations it can have. Telomerase, a specialized DNA polymerase, can add segments to telomeric DNA. It is almost absent in non-immortalized cells but expressed in high levels in spontaneously immortalized cells as well as human cancer cells. This indicates that tumours have the ability to maintain telomeric DNA at lengths that allow them to avoid crisis and apoptosis by up-regulating telomerase.

Inducing Angiogenesis. Tumours just as normal tissue requires nutrients and oxygen, as well as removal of wastes and carbon dioxide. These needs are addressed by the vasculature

generated through angiogenesis. The ability for neoplastic cells to initiate and sustain angiogenesis is purported to be gained in one or more discrete steps. This is termed the "angiogenic switch". This switch seems to be activated in early to mid-stage lesions. Evidence also indicates that this switch is controlled by factors that offset each other to either induce or oppose angiogenesis. Vascular endothelial growth factor-A (VEGF-A) is a gene that encodes signalling molecules involved in generating new blood vessels, and is one known angiogenesis inducer, another inducer is fibroblast growth factors 1 and 2 (FGF 1/2). Thrombospondin-1 (TSP-1) is known as a angiogenesis inhibitor. Some tumours activate the angiogenic switch by increasing expression of VEGF and or FGFs, while in others expression of inhibitors like TSP-1 are down-regulated.

There are indications that neo-vascularization is a necessity for rapid clonal expansion leading to macroscopic tumours, as anti-VEGF antibodies has been shown to impair neo-vascularization and subcutaneous tumour growth in mice.

With this chronically activated angiogenesis and an unbalanced mix of angiogenic signals the vasculature generated in tumours is convoluted, with distorted and enlarged vessels, erratic blood flow, leakiness and with abnormal levels of endothelial cell proliferation and apoptosis.

Activating Invasion and Metastasis. As cancers develop towards higher pathological grades of malignancy the cancer cells usually develop changes in their shape, attachment to other cells and the extracellular matrix (ECM). The frequently observed down-regulation or mutational inactivation of E-cadherin, a key cell-to-cell adhesion molecule, in human carcinomas provides compelling evidence toward its role as a key suppressor of metastasis and invasion. Genes encoding adhesion molecules have also been seen to be altered in highly aggressive carcinomas.

The process of invasion and metastasis has been depicted as a multi-step process termed the invasion-metastasis cascade. The succession of cell-biologic changes in this process are local invasion, then the invasion of cancer cells through the basal membrane into a blood or lymphatic vessel, passing cancer cells through the lymphatic and hematogenous systems, the cells then escape out of this system to distant tissues, formation of small nodules of cancer cells, finally growth into macroscopic tumours. A program referred to as Epithelial-mesenchymal transition (EMT) has been suggested as a means for epithelial cells can gain the ability to resist apoptosis, invade and spread. It appears that factors that induce EMT can arrange for most of the steps in invasion-metastasis cascade, except for colonization.

Reprogramming Energy Metabolism. In order to fuel the uncontrolled cell proliferation adjustments to energy metabolism are required. Under aerobic conditions normal cells process glucose and under anaerobic conditions glycolysis is favoured. Cancer cells can reprogram their glucose metabolism and use mostly glycolysis, even in the presence of oxygen. This state is therefore called the "aerobic glycolysis". This method of metabolism is however much less efficient. To compensate cancer cells up-regulate glucose transporters, increasing the glucose import into the cytoplasm. The use glycolysis can be amplified under hypoxic conditions, which is present in many tumours, thus tumour hypoxia can increase the levels of hypoxia inducible factor one alpha, HIF1 α , and HIF2 α which increases glycolysis. The reason for this switch in energy production is still not fully known, one hypothesis is that glycolysis allows the distribution of glycolytic intermediates into different pathways like ones that produce blocks for new cells.

Evading Immune Destruction. The immune system monitors cells and tissues, and is re-

sponsible for finding and removing most developing cancer cells. Solid tumours have managed to avoid detection or have been able to limit the immunological eradication. This is seen from the fact that in mice, with genetically induced deficiencies of the immune system, tumours emerged and grew faster relative to mice with normal immune systems. In addition when cancer cells grown in immunodeficient mice is transplanted into mice with normal immune systems the cancer cells are inefficient at creating secondary tumours relative to cancer cells grown in immuno-competent mice. This has been interpreted as cancer cells in normal hosts are frequently eliminated leaving only behind the strains that can grow in immuno-competent environments. This is known as "immunoediting". Anti-tumour immune responses can also be seen in some forms of human cancer. Patients with colon and ovarian tumours that have high levels of immuno-killer cells have better prognosis than those who lack this abundance.

Enabling Characteristics. The hallmarks mentioned are gained through two enabling characteristics. The most notable being genomic instability which creates mutations in the DNA. The second characteristic is the inflammatory state which serves to promote tumour progression.

Genome Instability and Mutation. For neoplastic cells to gain the hallmarks previously discussed there needs to be changes to their genomes. Therefore the multi-step process which is tumour progression can be viewed as a series of chance acquisitions of an enabling mutant genotype. Some steps may also be triggered by non-mutational changes affecting the regulation of gene expression. In order to achieve the number of mutational changes needed for tumourigenesis cancer cell increase rates of mutation by breaking down one or several components of the genomic maintenance system or the systems that survey the genomic integrity of cells.

Tumour-Promoting Inflammation. It is clear that virtually all neoplastic lesions contains immune cells from subtle infiltration to large inflammations apparent even by histochemical staining techniques. Inflammation can add to several hallmarks by providing active molecules to the tumour-environment, like growth factors, survival factors, pro-angiogenic factors, signals that lead to activation of EMT and enzymes that facilitate angiogenesis, invasion and metastasis. Inflammation is in some cases noticeable at the early stages of tumour progression and able to foster the development into fully developed cancers. In addition inflammation releases reactive oxygen that is mutationally accelerating the genetic progression to malignancy.

The Tumour Microenvironment. The understanding of tumour biology has shifted from the simple view of tumours, as a collection of homogeneous cancer cells whose biology could be fully understood by explaining the properties of these cells, to being recognized as organs whose complexity is close to or may exceed normal healthy tissue. Therefore the interplay between different biological systems and agents must be understood to create a holistic picture of cancer cells.

2.2.1 Tumour Node Metastasis System

The tumour-node-metastasis (TNM) classification of malignant tumours is a recognised standard for classifying the extent and spread of cancer. T describes the size of the original tumour and also describes if it has invaded nearby tissue. Accordingly, T0 means no evidence of tumour, whereas T1, T2, T3, T4, are increasing size or extension of the primary tumour. Sometimes extra identifiers are added to describe differences. For colon cancer, T4a means that the tumour perforates the colon lining and T4b means that the tumour directly invades other organs or structures. N describes nearby lymph nodes that are involved. N0 means no regional lymph

nodes metastasis, whereas N1 means regional lymph node metastasis present at some sites, tumour spread to closest or small number of regional lymph nodes. N2, tumour has spread to a large extent. M describes distant metastasis, M0, no distant metastasis, M1, metastasis found in distant organs. In rectal cancer metastasis is most frequently found in the liver and the lungs.

TNM stage determined by MRI is denoted mrT mrN. TNM stage determined by pathology of the specimen after oncologic treatment, is denoted ypT ypN. For patients without treatment the pathological TNM stage is pT and pN.

Tumour regression grade (TRG) is a measure of the response to neoadjuvant CRT in locally advanced rectal cancer. The TRG is determined by a pathologist after the tumour has been surgically removed. The TRG used in this study has been scored using the grading defined by American Joint Committee on Cancer (AJCC) AJCC/CAP (The College of American Pathologists) [2].

| Tumour Regression Grade (TRG) | |
|-------------------------------|---|
| 0 | No viable cancer cells (total regression, strong response) |
| 1 | Small group/groups of cancer cells (nearly total regression, moderate response) |
| 2 | Residual cancer with fibrous growth (moderate regression, low response) |
| 3 | Little to no tumour cells killed (minuscule regression, poor/no response) |

Table 1: Table explaining the different stages of tumour regression grading

2.3 Vascularization

The vascular system transports oxygen and nutrients around the body as well as removing waste products created by the cells. The essential parts of the vascular system are: the heart, the blood and the blood vessels. The latter are divided into arteries, veins and capillaries. The arteries transport oxygenated blood from the heart out to the body and veins transport de-oxygenated blood back to the heart. The arteries branch out into smaller vessels called arterioles, which then branch out into capillaries again. The capillaries deliver blood to the cells. The capillaries branch back together in venules, which branches back to the veins, after passage through body tissues. Vascular endothelial cells are found lining the entire circulatory system, from the heart to the capillaries. Endothelial cells are cells that line the inside surface of blood vessels and lymphatic vessels, they form a barrier between the blood or lymph in the vessel and the vessel wall.

To develop the vascular system the body employs different processes. There are three different processes of angiogenesis, which is the formation of new blood vessels, in normal tissue: Vasculogenesis is the process where blood vessels are created where no pre-existing ones exist, this is what creates the beginning of the vascular system in embryos. Next, sprouting angiogenesis is the formation of new blood vessels from pre-existing vessels. Finally there is intussusception, or splitting angiogenesis, where pre-existing vessels split to create new vessels. The two later processes will be of the most interest.

Sprouting angiogenesis is the typical form of angiogenesis and accounts for most of the new vessels in adults [49]. In sprouting angiogenesis endothelial cells from existing blood vessels travel to the surrounding tissue and form solid sprouts that connect back to the existing vessels to supply avascular areas [1]. With the exception of vascular remodelling during ovulation,

wound healing and weight gain (muscle, fat or other), no changes in the vascular system of healthy tissue is generally needed.

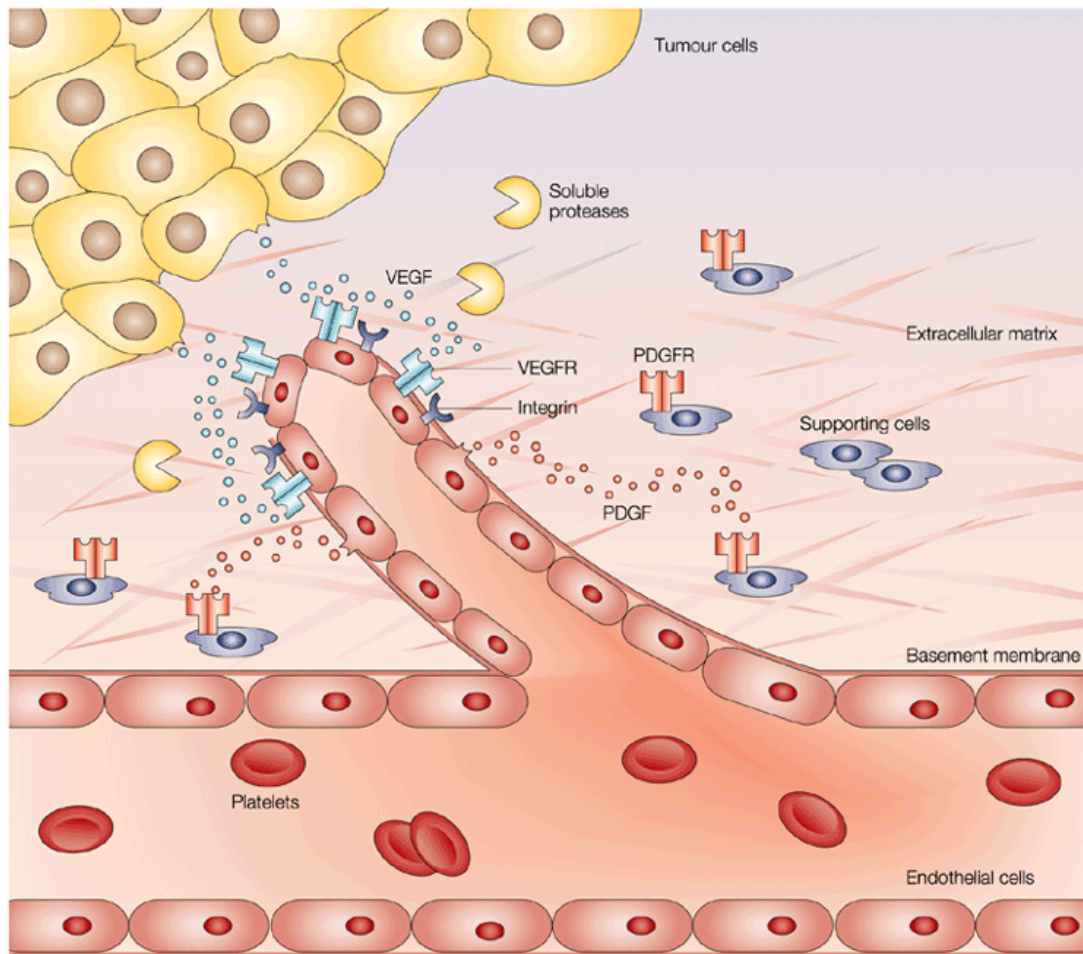


Figure 1: Illustration of sprouting angiogenesis in the vicinity of tumour cells. Recreated with permission from [7].

In tumours more blood vessels are needed to supply the generation and maintenance of new cells. As a consequence, most of the insight into angiogenesis has been gained because of angiogenesis' large role in tumour development and tumour vascularization.

2.4 Tumour Vascularization

For the tumour to generate new blood vessels the angiogenic switch must be turned on, as discussed earlier in 2.2. When activated and other supporting factors are achieved the formation of blood vessels takes place through the two aforementioned modes of vessel generation. However tumours also have two additional modes of vessel acquisition, these are non-angiogenic modes of vessel acquisition that exploit pre-existing vessels. Non-angiogenic tumour growth was overlooked for a long time, but is now suggested as one of the reasons why anti-angiogenic drugs have been somewhat ineffective in countering tumour growth and progression [9]. Non-angiogenic tumours are most often found in the lung, liver and brain, but a mixture of non-angiogenic and angiogenic areas is most likely to be found in almost all tumours. It should also be noted that in most tumours both angiogenic and non-angiogenic areas are present within the same tumour, and that angiogenic and non-angiogenic lesions can appear at different times during

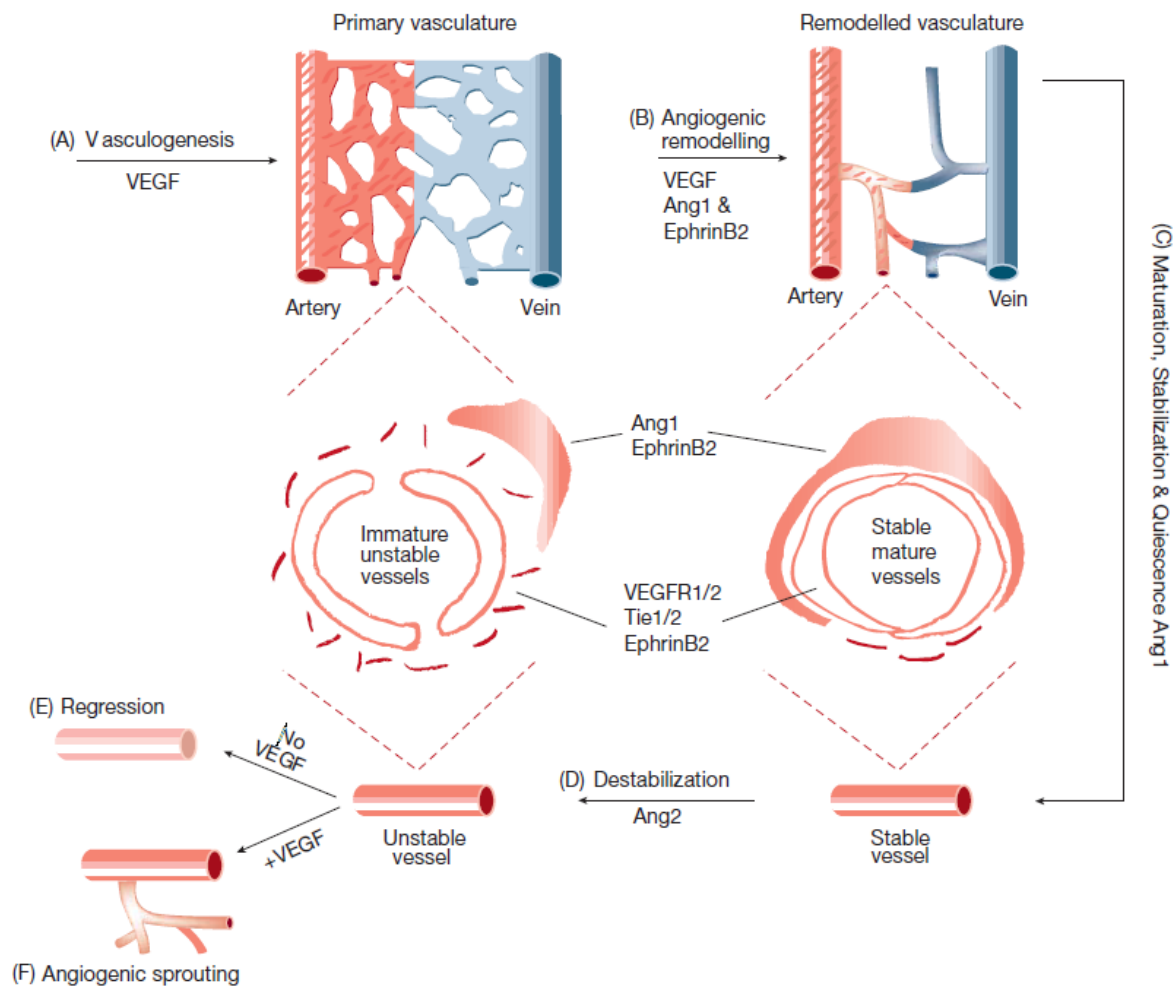


Figure 2: Illustration showing (a) Vasculogenesis (b) Angiogenic remodelling (c) Maturation (d) Destabilization (e) Regression and (f) sprouting angiogenesis. The roles different signalling molecules and proteins is shown for each process. Recreated with permission from [49].

the progression of cancer or in response to treatment [33] [9]. Also non-angiogenic neoplastic cells are highly metastatic and are associated with increased motility and the ability to invade surrounding tissues.

The two modes of non-angiogenic vessel acquisition are:

Vessel co-option, here the tumour cells infiltrate the pre-existing blood vessels by fusing with existing vessel cells. The term vessel co-option was first used by Holash and colleges in 1999 [18] to describe how tumour cells were observed to exploit pre-existing vessels rather than inducing angiogenesis. Much of the knowledge about how vessels are co-opted comes from brain tumours. In the process of co-option tumour cells need to travel towards vessels. In slices of rat brain it was shown that an activator of matrix metalloproteinases (MMPs) is expressed from brain-cancer cells and act as a chemo-attractant to guide the cell towards blood vessels [26]. The mechanisms by which the tumour cells interact with pre-existing vessels has also been investigated, but not yet fully understood. Caspani and colleges seeded glioblastoma cells (aggressive brain cancer cells), on mouse brain samples and showed vascular co-option within 15 hours [4]. The tumour cells developed contacts with vessel cells through special protein-based extensions, the results also indicated that cell division control protein 42 (CDC42) and CD44, a cell-surface glycoprotein involved in cell-cell interactions, cell adhesion and migration, support

vessel co-option by enabling fusion with the vessel cells.

Vasculogenic mimicry. In 1999 Maniotis and colleagues found vessel-like structures, in highly aggressive and metastatic melanomas, which were highly patterned. In these structures blood cells were detected, but endothelial cells were not. They also found that this structure, unlike those from angiogenesis, was lined by tumour cells. The vessel like structures were called 'VM', vasculogenic mimicry, [1]. Since then it has been found that many molecule mechanisms, especially vascular endothelial cadherin (VE-cadherin), ephrin type-A receptor 2 (EphA2), phosphatidylinositide 3-kinases (PI3K), MMPs, vascular endothelial growth factor receptor 1 (VEGFR1) and HIF-1 α , are involved in VM formation [34].

The channels formed through VM are not vessels but are made up of tumour cells mimicking normal endothelium. VM plays an important role in tumour growth by providing a perfusion pathway for blood and nutrition to the tumour as tumour cells lining these channels are directly exposed to blood. These systems facilitate a pathway for tumour growth without invoking the angiogenic switch, and may therefore be a way for tumours to continue their growth without the regular angiogenic pathways. VM's characteristics are as follows: Positive Periodic acid-shiff (PAS) staining and negative CD31 staining (endothelial cell adhesion molecule), the channel is lined by tumour cells, the expression of a stem cell-like phenotype, ECM remodelling and VM connects to the tumour circulation system, providing blood for tumour growth. VM has been linked with poor prognosis and shorter 5-year survival, in addition cancer patients with VM tend toward tumour metastasis.

2.4.1 General Tumour Vasculature Characteristics

Although vasculature can be generated through the same processes as in normal tissue, the balance of pro-angiogenic and anti-angiogenic factors as well as other vascular forming molecules and signalling factors are not controlled as they would be in normal tissue. This comes from the alterations neoplastic cells have made to their genomes. As a result tumour vasculature has different characteristics from normal vasculature. One consequence is that tumour vasculature has no clear classification into arterioles, venules or capillaries [3] [23]. Further the vessels have different characteristics that separate them from normal vessels, these are described below.

Tumour vessel permeability: It is well known that tumour vessels have high permeability [15]. This causes blood from the vessels to leak into the extracellular space. The reason for this permeability is that the diameter of the vessels are irregular and the walls are thin, in addition the walls are poorly developed and often have a discontinuous endothelial lining leading to holes in the vessel.

Defective Endothelial layer: Tumour endothelial cells have irregular shapes and sizes as well as poor organization, which can cause the cells to penetrate the vessel walls creating small finger-like holes. This in turn may lead to blood pooling up in the form of blood lakes.

Blood Lakes: Because of the permeability of the tumour vessels larger bodies of blood may be created, known as blood lakes. These blood lakes seem to not be in contact with the vascular system.

Tumour vasculature morphology: The formation of blood vessels in tumours is fast, unregulated and non-systematic therefore it becomes very chaotic and inconsistent. The tumour

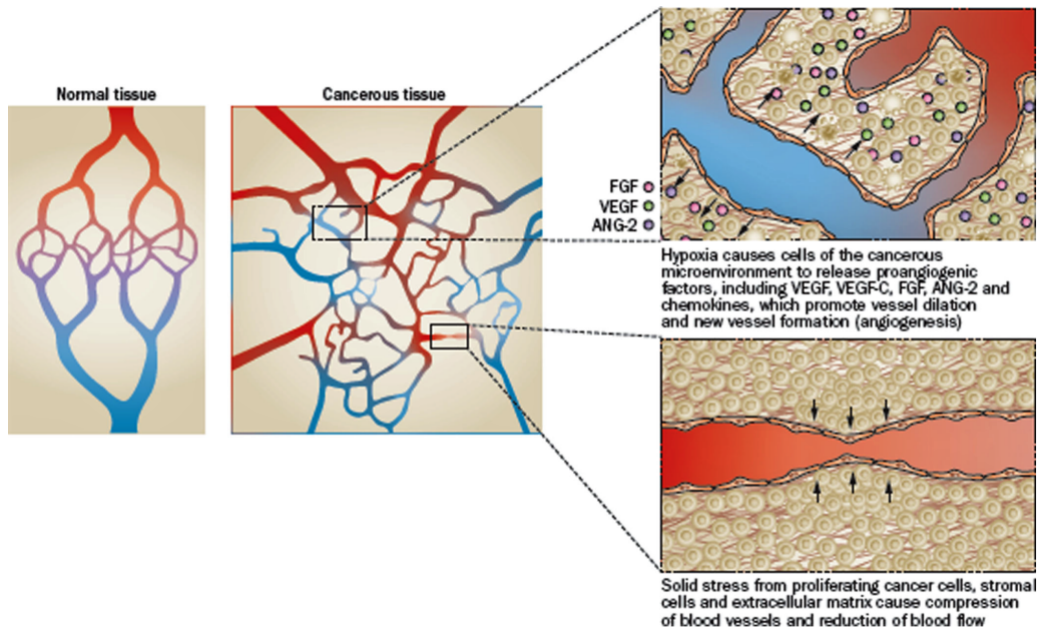


Figure 3: Illustration of normal (left) and cancerous (right) vasculature. In normal tissues, red vessels indicate oxygen-rich feeding arteries and arterioles, blue vessels are veins carrying deoxygenated blood and the connecting regions are the capillary stage with mixed colour. In cancerous tissues, slow blood flow is indicated by reduced colour intensity. Recreated with permission from [12].

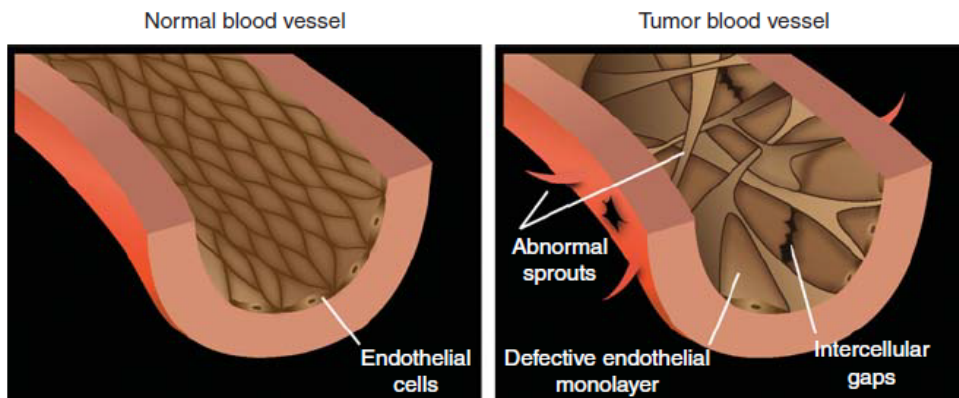


Figure 4: Illustration showing the blood vessels from normal (left) and tumour (right) vasculature. It also shows defects in the endothelial layer of tumour vessels. In a normal vessels endothelial cells for a tight grid. In tumour vessels the endothelial cells sprout and branch uncontrolled leading to a defective endothelial layer. The poor structure leads to gaps that can cause leakage. Recreated with permission from [10].

endothelial cells often present excessive branching and. This can cause areas of the tumour to become chronically-hypoxic this is explained in section 2.5.

Irregular blood flow: Because of the changes to vessel stability relative to normal vessels, tumour vessels have chaotic blood flow that changes in magnitude and may even reverse direction. Some vessels are not even perfused with blood at all. This is caused by the fact that the density of vessels may rise in bursts during the early stages of tumour development while decreasing in larger tumours when tumour growth is larger than the rate of blood vessel formation [10].

2.5 Hypoxia

Hypoxia refers to the oxygen deficiency that arises when a cell or part of the body is receiving less oxygen than it is consuming. The types of hypoxia are usually divided into two groups:

Acute hypoxia can occur when blood flow is restricted or absent in an area of the body, this can take place for many different reasons, but in tumours it is usually caused by the irregular blood flow. The malformed vasculature of the tumour also causes temporary closing of blood vessels from time to time and this can lead to acute hypoxia. Other reasons could be collapsed vessels or vessels that are too small being blockaded by tumour cells or red blood cells. An illustration is shown in figure 5. Dewhirst and colleagues studied acute hypoxia [30] and found vessels that experienced unstable flow magnitude and direction, in these the vessels would be empty for only a few seconds at a time. Other vessels experienced cyclic patterns of acute hypoxia in intervals of 20-60 minutes. Finally 9% of vessels had very low or absent red blood flow over longer periods.

Chronic hypoxia is when a part of the body is not getting enough oxygen on a consistent basis, this can occur if the vascular system is not well constructed in some part of the body. An illustration is shown in figure 5. If there is a poorly organized capillary system, like in most tumours, some cells are too far from the vessel for the oxygen to reach it. This typically occurs at around 100-190 microns from the blood vessel [32]. Many factors influence the distance which oxygen can diffuse, like the ability of haemoglobin to release oxygen, the intra-vascular pressure gradient, the use of oxygen by cells close to the blood vessel as well as the amount of oxygen in the blood in the vessel. If cells are completely deprived of oxygen for a long period, they will become necrotic and die. Necrosis indicates a more severe diagnosis, because of the complicating role of hypoxia as well as its role in malignant tumour progression.

For human tumours it is likely that there exist regions with both acute and chronic hypoxia and both have been described in pre-clinical models [28] [29]. One of the primary consequences of acute hypoxia in tumours is the increase in HIF-1 activity [50] [14].

2.5.1 Consequences of Tumour Hypoxia

Hypoxia is very important to consider when treating a tumour with radiotherapy, this is because the amount of oxygen in the tissue will greatly affect the effectiveness of radiation as well as affecting cells metabolism and cell cycle progression. The change in radiotherapy effectiveness as a consequence of oxygen is known as the oxygen effect. It is caused by the fact that radiotherapy with photons heavily relies on oxygen to create damage in the DNA via the creation of free radicals. The creation of free radicals is indirect damage to the DNA and is caused by the incoming photon interacting with an electron. The electron then interacts with other molecules like water to create free radicals. The free radicals can then diffuse far enough to damage the DNA, if there is oxygen available this damage will be fixed. This can be seen in figure 3. This fixation is the reason oxygen increases the effectiveness of indirect action, as repair is no longer possible. In direct action the photon interacts with an electron which then creates the damage in the DNA directly. About two thirds of the damage caused by photons is caused through indirect damage [51]. Without oxygen or with low amounts of oxygen the damage to the tumour cells will be lower and the treatment less effective as some of the damage caused can be repaired.

Because of the radioresistance in hypoxic tumours, a poorer prognosis is generally seen for patients with hypoxic tumours. This was first shown by Hockel and colleagues [22]. In addition

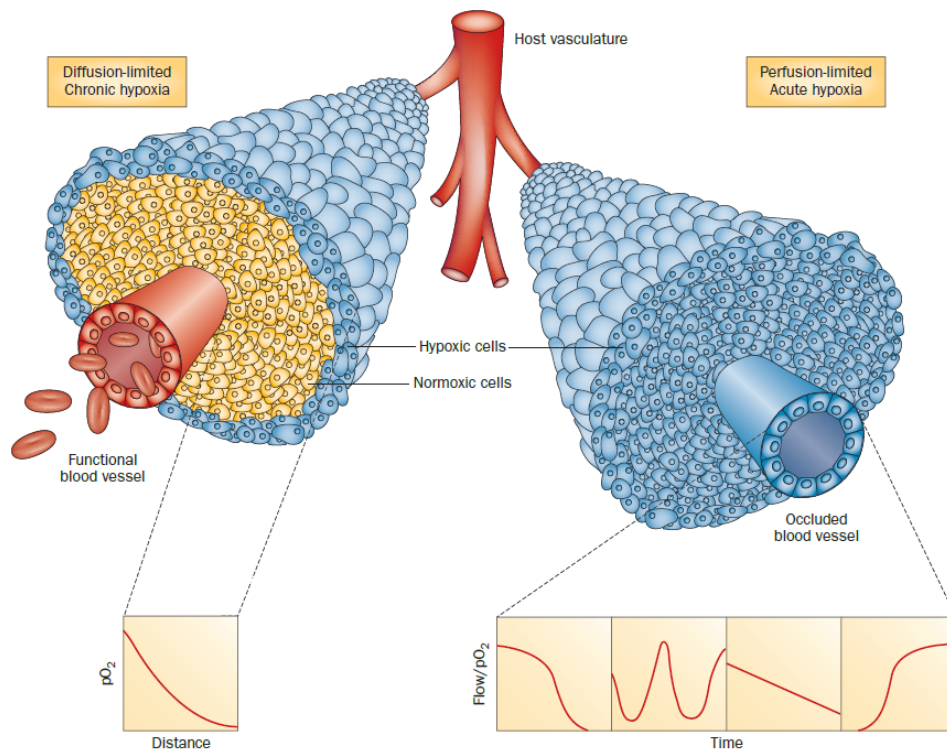


Figure 5: Illustration of chronic and acute tumour hypoxia. In the figure on the left we can see how chronic tumour hypoxia is limited by the diffusion distance of the blood. As a consequence the oxygen concentration decreases with distance from the vessel. On the right we can see all tumour cells surrounding the vessel are in a temporary state of hypoxia. The graph illustrates how the blood flow, or blood perfusion, can vary over time and therefore leave the cells without oxygen for short periods. Recreated with permission from [17].

to this it is suspected that hypoxia may produce a more aggressive phenotype as an association has been seen between distant metastases and hypoxic tumours as shown by Brizel and colleagues [8].

Tumour vascularization and hypoxia are important factors in radiotherapy, since the the tumour vascular function determines the effectiveness of the treatment. Therefore having good tools and techniques to study tumour vascularization is of high value. Two promising techniques to gather vascular information of tumours non-invasively are: dynamic contrast-enhanced magnetic resonance imaging (DCE-MRI) and dynamic susceptibility contrast MRI (DSC-MRI). However these methods are not yet in clinical routine and therefore it is needed to determine whether they reliably reflect the tumour vascular function. One way to to asses this is to correlate the MRI findings to quantitative analysis of IHC using vascular markers. Now follows a section on MRI, before the theory behind IHC is presented 2.7.

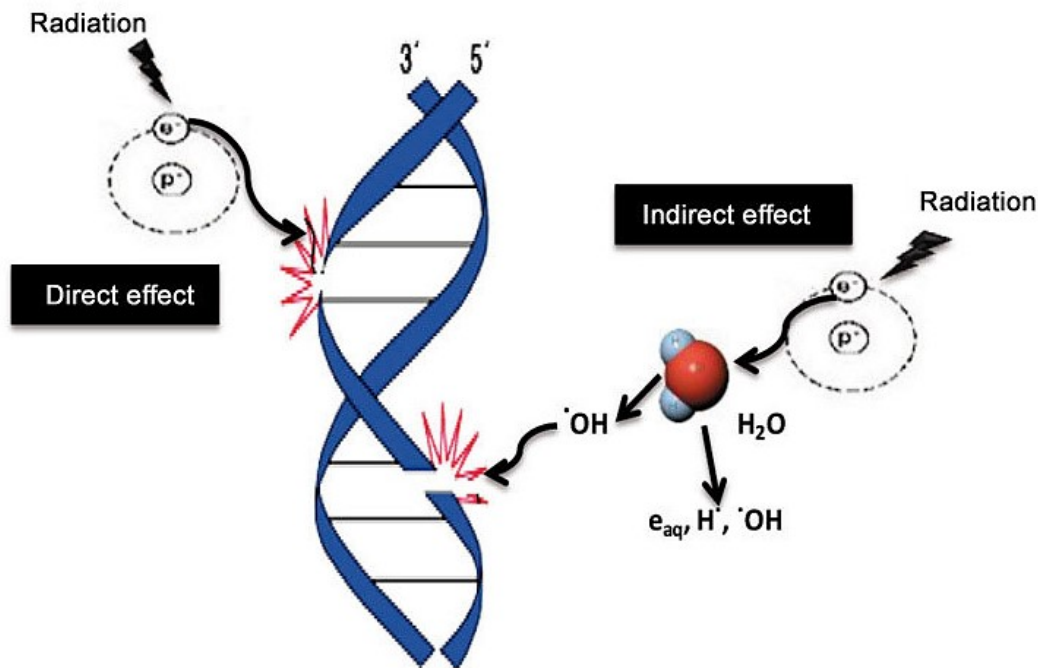


Figure 6: Illustration of the indirect and direct effects of readiation on DNA. In the direct effect the radiation interacts with an electron which damages the DNA. In the indirect effect the radiation strikes an electron which creates a free radical by interacting with a water molecule. The free radical goes on to fixate the damage of the DNA. Recreated with permission from [36].

2.6 Magnetic Resonance Imaging

MRI is a medical imaging modality based on the concepts of nuclear magnetic resonance (NMR). MRI gives anatomical and physiological images of bodies by using strong magnetic fields, radio-frequency waves and electrical gradients.

MRI is widely used in hospitals and its popularity and uses are increasing.

2.6.1 History

The concept of nuclear magnetic resonance was first described by Isidor I. Rabi in 1938. While the principles used for imaging originate with two other physicists, Felix Bloch and Edward Purcell. They received the Nobel prize in physics for their work in 1952, 5 years after they first submitted their discoveries. It was not until the late 1970s before the techniques were used to create images. In 1971 Raymond Damadian discovered that the hydrogen signal from cancerous cells was stronger than that of normal tissue since it contains more water and in the following year applied for a patent for the concept of NMR being used for cancer detection. By 1973 Peter Mansfield and Paul C. Lauterbur had made discoveries concerning magnetic resonance imaging. Lauterbur realized that magnetic field gradients could be used to determine spatial location, which lead to the possibility of rapid acquisition of two dimensional images. Mansfield had developed the mathematical formalism for MRI and developed techniques for efficient gradient utilization as well as fast imaging. In 1977 Damadian built the first MRI scanner along with two of his post-doctoral students and acquired the first MRI scan.

Since then the development has moved forward very quickly. Today we can get anatomical images with high resolution and very good soft tissue contrast accompanied by a large array of imaging techniques including different magnetic pulse sequences and contrast agents. MRI

can even be combined with other imaging methods such as computed tomography (CT) or positron emission tomography (PET) to give overlapping imaging information or combined with treatment hardware like a linear accelerator (MR-linac) for radiation treatment or with Electroencephalography (EEG) to monitor brain activity.

2.6.2 Working Principle

The working principle for MRI is the use of powerful magnets and radio-wave pulses to create a varying magnetic field in matter, which then induces electric signals in a receiver coil. This electric signal can give spatial information, by the help of magnetic gradients, to create an image of the matter within the magnetic field. This chapter will explore how this is accomplished, but will not go into the specifics of the components of the machine itself, but focus mainly on the mathematical and physical ideas behind the concept.

The proton is a subatomic particle that is present in every single atom. It possesses a positive electric charge and spin, a quantum mechanical property. Spin is a form of angular momentum. Spin is often represented as a spinning object, and spin follows the same mathematical laws, however this is not an accurate representation of what spin actually is and spin has some properties which distinguish it from orbital angular momenta. The spin cannot change its rotation speed and the spin of a charged particle is associated with a magnetic dipole moment. It is this magnetic dipole moment that creates the phenomenon of magnetic resonance.

Spin has two available eigenstates α and β . The energy of α and β for any nucleus have the same energy in their natural state, but if a magnetic field is applied in some direction, then the spin α state will be aligned with the field and the β state against the field. The β state has higher energy since it is aligned against the field and the difference between the two states is $\Delta E = \lambda h B_0$. Here λ is the gyromagnetic ratio, a constant that is specific to every nucleus, and B_0 is the strength of the applied magnetic field.

For a large collection of spins the distribution of α and β states will be equal, but with an applied magnetic field there is a slight preference towards the α state, this difference scales with the strength of the applied field. This difference gives a small net magnetization in the α -direction, this net magnetization is usually called M or M_0 and is the main focus of all work on MR. At equilibrium the magnetization (M_0) is aligned with the magnetic field (B_0). However any magnetic vector not aligned with B_0 will precess around the B_0 -direction, this is known as Larmor precession, as the external magnetic field exerts a torque on the magnetic moment. This can be expressed as:

$$\vec{\tau} = \vec{\mu} \times \vec{B} = \lambda \vec{J} \times \vec{B} \quad (1)$$

where $\vec{\tau}$ is the torque, $\vec{\mu}$ is the magnetic dipole moment, \vec{B} is the external magnetic field and \vec{J} is the angular momentum. The magnetic vector will precess about the external magnetic field with an angular frequency ω of

$$\omega = -\lambda B \quad (2)$$

This frequency is known as the Larmor frequency.

The behaviour of the magnetization can be described by the Bloch equations, here given in a reference system that rotates around the z-axis:

$$\frac{dM_z}{dt} = \frac{M_z - M_0}{T_1} \quad (3)$$

$$\frac{dM_{x'}}{dt} = -(\omega_0 - \omega)M_{y'} - \frac{M_{x'}}{T_2} \quad (4)$$

$$\frac{dM_{y'}}{dt} = (\omega_0 - \omega)M_{x'} - \frac{M_{y'}}{T_2} \quad (5)$$

Where ω minus ω_0 is the difference in the angular frequencies for the rotating frames of reference and the precession angular frequency. M_z describes the magnetization along the external field (longitudinal component), M'_x and M'_y describe the magnetization perpendicular to the field (transverse component). The fractions on the right side in the three equations describe the relaxation from an excited state of the system back to equilibrium where T_1 and T_2 are the relaxation times, these depend on the magnetic landscape within the material being used.

The fraction on the right side of equation 3 describes longitudinal relaxation back to the original, low energy, state of the system with M_z equal M_0 and aligned with B_0 . This is caused by thermal relaxation, as energy is transferred into nearby atoms, and molecules through collisions, rotations, or electromagnetic interactions. The fractions on the right side of equations 4 and 5, describe the transverse relaxation or de-phasing of the transverse signal. This usually occurs if a spin is located in an environment where it experiences a local magnetic field, B_{loc} , in addition to the main magnetic field, B_o . If B_{loc} is in the same direction as B_o , the two fields add together and a spin in that changed magnetic field will now precess at frequency $\lambda(B_o + B_{loc})$, according to 2. The other spins, which did not have this local field, will be precessing at the original Larmor frequency $f_o = \lambda B_o$. Over time a time t the phase difference of $\phi = \lambda B_{loc}t$ would develop between the altered spin and the rest, the net transverse magnetization M_{xy} would be reduced as a result. The observed T_2 is shorter than what we would expect, this is because in the real world we will never be able to create perfect B_0 fields, there will always be some small inaccuracies in the field, this leads to an additional affect to the intrinsic T_2 and a shorter relaxation time. This relaxation time is called T_2 -star written T_2^* and is the combination of the intrinsic relaxation and the contributions from the field inhomogeneities. In addition to this we also have the same thermal relaxation in the transverse plane.

$$\frac{1}{T_2^*} = \frac{1}{T_2} + \frac{1}{T_2'} \quad (6)$$

The relaxation time T_2 is often replaced by the rate of relaxation. The rate is called R_2 and is the reciprocal of T_2 , $R_2 = \frac{1}{T_2}$. So equation 2.6.2 becomes:

$$R_2^* = R_2 + R_2' \quad (7)$$

To reach an excited state the system, there is a need to convert M_0 into transverse magnetization. This is done using a magnetic field perpendicular to B_0 , called B_1 . For the field to have the wanted effect it needs to be applied near the Larmor Frequency (equation: 2). When this field is applied the direction of the net magnetization M is rotated according to:

$$\theta = \lambda B_1 t \quad (8)$$

Where t is the time the field is applied and θ is the angle of rotation. This field is used in short pulses to make the necessary rotation and is referred to as an RF-pulse (radio-frequency) as the frequency is close to that of regular radio waves. The most common pulses are the 90 and 180 degree pulses, which rotate the magnetization 90 or 180 degrees respectively.

Through the use of these pulses and changing of the timing between pulses different experiments or pulse sequences can be created. The most common ones will be discussed in the following parts.

2.6.3 Pulse Sequences

The simplest one would be just a single 90 degree pulse. This will tip the initial magnetization from the B_0 -direction into the transverse plane where it will decay and de-phase until we have returned to the initial set-up with all magnetization in the B_0 -direction again. This is known as Free Induction Decay (FID). The signal we receive is a sine-wave dampened by the T_2^* effects.

One of the most used pulse sequences is the spin echo (SE). It consists of one 90 degree pulse and a 180 degree pulse separated by a time TE , the echo time. The first pulse flips the magnetization into the transverse plane where it begins to de-phase. The second pulse flips the spin-system around so that the spins start to re-phase. After another interval of TE all spins are in phase and we get a strong signal, this is called a spin-echo. This re-phasing is equivalent to having cars racing away from a point with different speeds and then after a certain time return back the same way they came with their respective speeds. They will reach the starting point at the same time. In the same way all the spins reach the starting phase after the same time, TE . However some de-phasing will still remain the 180 degree flip can only recover the de-phasing caused by the T_2' effects, the intrinsic T_2 de-phasing will still remain. Therefore this sequence is often used if we want an image which can show the materials T_2 effects, called a T_2 -weighted image. The longer the TE the stronger the weighting.

When a sequence is performed multiple times in a row the period of time between the beginning of a pulse sequence and the beginning of the succeeding pulse sequence is called repetition time and is commonly used as TR .

SE sequences can be very slow to use because higher T_2 -weighting requires longer TE and TR is very long. A way to speed up image acquisition is to re-use the excitation created for the first echo by applying another 180 degree pulse after the first echo. In this way there is no need to reset and do a new excitation with the 90 degree pulse and a second echo can be achieved. This is what is called a fast spin echo (FSE) sequence. The signal for each echo after the excitation decreases according to the T_2 de-phasing, therefore after a certain number of echoes a new excitation must be performed. The number of echoes acquired in one TR is called the echo train length (ETL) or turbo factor. The ETL typically ranges from 4 to 32 for routine imaging, but can be over 200 for rapid imaging and echo planar techniques. To increase signal to noise ratio the signal may be sampled multiple times and averaged. This is called the number of excitations or averages.

If a T_1 -weighted image is desirable one would use a sequence called inversion recovery (IR). This sequence is started with a 180 deg pulse followed by a 90 degree pulse and then another 180 degree pulse. The first pulse turns the magnetization in the opposite direction of B_0 and the T_1 relaxation begins. The time between the 180 degree pulse and the 90 degree pulse is

called the inversion time T_I and is the determining factor for the amount of T_1 -weighting.

$$S(t, TE_n) = S_{PD}(t)e^{\frac{-TE_n}{T_2^*(t)}} \quad (9)$$

In order to get an image which could be T_2^* -weighted one would apply magnetic gradients. The underlying pulses is just a FID, but after the 90 degree pulse a gradient is applied which scrambles the signal to accelerate the de-phasing, it is known as a de-phasing gradient. Shortly after a re-phasing gradient is applied, with the opposite direction and the same strength and with this an echo is generated and a T_2^* -weighted image is created. Note that the gradients do not undo the de-phasing caused by the inhomogeneities in the field.

2.6.4 Dynamic Susceptibility Contrast MRI

In addition to using different sequences, a contrast can be created by injecting a contrast agent (CA). This is done in dynamic susceptibility contrast MRI (DSC-MRI) and dynamic contrast enhanced MRI (DCE-MRI).

In DSC-MRI a gadolinium-based CA is administered. This CA decreases the local T_2^* since the agent has positive magnetic susceptibility, which means its paramagnetic properties enhances nuclear relaxation rates. The CA will follow the blood stream and affect the relaxation of the tissue compared to the relaxation times without the CA, giving rise to a difference in signal. For the gadolinium-based CA, the signal intensity will transiently decrease because of shortened T_2^* . T_1 is also affected but has a shorter range and if the CA remains within the vessels, it can be neglected. We can assume a linear relationship between CA concentration and change in T_2^* . The signal will increase again as the CA diffuses out of the image volume.

Images are taken before, during and after the injection of the CA, and a signal intensity difference can be seen across the images as the CA enters and dissipates in the image volume. To observe the influence of CA over time an imaging sequence with high temporal resolution needs to be used. Echo-planar-imaging (EPI) is a commonly used sequence and fits this role well. Echo-planar-imaging creates multiple gradient echoes from an initial excitation by using a frequency-encoding gradient that switches directions multiple times, as well as a low-magnitude phase-encoding gradient that is transiently applied when the frequency gradient changes direction. This speeds up acquisition as it gathers several lines of k-space in one excitation. The number of lines acquired per excitation is known as the EPI factor. The data from DSC-MRI can be acquired with a T1-weighted multi-echo EPI. By using multiple echoes both T_2^* and T_1 weighted data can be acquired by the same sequence. This is the same idea as in FSE to create more than one echo from a single excitation.

Merged fast field echo (mFFE) is a sequence to create static T_2^* -weighted images. By rapidly reversing the direction of the frequency-encoding gradient, many gradient echoes can be created at different echo times. This process is limited in that the number of echoes is limited by T_2^* -decay, so a couple of echoes are normally used.

As discussed earlier tumours have high permeability, this means that when the CA enters the tumour volume it will leak out of the vessels. Therefore the linear relationship assumed earlier will no longer be accurate. T_2^* can be calculated from equation 9, as long as a multi-echo sequence was used.

2.7 Histology and Immunohistochemistry

Histology concerns the study of biological material, in the form of intact tissue, using microscopes. To use microscopes the specimens are usually sectioned and mounted on microscope slides. In order to visualize different biological processes and structures the sections can be stained with appropriate dyes.

In this project we have looked at both histology and IHC, but there is a lot that applies to other areas of histology.

The process for creating histological sections will be given a short overview and some details about certain markers will be given. Unless otherwise stated the following section will be based on lectures and lecture notes from the course Biophysical Micromethods at NTNU from 2017 and the book *Histology: A Text and Atlas* by M.H.Ross and W.Pawlina. [37]

2.7.1 Fixation, Embedding, Sectioning, Staining and Mounting

The initial step of sample preparation is fixation. The sample must be fixated, so that it is stored in the same state as when it is removed from the body, otherwise the biological material might break down or be altered by enzymes or microorganisms. Fixation also terminates cell metabolism and hardens the specimen without significantly altering its molecular structure. The most popular fixation agent is formalin (formaldehyde), which can be applied either through vascular perfusion of the specimen, or by immersion of the specimen. Because formaldehyde does not alter the three-dimensional structure of the sample the proteins maintain their ability to react with antibodies which allows for the later staining. The sooner fixation is initiated after the specimen is detachment from its blood supply, the better.

The second step in sample preparation is embedding. In paraffin-embedding the specimen is surrounded by a paraffin wax-based agent. The agent solidifies and thereby provides the mechanical support to section the sample. After being embedded the specimen can be stored for several years. After fixation the sample is washed and dehydrated with a series of increasing alcohol concentration solutions. Thereafter the alcohol removed using organic solvents like xylol or toluol. Now the sample is ready for paraffin-embedding.

In order to create the very thin slices needed for histological study a microtome is used. The microtome is a precision machine that sections biological tissue, it employs sharp steel, glass or diamond-edged knives to section tissue into thin slices in the micron-size range.

For the staining, the paraffin must be removed and the specimen rehydrated with decreasing alcohol concentration solutions. The sample can then be stained with the appropriate dye. The most common stain is hematoxylin and eosin (H&E-stain), it displays the general structural features of the sample an example of an H&E image is shown in figure 7.

2.7.2 Immunohistochemistry

Antibodies are glycoproteins that are made by specific cells of the immune system as a reaction to a foreign protein, or antigen. Antibodies can be extracted and attached to fluorescent dyes. Antibodies with attached dyes can be used to localize an antigen in cells and tissue. Two types

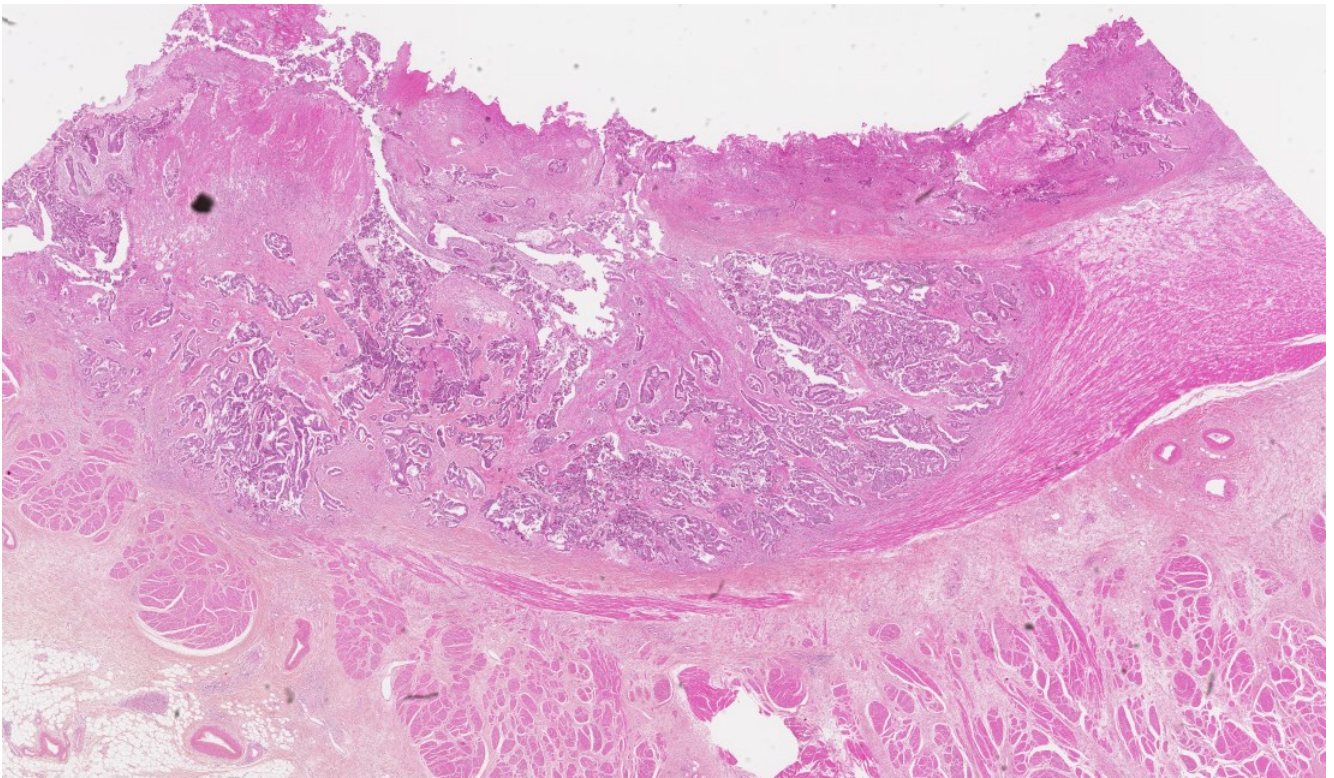


Figure 7: Image of an H&E image. The structure of the tissue is well resolved thanks to the H&E stain.

of antibodies are used in IHC:

Polyclonal antibodies are produced by immunized animals. In the process of creating an antibody, a specific protein is isolated from a cell of one species and injected into another species. In the injected, immunized, subject the foreign protein is recognized by the immune system and triggers specific immunologic reactions involving many clones immune cells called B lymphocytes. The cloning of B lymphocytes eventually creates the antibodies for the injected protein. These polyclonal antibodies represent mixtures of different antibodies made by multiple clones of B lymphocytes that each react to different parts of the protein molecule. The antibodies are then removed from the blood, purified and modified with fluorescent dye. Now these antibodies can be used to locate the original protein in the species the protein was originally taken from. As the antibody binds to it and this connection can be visualized by fluorescence microscopy.

Monoclonal antibodies are produced by immortalized antibody-producing cell lines. The origin of this cell line comes from an individual with multiple myeloma, a tumour originating from an antibody-producing plasma cell. These antibodies consist of a single group of identical B lymphocytes. To create monoclonal antibodies for a specific antigen, a species is immunized with that antigen and the B lymphocytes isolated and fused with the myeloma cell line. This combination creates hybridoma, an immortalized individual antibody-secreting cell line.

When one is trying to locate a specific antigen in a sample both indirect and direct methods are used, but indirect methods are replacing direct methods because of suboptimal sensitivity. In the direct method of immuno-fluorescence a fluochrome-labelled antibody (poly- or mono-clonal) that reacts with the antigen in the sample is used. While in indirect immuno-fluorescence the fluochrome is attached to a secondary antibody which reacts to the antibody of the antigen in the sample. This method enhances the fluorescence signal from the tissue as

multiple of the secondary antibodies can attach to a single primary antibody. In addition a single secondary antibody can localize the binding of several different primary antibodies and the secondary antibody can be attached to different dyes so that multiple labels can be shown in the same tissue section. The drawbacks of the indirect method is that it is expensive, labour intensive and not easily adapted to automated procedures.

When applying antibodies to a prepared sample, the sections are heated in order to unmask the connecting point of the antigen, and treated with hydrogen peroxide to block the enzyme that catalyses the oxidation of hydrogen peroxide. Thereafter the sections are incubated with antibodies and later can be imaged.

2.7.3 Histological and Immunohistological Markers Used in This Study

H&E: DNA in the nucleus, RNA in ribosomes and in the rough endoplasmic reticulum are all acidic, and so haematoxylin binds to them and stains them purple. Most proteins in the cytoplasm are basic, and eosin binds to these proteins and stains them pink. This includes cytoplasmic filaments in muscle cells, intracellular membranes, and extracellular fibres. [37].

CD34: is widely regarded as a marker of vascular endothelial progenitor cells and is a trans-membrane protein. Cells expressing CD34 are normally found in mesenchymal stem cells, endothelial progenitor cells, endothelial cells of blood vessels. [27].

Carbonic anhydrase IX (CAIX): The expression of CAIX is upregulated during hypoxic conditions [5] and CAIX is a cellular biomarker of hypoxia. It is over-expressed in hypoxic solid tumors, but is not expressed in most other normal tissues.

HIF-1 α : Monoclonal anti-HIF-1 α antibody can be used in immuno-staining to detect HIF-1 α localization [43]. HIF-1 α is a regulator of cellular and developmental responses to hypoxia. HIF-1 α is over-expressed in many human cancers and HIF-1 α over-expression is heavily implicated in promoting tumour growth and metastasis through its role in initiating angiogenesis and regulating cellular metabolism to overcome hypoxia.

2.7.4 Automated Image Analysis

Tumour angiogenesis is a prognostic factor in many tumour types and has been well studied. The usual way to quantify it is to manually count the number of vessels in a specific region and thereby estimate the microvessel density (MVD). An automatic analysis would be beneficial to make this process less time-consuming and also more quantitative. One example of such a method was the computer program developed by [24] and [25]. In this program CD34 stained IHC images were used to quantify a range of vascular parameters. The program was compared to manual counting by an experienced pathologist. The agreement, over 50 cases, between the two methods achieved an intraclass correlation coefficient of $r_a^2 = 0.96$ and a 95% confidence interval for the percentage difference between the counts from -26.1% to 10.8% . In addition the automated program could provide a range of additional vascular characteristics.

A version of these programs were made available for use in this thesis.

3 Method

In this section the materials used as well as the procedures used to gain the results in this project will be presented. The materials and methods of the MRI investigation will be discussed first and then the histology and IHC. The structure of the section is on the format where, acquisition, analysis and statistics are all explained fully for one modality before moving on to the next.

3.1 R_2^* MRI Study

A project thesis was written by Ingrid Framås Syversen in 2017, where the R_2^* of 26 patients with rectal cancer was studied [41]. The patient data was taken from prospective study in rectal cancer named OxyTarget, conducted at Akershus University Hospital from 2013 to 2017 [35]. Both standard and study-specific MR images were taken before and after CRT, the patients then underwent surgery. Image analysis was performed using Matlab programs, where it was attempted to look for markers of cancer aggressiveness. The findings were that one parameter correlated with CRT response and was related to poor prognosis.

After this analysis was performed, more patient data has become available, and further analysis can be performed to see if it is in agreement with what was found previously. The programs and data from the earlier project have been made available for use in this thesis so a comparison can be made.

3.2 Patients

The patients in this study are taken from the OxyTarget study mentioned above. Data from a total of 113 patients were received, 102 of these patients had MR images and 39 had IHC images. 16 patients received neoadjuvant CRT but did not get surgery, 11 of these patients only had palliative (non-curative) treatment. 28 of the patients had both. Further information is found in table 2.

| | | | | |
|---------------------------------|-----------------------------|---------------|------------------|-----------------------------------|
| Total number of patients | Histological and IHC images | MRI | IHC and MRI | |
| 113 | 39 | 102 | 28 | |
| Treatment | Only Surgery | CRT + Surgery | CRT + no surgery | Palliative treatment + no surgery |
| 113 | 52 | 45 | 5 | 11 |
| Treatment for patients with MR | Only Surgery | CRT + Surgery | No Surgery | |
| 102 | 43 | 41 | 17 | |
| Treatment for patients with IHC | IHC + CRT | IHC + No CRT | | |
| 39 | 20 | 19 | | |

Table 2: Patients divided into groups according to what was collected and what treatments they received.

3.3 MRI

In this project the initial TNM classification was performed with MRI for the TN and computed tomography (CT) was used to classify the M, the CT was taken for thorax and abdomen.

The MRI was done using a Philips Achieva, 1.5 T, (Philips Healthcare, Best, The Netherlands) with NOVA Dual HP gradients ($33mT/m$ maximum gradient amplitude, $180T/m/s$ slew rate) and a five-channel cardiac coil with parallel imaging capabilities. Before and during imaging

glucagon ($1\text{mg}/\text{mL}$, 1mL intramuscularly) and Buscopan ($20\text{mg}/\text{mL}$, 1mL intravenously) was given to the patients, to reduce bowel movements.

An FSE sequence was used for the T_2 -weighted images 8a, with $TR = 2386 - 4122\text{ms}$, $TE = 80\text{ms}$, acquisition matrix = $224 \times 220 - 256 \times 254$, field of view (FOV) = $180 \times 180\text{mm}$, slice thickness = 2.5mm , number of excitations = 3 – 6, and ETL = 20. 21 – 37 slices were acquired. Based on these images tumour masks were drawn for the tumours by two radiologist with 20 years of experience. Addition, axial T_2^* -weighted images 8d were acquired using an mFFE sequence with five echoes, where $TR = 855 - 1137\text{ms}$, $TE_1 = 4.6\text{ms}$, echo spacing = 9.2ms , acquisition matrix = $152 \times 101 - 180 \times 120$, FOV = $180 \times 180\text{mm}$, slice thickness = 3mm , number of excitations = 1 – 3, and flip angle = 45 deg. The number of slices acquired for the mFFE sequence was 18 – 24.

For the DSC data a 3D T_1 -weighted EPI sequence with three echoes were used. Here $TR = 38 - 45\text{ms}$, $TE_1 = 4.6\text{ms}$, echo spacing = 9.2ms , acquisition matrix = 92×90 , FOV = $180 \times 180\text{mm}$, slice thickness = 10mm , flip angle = 28 deg, and EPI factor = 9. 12 – 22 slices were acquired, $2\text{s}/$ imaging volume - time resolution, and in total 60 time points were recorded. The DSC data was acquired in intervals using a split dynamic sequence, interleaved with a high spatial resolution T_1 -weighted sequence. To suppress fat signals a ProSet fat suppression technique was applied. The CA used was the gadolinium-based CA Dotarem which was given as a bolus injection. Dynamic R_2^* values were calculated from the DSC data using equation 9. Maps of the R_2^* values were made for the images.

DWI and DCE images where also taken, but were not used in this project.

3.3.1 Image Analysis

The images were analysed in MATLAB (R2016b, The MathWorks, Inc., Natick, Massachusetts, United States). The scripts used for the analysis can be found in the appendix A. To begin with all 2D-images were sorted, using the info from the DICOM-info-file, into 3D and 4D matrices. Here the two first dimensions are the image info and the third dimension is the slice position. For the FFE and DSC images the echo time was the fourth dimension.

In order for the program to perform its calculations in the tumour area the tumour masks were applied. The tumour masks were drawn on the T_2 -weighted images and guided by the DW images, these have a different resolution and thickness than the mFFE and DSC images, so the tumour masks had to be adapted to fit these images. This was done by multiplying the number of pixels in the tumour mask by the spatial resolution and placing the tumour mask on the nearest pixel. Tumour masks were in the NifTI-format, and was converted into binary 3D-matrices usable by MATLAB. The masks were all visually inspected for their fit with the images.

The static R_2^* values were calculated from the static mFFE images, using equation 9. For each tumour, median R_2^* values, as well as minimum and maximum values were obtained. For one patient there was no tumour mask and for some the mFFE file was missing, in addition some images had large artefacts that made the images unusable, these were then excluded in the analysis, see table 3.3.1.

Dynamic R_2^* maps were calculated from the DSC data. The pixel value at different time points,

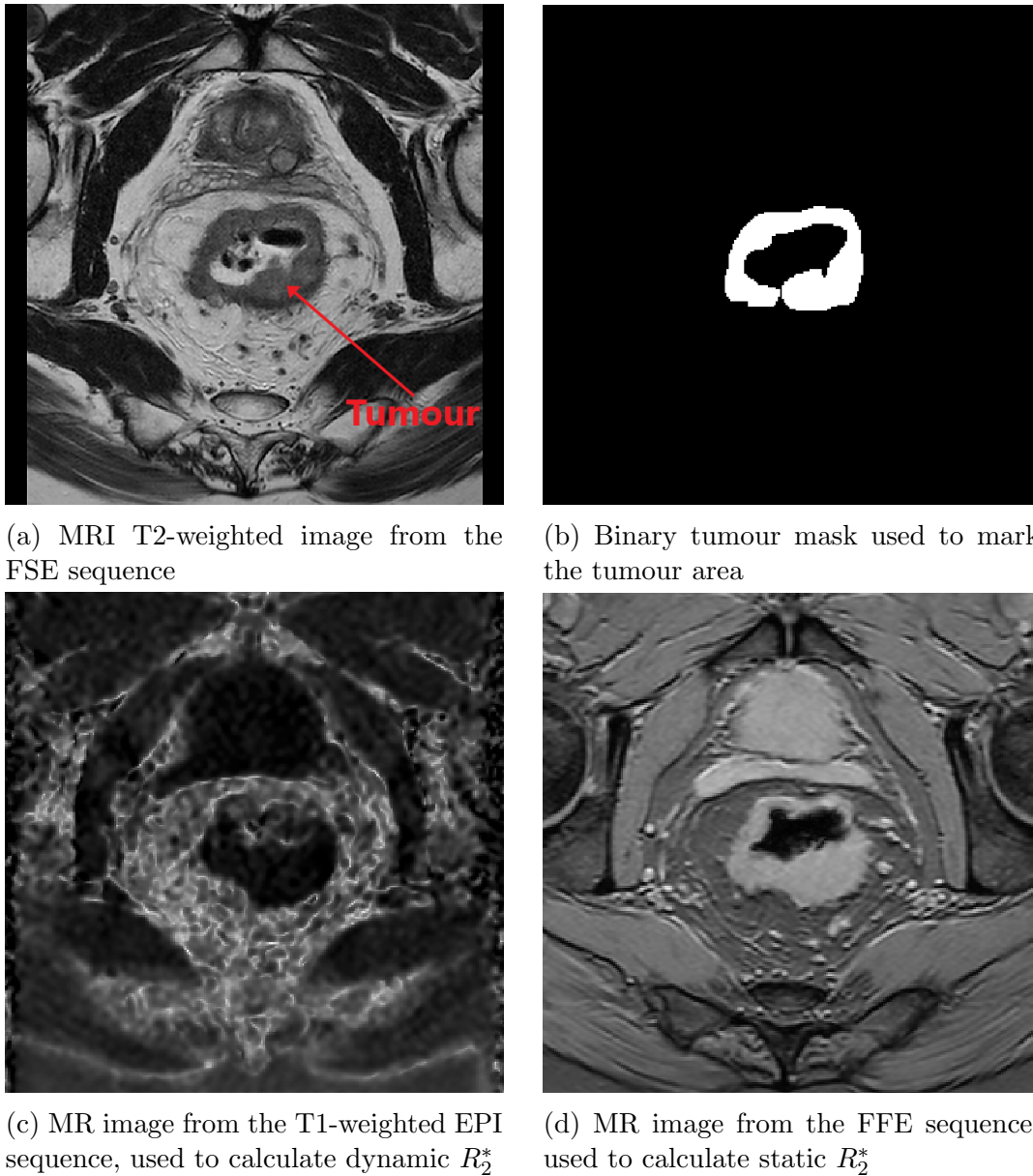


Figure 8: MRI pictures from the different sequences in the same patient.

| Total number | Included in all | Included in static | included in dynamic |
|--------------|-----------------|--------------------|---------------------|
| 102 | 82 | 90 | 82 |

Table 3: Patients included or excluded from results in the MR analysis.

for each pixel inside the tumour mask, were stored in an array. To create a baseline for the image intensity an average was calculated from the first few images, these are the images before CA injection. The number of baseline images varied between patients (from 5 to 23) and the number had to be found manually for each patient, this was done by plotting the pixel arrays against time and counting how many time points were acquired before the signal started to rise towards the peak. A higher count of baseline images gives a more robust baseline so as many as possible were used. The pixel arrays were then normalised according to the baseline, so the mean values of the baseline images were set to zero. The values of the array are now the change in dynamic R_2^* from baseline, ΔR_2^* . From this, the maximum enhancement of R_2^* (R_2^* -peak_{enh}) was found. By plotting the pixel array against time and integrating the curve, the area beneath the curve (R_2^* -AUC) was found. Illustrations of R_2^* -peak_{enh} and R_2^* -AUC

are shown in figure 9.

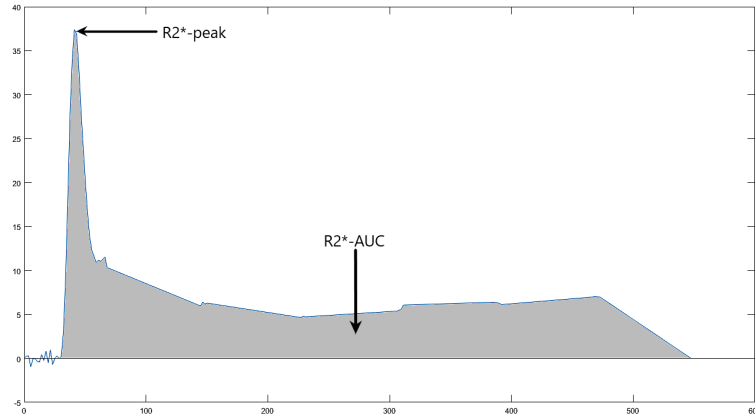


Figure 9: Curve of the signal averaged over all pixels in the mask. The gray area is the area under the curve (AUC) and the top of the initial curve is the peak. The baseline in this image was set according to the process explained in section 3.3.1.

To see if the correlation changed with different endpoints, multiple different time intervals were chosen. The time intervals were 0 to $49 \pm 1s$, 0 to $135 \pm 10s$, 0 to $222 \pm 15s$, and 0 to $525 \pm 25s$. The interval lengths have some variation because the images were acquired at slightly different time points for different patients. Median $R_2^* - peak_{enh}$ and $R_2^* - AUC$ values, as well as minimum and maximum values, were obtained for each patient.

3.3.2 Statistics

The Mann-Whitney U-test was used to check the calculated values for correlation with patient clinicopathologic information and therapy response. The U-test was used as there is a relatively small number of patients and it is unreasonable to assume that they are normally distributed. The test uses median instead of mean values, which limits the error caused by the low number of patients. The endpoints analysed with the U-test were mrTN, ypTN and TRG. Based on these endpoints the patients were divided into groups and can be seen in table 4.

The null hypothesis is that all patients come from a continuous distribution with one median value. This hypothesis is rejected if the p-value, the probability that the null-hypothesis is true, is below 0.05. So if the probability that the two groups have the same distribution is below 5% it is rejected. The alternative hypothesis is that the distributions of the two groups are not equal. If the null-hypothesis is rejected the alternative hypothesis must be accepted, meaning that it is highly likely that there is some intrinsic difference between the groups, as they have different distributions.

The different patients groups are shown in table 4. $\Delta T0-1$ and $\Delta T2-4$ are patients who had a difference in T-stage of 1, 0, 2, 3 or 4 compared between the initial TNM classification and the one given after surgery. $\Delta N0$ and $\Delta N1-2$ are the same, but for the N-stage. Downstaging and no-downstaging are groups defined by whether there was a lower T-stage or not after CRT as compared to pre-CRT. Patients with TRG0-2 were defined as good patients with good histopathologic response to CRT and TRG3 as poor tumour response.

| Endpoint | N_{static} | | $N_{dynamic}$ | |
|---------------------------------|--------------|---------|---------------|---------|
| | Group 1 | Group 2 | Group 1 | Group 2 |
| TRG0-2 vs. TRG3 | 28 | 10 | 29 | 10 |
| ypT0-2 vs. ypT3-4 | 13 | 22 | 12 | 24 |
| ypN0 vs. ypN1-2 | 31 | 29 | 43 | 27 |
| Δ T0-1 vs. Δ T2-4 | 28 | 7 | 30 | 6 |
| Δ T0-2 vs. Δ T3-4 | 30 | 5 | 31 | 5 |
| Δ N0 vs. Δ N1-2 | 21 | 15 | 20 | 17 |
| Downstaging vs. no-downstaging | 25 | 11 | 25 | 12 |
| <hr/> | | | | |
| No CRT | | | | |
| pT0-2 vs. pt2-4 | 13 | 20 | 13 | 20 |
| pN0 vs. pN1-2 | 23 | 15 | 24 | 13 |

Table 4: Grouping info showing number of patients in each group.

| Endpoint | Number of patients |
|----------|--------------------|
| mrT2 | 19 |
| mrT3 | 47 |
| mrT4 | 35 |
| mrN0 | 42 |
| mrN1 | 36 |
| mrN2 | 22 |
| pT1 | 4 |
| pT2 | 16 |
| pT3 | 21 |
| pT4 | 2 |
| pN0 | 24 |
| pN1 | 14 |
| pN2 | 4 |
| TRG0 | 4 |
| TRG1 | 13 |
| TRG2 | 15 |
| TRG3 | 11 |
| ypT0 | 5 |
| ypT1 | 4 |
| ypT2 | 4 |
| ypT3 | 25 |
| ypT4 | 3 |
| ypN0 | 23 |
| ypN1 | 11 |
| ypN2 | 7 |

Table 5: Parameters used for staging and evaluation of response.

3.4 Histology and Immunohistochemistry

Histology and IHC sections for 39 patients were examined. Only 33 of them were used in the actual data, the reasons are noted in introduction to the results 4.2. The following four stains were used for each patient: H&E, CD34, CAIX and HIF-1 α . The files were in the Aperio SVS TIFF format. The program PMA.start (Pathomation BVBA, Berchem, Belgium) was used to view the images.

TRG was determined after surgery and pathology.

3.4.1 Staining

The tumour sections were staining was performed at AHUS (Akershus university hospital) by an technician. CD34 staining was done with CD34 klon QBEND10, from Nordic BioSite (Nordic BioSite AB, Sweden). CAIX staining was performed with CAIX, from Bionordica (Bionordica AS, Norway). HIF-1 α staining was performed with HIF1-alpha klon 54, from BD Biosciences (BD Biosciences, USA). A routine H&E stain was also made. Stains for CD3 and CD8 were made, but since they are not used in this project they are not discussed further.

3.4.2 Scanning of Images

After the sections were stained they were imaged under a microscope and converted to digital images. The sections were imaged at $\times 20$ and $\times 40$ magnification. The digital files were later stored on a portable hard drive which was made available to the project.

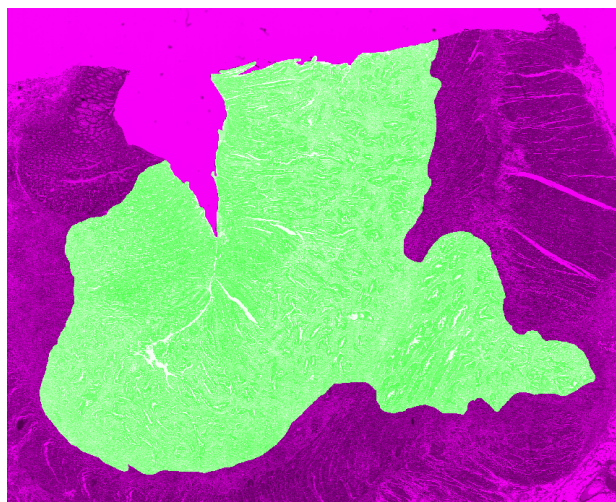
3.4.3 Tumour Mask creation

The images of the sections contained a mixture of normal tissue and tumour tissue, therefore tumour mask masks were made to separate tumour tissue from the normal tissue. The masks were made by the author of this thesis together with a PhD student in the department.

The tumour mask were drawn in GNU Image Manipulation Program (GIMP) on the H&E images. A threshold was applied afterwards to remove any non binary values. 19 of the images were sent to an experienced pathologist for inspection, to verify the tumour masks drawn and to clarify in the more uncertain areas whether or not they contained tumour cells. The tumour masks were then corrected and refined. An example of a mask is shown in figure 10a, an example of the applied mask is also shown in figure 10b.



(a) Binary tumour mask used to mark the tumour area, created for on an H&E image.



(b) Binary tumour mask applied to the corresponding H&E image.

Figure 10: Tumour mask and H&E image.

In drawing the tumour masks, the masks were drawn over the areas that contained the tumour and not specifically on only tumour cells, this was done as the masks would later be used for all

stains and some error was to be expected in the process so having some room for error was necessary to contain the tumours within the tumour masks. In addition it is not always possible to say where the tumour ends and normal tissue begins as tumours will recruit surrounding tissue like connective tissue and vessels as it grows. Further the extent of the tumour masks should be somewhat determined by the endpoint for the study as the different biological processes to be studied have different ranges impact. For example, for studying a feature with a low number of coloured pixels drawing a very tight mask could exclude stained pixels and greatly decrease the the number of data points since there are so few in total. For a feature with a high fraction of stained pixels a tight mask only excludes a small percentage of the data.

Artefacts were present in some of the images, but did not seem to affect results in any of the cases. Therefore no actions were taken, but if a consequence was found the area of the artefact would have been excluded from the masked area.

3.4.4 Image Analysis

A Matlab program developed for this project was used in the analysis of the stained images. The program is based on previous projects [24] [25] , a summary of the actions will be given as well as a brief explanation for the implementation.

Summary:

- The program loads in the files for a given patient.
- The tumour mask is applied to the H&E stain.
- The masks are applied to all other stains (registration based on the full image at a low resolution).
- The images are cropped to the area of the mask.
- To improve the mask-fit, the initial registration is re-done for the cropped images.
- The images are segmented and minuscule stains are removed.
- The features from the segmented and processed images are extracted.
- The features are saved to a file in the patients folder.

The registration in the application of the mask to the different stains is performed the first time with the thumbnail of the full image. The stains the mask will not fit perfectly since the images have slightly different sizes (in the range 10 – 500 pixels) and there are quite a few possible ways for the slice to be altered, examples are: stretching, ripping and folding. Because of these differences a more detailed registration between the H&E and the other stains is performed to improve the fit. The initial registration places the mask in the right vicinity, but rarely in the exact spot it needs to be. This is caused by the fact that the registration affects the entire image so it registers parts of the image we are not interested in with the same weight as the masked area. The second registration is only done in the area (bounding box) directly affected by the mask. This way the registration ignores values outside the area to be analysed. An example of the registration is shown in figure 3.4.4.

For the images where the image registration still did not fit well, the masks were scaled down (eroded) to keep them within the tumour region. An example of the scaling is seen in figure

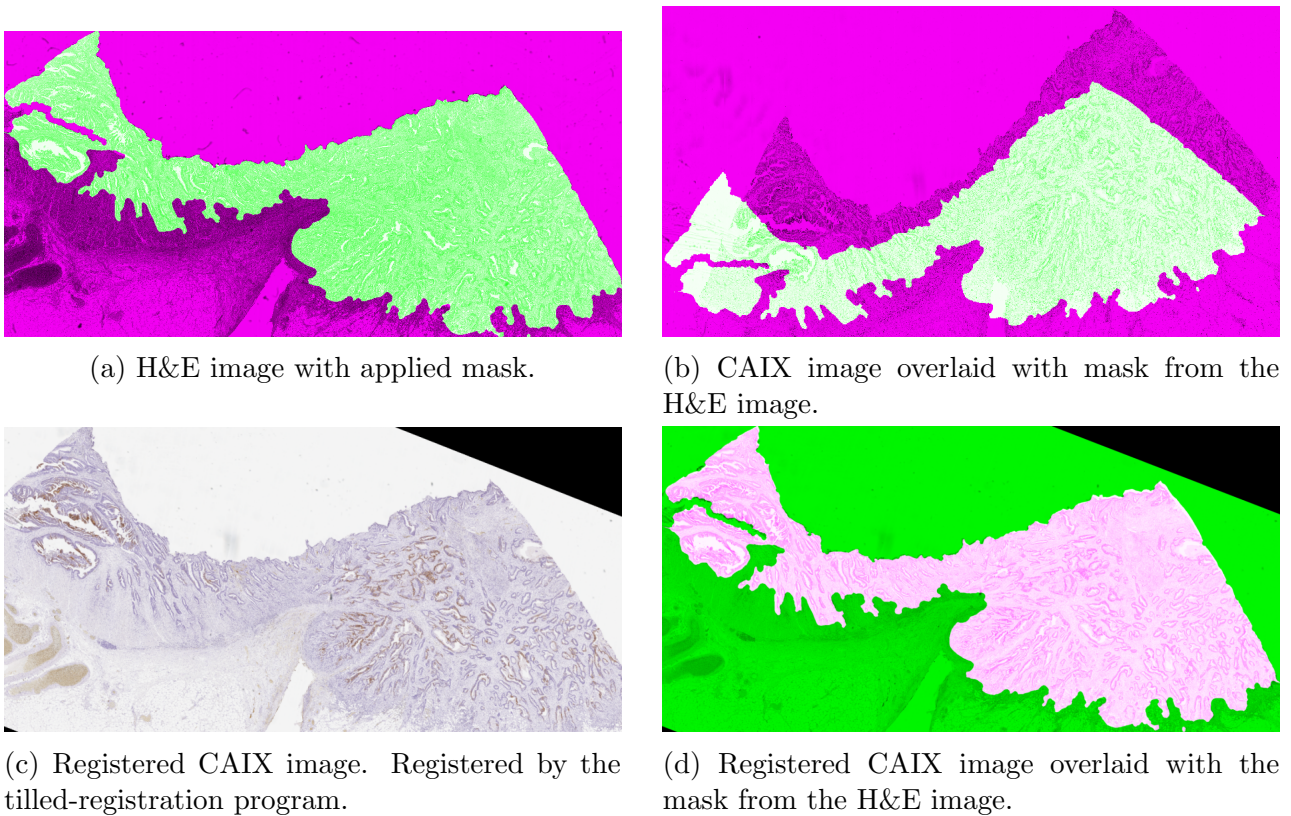


Figure 11: Images from different parts of the image registration. The first figure (a) shows how the mask should fit on the image based on how it was drawn on the H&E image. The second figure (b) shows how the initial registration fails to align the mask and image correctly compared to the first figure. In this example it is caused by a mixture of rotation, contraction. In the third figure (c) we see that the image from the second figure (b) is now aligned with the H&E image. When the mask is applied in the last figure (d) it now fits a lot better.

12. The images that still did not match up with the tumour region were excluded.

In the segmentation the HSV transform (hue, saturation, value) and the B value of the RGB are combined. The B layer has the highest contrast of the three RGB layers and provides better contrast than the RGB to gray function.

The post processing removes stains that are too small. The stains on the HIF-1 α images were weak, to compensate, these images were post-processed with slightly different parameters. This was done to make sure that most of the stains were conserved.

Examples of the images after segmentation and post-processing can be seen in figure 3.4.4.

The following features were extracted:

- Total Stained area, given as a fraction of total masked area. Generated for all stains. Abbreviated as SF (stained fraction), CAStf (CAIX stained fraction) and HIFsf (HIF-1 α stained fraction) in the for respectively CD34, CAIX and HIF-1 α .
- Average stain size. Generated for all stains (In the CD34 stain this is defined as average vessel size). Abbreviated as vessel size (VS), CAss (CAIX stain size) and HIFss (HIF-1 α stain size).



Figure 12: Image of an tumour mask that has been scaled/eroded. The coloured part has been removed from the mask to make sure the mask stays within the tumour area.

- Average Inter capillary distance (ICD), which is the distance to the closest vessel from a given vessel.(for CD34)
 - Average Solidity (a measure of convex-ness) (for CD34)
 - Micro Vessel density (MVD) (for CD34)
 - Number of Vessels (for CD34)
 - Average vessel radius (for CD34)
- The features were calculated in the following way:
- Stained fraction: The number of pixels in the masked area divided by the number of pixels that had a value above the threshold value.
 - Number of vessels: Each region of connected pixels with values over the threshold are grouped together and considered as one vessel.
 - Average stain size: The average number of pixels for each vessel (group of connected pixels).
 - Vessel radius: For each group the major and minor axis lengths were found and the average of these gives the diameter.

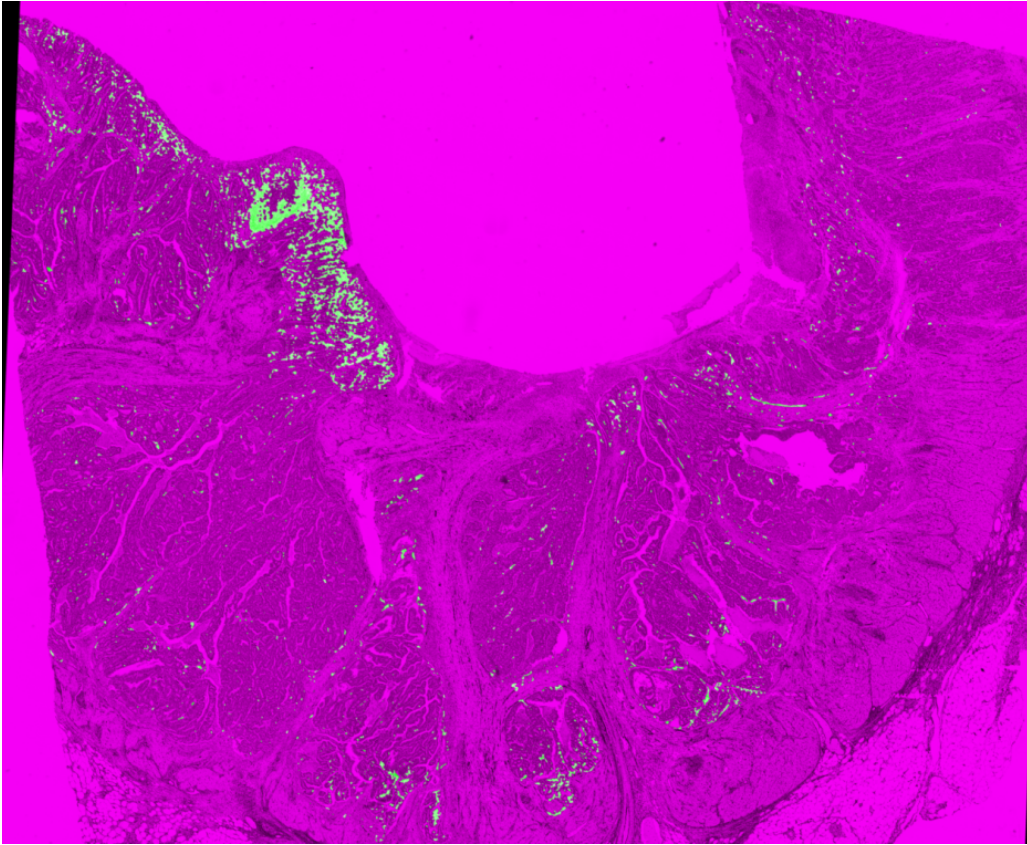


Figure 13: CD34 image after segmentation and post-processing. The green pixels are stains of CD34, vessels.

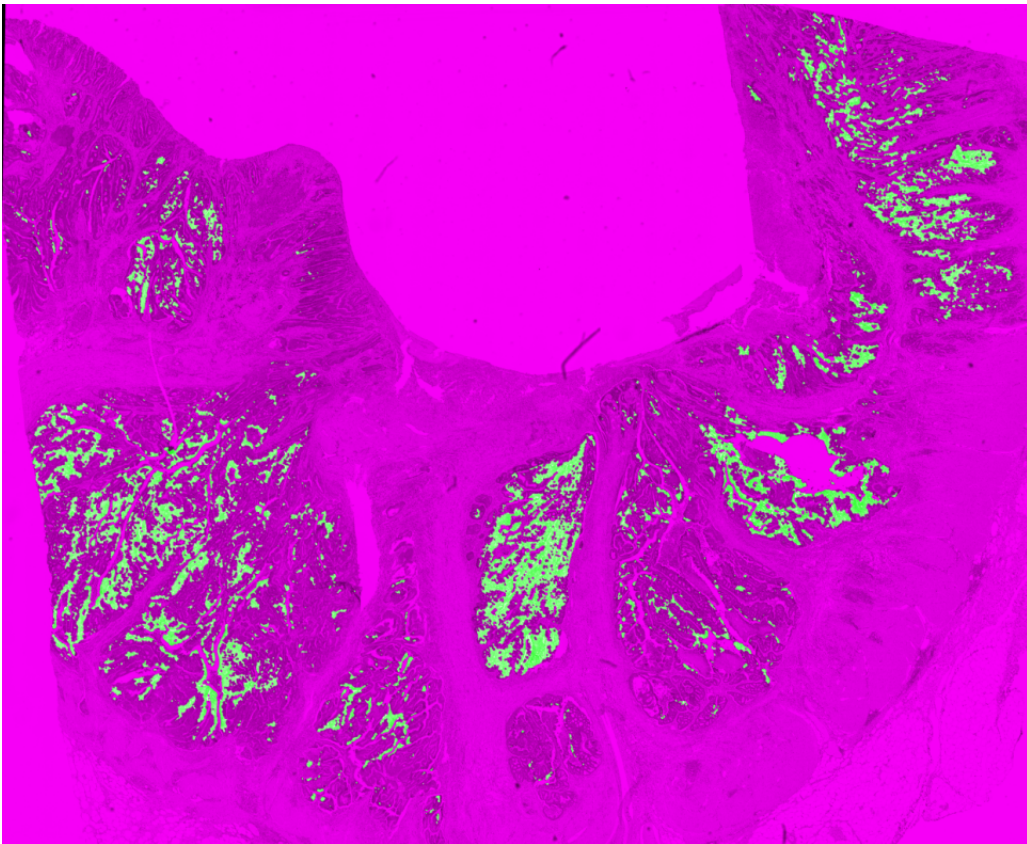


Figure 14: CAIX image after segmentation and post-processing



Figure 15: HIF1- α image after segmentation and post-processing

- Intra Capillary Distance (ICD): For each group the centroid of the region was found and the position of the centroid was stored. From this the shortest distance to any other centroid was calculated.
- Solidity: The convex hull of each group was found. The solidity was then calculated as the proportion of pixels in the convex hull that were also in the region of the group.
- Micro Vessel density (MVD): Found by taking number of vessels divided by the total masked area.

3.4.5 Statistics

The Spearman rank correlation coefficient was calculated for the pathological results to look for correlation with clinicopathologic information and CRT response, as well as correlation within the pathological results, and the p-values for these correlations were also calculated.

Survival statistics were calculated in IBM SPSS (IBM, New York, USA) ref. In SPSS Kaplan-Meier plots were made to see if survival differed for patients with different feature values. These are shown in appendix A.

| No TRG | 16 | |
|---------------------------------|---------|---------|
| Endpoint | Group 1 | Group 2 |
| TRG0-1 vs. TRG2-3 | 6 | 15 |
| TRG0-2 vs. TRG3 | 12 | 3 |
| ypT0-2 vs. ypT3-4 | 13 | 20 |
| ypN0 vs. ypN1-2 | 14 | 19 |
| Δ T0-1 vs. Δ T2-4 | 32 | 0 |
| Δ T0-2 vs. Δ T3-4 | 32 | 0 |
| Δ N0 vs. Δ N1-2 | 26 | 7 |
| Downstaging vs. no-downstaging | 13 | 20 |

Table 6: Grouping info for the pathological data. Notice that there are no patients in Δ T2-4 or Δ T3-4

4 Results

4.1 MRI Results

The analysis of the MRI data yielded the results given below. Of the 103 patients with MRI data 79 were included in all results, 20 were only included in either static or dynamic R_2^* results and four were not used in either. The four patients not included in either were as a consequence of having images with artefacts or faulty tumour masks.

The results for static R_2^* , dynamic R_2^* -peak_{enh} and dynamic R_2^* -AUC are given below.

4.1.1 Results for Static R_2^*

Calculated from the mFFE images the static R_2^* values were not statistically significant for any of the different endpoints, although there were differences in median values. This can be seen in table 7.

| For patients with CRT Endpoint | Median static R_2^* (s^{-1}) | | p-value |
|--------------------------------------|------------------------------------|-------------------|---------|
| | Group 1 | Group 2 | |
| TRG0-2 vs. TRG3 | 32.2 (12.7-482) | 18.9 (13.1-353) | 0.135 |
| ypT0-2 vs. ypT3-4 | 39.6 (13.6-482) | 22.6 (12.7-463) | 0.621 |
| ypN0 vs. ypN1-2 | 24.2 (13.1-463) | 23.1 (12.7-482) | 0.608 |
| Δ T0-1 vs. Δ T2-4 | 22.6 (13.1-482) | 42.4 (13.6-452) | 0.578 |
| Δ T0-2 vs. Δ T3-4 | 23.6 (13.1-482) | 39.6 (13.6-452) | 0.869 |
| Δ N0 vs. Δ N1-2 | 39.6 (12.7-452) | 21.0 (15.3-482) | 0.608 |
| Downstaging vs. No-downstaging | 33.3 (13.1-482) | 18.8 (12.7-463.2) | 0.229 |
| For patients without CRT Endpoint | Median static R_2^* (s^{-1}) | | p-value |
| | Group 1 | Group 2 | |
| pT0-2 vs. pt2-4 | 24.2 (13.8-459) | 20.6 (13.1-437) | 0.453 |
| pN0 vs. pN1-2 | 22.6 (13.8-459) | 20.8 (14.2-437) | 0.929 |

Table 7: Results from the statistical analysis of the static R_2^* -values of different endpoints. The Results are given as median values and the range given in parenthesis. The full dataset can be found in the appendix 192021

4.1.2 Results for Dynamic R_2^* -peak_{enh}

Calculated from the dynamic images the R_2^* -peak_{enh} values were not statistically significant for any of the different endpoints, although there were some differences between the median values. The group ypN0 vs. ypN1-2 showed a strong trend ($p = 0.065$). All these results can be seen in table 8.

| Endpoint | Median R_2^* -peak _{enh} (s^{-1}) | | p-value |
|---------------------------------|--|------------------------|--------------|
| | Group 1 | Group 2 | |
| TRG0-2 vs. TRG3 | 29.3 (0.0-75.2) | 36.5 (14.9-51.3) | 0.257 |
| ypT0-2 vs. ypT3-4 | 29.6 (0.0-75.2) | 31.8 (24.7-51.3) | 0.987 |
| ypN0 vs. ypN1-2 | 37.1 (0.0-75.2) | 31.6 (14.9-60.9) | 0.065 |
| Δ T0-1 vs. Δ T2-4 | 32.0 (14.9-53.3) | 29.1 (0.0-75.2) | 0.823 |
| Δ T0-2 vs. Δ T3-4 | 32.0 (0.0-53.3) | 29.1 (13.0-75.2) | 1.000 |
| Δ N0 vs. Δ N1-2 | 32.3 (0.0-75.2) | 31.2 (13.0-51.3) | 0.498 |
| Downstaging vs. No-downstaging | 31.8 (0.0-75.2) | 29.1 (14.9-47.9) | 0.695 |
| For patients without CRT | | | |
| Endpoint | Median R_2^* -peak _{enh} (s^{-1}) | | p-value |
| | Group 1 | Group 2 | |
| pT0-2 vs. pt2-4 | 36.9 (0.0-56.0) | 37.8 (0.0-62.7) | 0.921 |
| pN0 vs. pN1-2 | 39.2 (0.0-62.7) | 31.0 (0.0-60.9) | 0.024 |

Table 8: Results from the statistical analysis of the dynamic R_2^* - peak_{enh}-values of different endpoints. The Results are given as median values and the range given in parenthesis. The full dataset can be found in the appendix 192021.

4.1.3 Results for Dynamic R_2^* -AUC

The dynamic R_2^* -AUC values were calculated from the DSC data, for different endpoints and for different ranges of time points. The time points chosen were the same as in [41] so a comparison of the results can be made. The following time points (in seconds) were used: 525 ± 25 , 222 ± 15 , 135 ± 10 , 49 ± 1 .

For the time point 525 ± 25 the statistical analysis found two significant results, TRG0-2 vs TRG3 ($p = 0.008$) and Δ T0-1 vs. Δ T2-4 ($p = 0.014$). This can be seen in table 12. For the time point 222 ± 15 , TRG0-2 vs TRG3 showed a strong trend ($p = 0.074$) and Δ T0-1 vs. Δ T2-4 ($p = 0.029$) was significant. For the time point 135 ± 10 TRG0-2 vs TRG3 was once again significant ($p = 0.047$) and for ypN0 vs. ypN1-2 ($p = 0.075$) as well as Δ T0-1 vs. Δ T2-4 there was a strong trend ($p = 0.083$). The timepoint 49 ± 1 showed a strong trend ($p = 0.055$) for the Δ T0-1 vs. Δ T2-4 group as well as the Δ T0-2 vs. Δ T3-4 ($p = 0.084$).

4.2 Results from the immunohistochemical analysis

4.2.1 CD34 Results

Of the 39 patients with IHC images, 20 received CRT, features were calculated for 33 of them. Of the six patients that features were not calculated for, three of them had no more tumour in the image slices as a result of successfully CRT. Two of the other three had very poor image registration leading to the tumour mask landing largely outside the tumour region. This was a result of the tumour areas being very spread out and very small. The last patient had a very small tumour area which contained no to little staining, therefore after thresholding no features

| Endpoint | Median R_2^* -AUC, 49 ± 1 | | p-value |
|---------------------------------|---------------------------------|---------------|---------|
| | Group 1 | Group 2 | |
| TRG0-2 vs. TRG3 | 214 (0-546) | 248 (83-431) | 0.385 |
| ypT0-2 vs. ypT3-4 | 229 (0-546) | 228 (42-474) | 0.535 |
| ypN0 vs. ypN1-2 | 241 (0-617) | 223 (0-546) | 0.573 |
| Δ T0-1 vs. Δ T2-4 | 268 (34-593) | 132 (0-331) | 0.055 |
| Δ T0-2 vs. Δ T3-4 | 268 (0-593) | 132 (105-323) | 0.084 |
| Δ N0 vs. Δ N1-2 | 226 (0-474) | 281 (34-546) | 0.291 |
| Downstaging vs. No-downstaging | 238 (0-546) | 227 (134-404) | 0.863 |
| For patients without CRT | | | |
| Endpoint | Median R_2^* -AUC, 49 ± 1 | | p-value |
| | Group 1 | Group 2 | |
| pT0-2 vs. pt2-4 | 202 (0-473) | 306 (0-617) | 0.343 |
| pN0 vs. pN1-2 | 261 (0-617) | 206 (0-522) | 0.192 |

Table 9: Results from the statistical analysis of the dynamic $R_2^* - AUC$ -values of different endpoints. The Results are given as median values and the range given in parenthesis. The full dataset can be found in the appendix 192021.

| Endpoint | Median R_2^* -AUC, 135 ± 10 | | p-value |
|---------------------------------|-----------------------------------|-----------------------|--------------|
| | Group 1 | Group 2 | |
| TRG0-2 vs. TRG3 | 528 (0-1270) | 787 (264-1140) | 0,047 |
| ypT0-2 vs. ypT3-4 | 430 (0-1073) | 586 (231-1270) | 0.578 |
| ypN0 vs. ypN1-2 | 678 (0-1337) | 434 (0-1735) | 0,075 |
| Δ T0-1 vs. Δ T2-4 | 678 (256-1292) | 423 (0-918) | 0,083 |
| Δ T0-2 vs. Δ T3-4 | 622 (0-1292) | 430 (84-918) | 0,412 |
| Δ N0 vs. Δ N1-2 | 575 (0-1073) | 734 (320-1270) | 0.378 |
| Downstaging vs. No-downstaging | 598 (0-1073) | 589 (256-1270) | 0.307 |
| For patients without CRT | | | |
| Endpoint | Median R_2^* -AUC, 135 ± 10 | | p-value |
| | Group 1 | Group 2 | |
| pT0-2 vs. pT3-4 | 654 (0-498) | 601 (0-1735) | 0.064 |
| pN0 vs. pN1-2 | 656 (0-1334) | 274 (0-1735) | 0.681 |

Table 10: Results from the statistical analysis of the dynamic $R_2^* - AUC$ -values of different endpoints. The Results are given as median values and the range given in parenthesis. The full dataset can be found in the appendix 192021.

could be extracted.

Results of the image analysis for 33 patients is given in the rest of this section. First are the feature values given in the same grouping as in the MRI results. This is followed by correlation between different IHC features and the correlation between the MRI results and the IHC features.

The correlation plots are shown in figure 16 and the p-values in the table 17. For some features correlation with the MRI results were also calculated and are shown in figure 17. All values were calculated in Matlab.

| Endpoint | Median R_2^* -AUC, 222 ± 15 | | p-value |
|---------------------------------|-----------------------------------|-----------------------|--------------|
| | Group 1 | Group 2 | |
| TRG0-2 vs. TRG3 | 859 (-22-1872) | 1291 (382-2992) | 0.058 |
| ypT0-2 vs. ypT3-4 | 864 (-22-2287) | 1095 (0-2992) | 0.332 |
| ypN0 vs. ypN1-2 | 936 (-22-2304) | 732 (-3383-2222) | 0.466 |
| Δ T0-1 vs. Δ T2-4 | 1099 (0-2992) | 597 (-22-1322) | 0.029 |
| Δ T0-2 vs. Δ T3-4 | 1091 (0-2992) | 864 (-22-1322) | 0.244 |
| Δ N0 vs. Δ N1-2 | 1016 (-22-2992) | 921 (162-1872) | 0.883 |
| Downstaging vs. No-downstaging | 903 (-22-2992) | 1106 (0-1872) | 0.718 |
| For patients without CRT | | | |
| Endpoint | Median R_2^* -AUC, 222 ± 15 | | p-value |
| | Group 1 | Group 2 | |
| pT0-2 vs. pt2-4 | 997 (0-2287) | 827 (0-2222) | 0.810 |
| pN0 vs. pN1-2 | 967 (0-2287) | 649 (0-2222) | 0.114 |

Table 11: Results from the statistical analysis of the dynamic $R_2^* - AUC$ -values of different endpoints. The results are given as median values and the range given in parenthesis. The full dataset can be found in the appendix 192021.

| Endpoint | Median R_2^* -AUC, 525 ± 25 | | p-value |
|---------------------------------|-----------------------------------|------------------------|--------------|
| | Group 1 | Group 2 | |
| TRG0-2 vs. TRG3 | 1590 (-216-3749) | 2901 (867-6015) | 0.008 |
| ypT0-2 vs. ypT3-4 | 1266 (0-2417) | 1844 (-216-6015) | 0.063 |
| ypN0 vs. ypN1-2 | 1616 (-545-6175) | 1825 (-219-6015) | 0.745 |
| Δ T0-1 vs. Δ T2-4 | 1869 (-216-6015) | 730 (0-2320) | 0.014 |
| Δ T0-2 vs. Δ T3-4 | 1820 (-216-6015) | 949 (247-2320) | 0.167 |
| Δ N0 vs. Δ N1-2 | 1869 (-216-6175) | 1633 (520-3750) | 0.977 |
| Downstaging vs. No-downstaging | 1604 (-216-6015) | 2042 (881-4750) | 0.388 |
| For patients without CRT | | | |
| Endpoint | Median R_2^* -AUC, 525 ± 25 | | p-value |
| | Group 1 | Group 2 | |
| pT0-2 vs. pt2-4 | 1708 (-171-6175) | 1527 (-545-3924) | 0.542 |
| pN0 vs. pN1-2 | 1607 (-545-6175) | 1040 (-219-3924) | 0.944 |

Table 12: Results from the statistical analysis of the dynamic $R_2^* - AUC$ -values of different endpoints. The Results are given as median values and the range given in parenthesis. The full dataset can be found in the appendix 192021.

4.2.2 CAIX Results

The results for the CAIX-stain are shown below in table 15 and the full data for all patients are show in the appendix 26, some groups with no data as there were a number of images with no staining.

4.2.3 HIF1- α results

The results for the analysis of the IHC stained HIF1- α images are shown in table 26. For some groups there was no data as there were a number of images with no staining.

| Endpoint | Number of Vessels. | | p-value |
|--------------------------------|-------------------------------------|------------------|---------|
| | Group 1 | Group 2 | |
| TRG0-2 vs. TRG3 | 109 (8-954) | 714 (333-1742) | 0.101 |
| ypT0-2 vs. ypT3-4 | 908 (29-2749) | 919 (8-4048) | 0.927 |
| ypN0 vs. ypN1-2 | 931 (8-2749) | 781 (16-4048) | 0.785 |
| Δ N0 vs. Δ N1-2 | 931 (8-4048) | 897 (83-1742) | 0.775 |
| Downstaging vs. No-downstaging | 781 (8-2749) | 1182 (16-4048) | 0.367 |
| Endpoint | Vessel Size, in μm | | p-value |
| | Group 1 | Group 2 | |
| TRG0-2 vs. TRG3 | 408 (272-772) | 412 (330-516) | 0.734 |
| ypT0-2 vs. ypT3-4 | 512 (330-828) | 454 (330-976) | 0.367 |
| ypN0 vs. ypN1-2 | 528 (330-828) | 446 (298-976) | 0.222 |
| Δ N0 vs. Δ N1-2 | 462 (330-976) | 516 (330-690) | 1.000 |
| Downstaging vs. No-downstaging | 516 (330-828) | 454 (272-976) | 0.428 |
| Endpoint | Vessel Radius, in μm | | p-value |
| | Group 1 | Group 2 | |
| TRG0-2 vs. TRG3 | 15 (12.8-20.8) | 15.8 (14.0-17) | 0.945 |
| ypT0-2 vs. ypT3-4 | 17.2 (13.2-20.8) | 16.4 (12.8-22.0) | 0.672 |
| ypN0 vs. ypN1-2 | 17.6 (13.0-20.8) | 16.4 (12.8-22.0) | 0.251 |
| Δ N0 vs. Δ N1-2 | 16.8 (12.8-22.0) | 16.8 (14.0-19.6) | 0.809 |
| Downstaging vs. No-downstaging | 17 (14.4-20.8) | 16.2 (12.8-22.0) | 0.387 |
| Endpoint | MVD, in $X1/\text{m} \cdot 10^{-5}$ | | p-value |
| | Group 1 | Group 2 | |
| TRG0-2 vs. TRG3 | 3.0 (1.1-14) | 5.0 (1.4-7) | 0.448 |
| ypT0-2 vs. ypT3-4 | 3.9 (1.2-14) | 3.6 (1.1-8) | 0.868 |
| ypN0 vs. ypN1-2 | 4.1 (1.2-8) | 3.9 (1.1-14) | 0.702 |
| Δ N0 vs. Δ N1-2 | 3.9 (1.1-14) | 3.9 (1.4-6) | 0.582 |
| Downstaging vs. No-downstaging | 3.9 (1.2-14) | 3.9 (1.1-8) | 0.782 |

Table 13: Results from the quantitative IHC analysis of the features: vessels, vessel size, vessel radius and MVD from pathological CD34-images. The Results are given as median values and the range (min-max) given in parenthesis. The full dataset can be found in the appendix 24 and 25

4.2.4 Results for the Correlation Between MRI Parameters and IHC Features

The correlation matrix showing the scatter plots and correlation values are shown in figure 17 and the p-values are shown in table 18.

| Endpoint | ICD, in μm | | p-value | |
|--------------------------------|----------------------------------|-----------------|---------|---------|
| | Group 1 | Group 2 | | |
| TRG0-2 vs. TRG3 | 161.4 (70-304) | 94.2 (92-172) | 0.734 | |
| ypT0-2 vs. ypT3-4 | 104.8 (70-192) | 116.0 (78-304) | 0.868 | |
| ypN0 vs. ypN1-2 | 102.4 (70-304) | 105.8 (78-236) | 0.500 | |
| Δ N0 vs. Δ N1-2 | 106.4 (70-304) | 104.8 (90-172) | 0.613 | |
| Downstaging vs. No-downstaging | 52.5 (70-304) | 105.2 (78-236) | 0.839 | |
| Endpoint | Solidity, in $X \cdot 10^{-3}$ | | Dif | p-value |
| | Group 1 | Group 2 | | |
| TRG0-2 vs. TRG3 | 930.8 (889-945) | 923.4 (922-940) | 7.4 | 0.734 |
| ypT0-2 vs. ypT3-4 | 929.5 (889-945) | 923.3 (884-945) | 6.2 | 0.277 |
| ypN0 vs. ypN1-2 | 925.5 (889-945) | 923.6 (884-945) | 1.9 | 0.956 |
| Δ N0 vs. Δ N1-2 | 923.6 (884-945) | 929.5 (906-940) | -5.9 | 0.613 |
| Downstaging vs. No-downstaging | 923.8 (884-945) | 925.3 (897-945) | -1.5 | 0.519 |
| Endpoint | Stained Fraction, in percentages | | p-value | |
| | Group 1 | Group 2 | | |
| TRG0-2 vs. TRG3 | 1.06 (0.4-10.3) | 2.55 (0.5-2.7) | 0.536 | |
| ypT0-2 vs. ypT3-4 | 2.01 (0.5-10.3) | 1.71 (0.4-7.9) | 0.568 | |
| ypN0 vs. ypN1-2 | 2.13 (0.5-10.3) | 1.78 (0.4-7.9) | 0.500 | |
| Δ N0 vs. Δ N1-2 | 1.79 (0.4-10.3) | 2.01 (0.5-4.2) | 0.676 | |
| Downstaging vs. No-downstaging | 2.01 (0.5-10.3) | 1.79 (0.4-7.9) | 0.897 | |

Table 14: Results from the quantitative IHC analysis of the features: ICD, solidity and stained fraction from the CD34-images. The Results are given as median values and the range (min-max) given in parenthesis. The full dataset can be found in the appendix 24 and 24

| CAIX Endpoint | Stained Fraction, in percentages | | p-value |
|--------------------------------|----------------------------------|------------------|---------|
| | Group 1 | Group 2 | |
| TRG0-2 vs. TRG3 | 2.58 (0.01-9.2) | 0.84 (0.01-1.2) | 0.183 |
| ypT0-2 vs. ypT3-4 | 2.58 (0.00-15.1) | 0.84 (0.00-5.7) | 0.500 |
| ypN0 vs. ypN1-2 | 0.31 (0.00-12.6) | 1.08 (0.00-15.1) | 0.554 |
| Δ N0 vs. Δ N1-2 | 0.86 (0.00-15.1) | 0.84 (0.14-9.2) | 0.686 |
| Downstaging vs. No-downstaging | 0.69 (0.00-12.6) | 0.89 (0.00-15.1) | 0.979 |
| CAIX | Stain Size, in μm | | p-value |
| | Group 1 | Group 2 | |
| TRG0-2 vs. TRG3 | 1452 (196-5404) | 1452 (196-1752) | 0.833 |
| ypT0-2 vs. ypT3-4 | 1342 (30-6284) | 1056 (72-3928) | 0.468 |
| ypN0 vs. ypN1-2 | 1200 (30-6284) | 1072 (72-4828) | 0.817 |
| Δ N0 vs. Δ N1-2 | 1056 (30-6248) | 1342 (428-5404) | 0.729 |
| Downstaging vs. No-downstaging | 573 (30-5404) | 536 (74-6284) | 0.854 |

Table 15: Results from the quantitative IHC analysis of the CAIX-images. Stain fraction is the fraction of coloured pixels versus number of pixels in the tumour mask. Median number of pixels for each vessel in the tumour mask. The Results are given as median values and the range (min-max) given in parenthesis. The full dataset can be found in the appendix 26

Kaplan-Meier plots were made to assess differences in long-term survival based on separating the CD34 IHC parameters in groups above and below their median values. This was not done for the CAIX and HIF-1 α parameters as there were so few patients with data in these groups. The results did not reveal any significant differences in survival. The plots can be found in the appendix A.

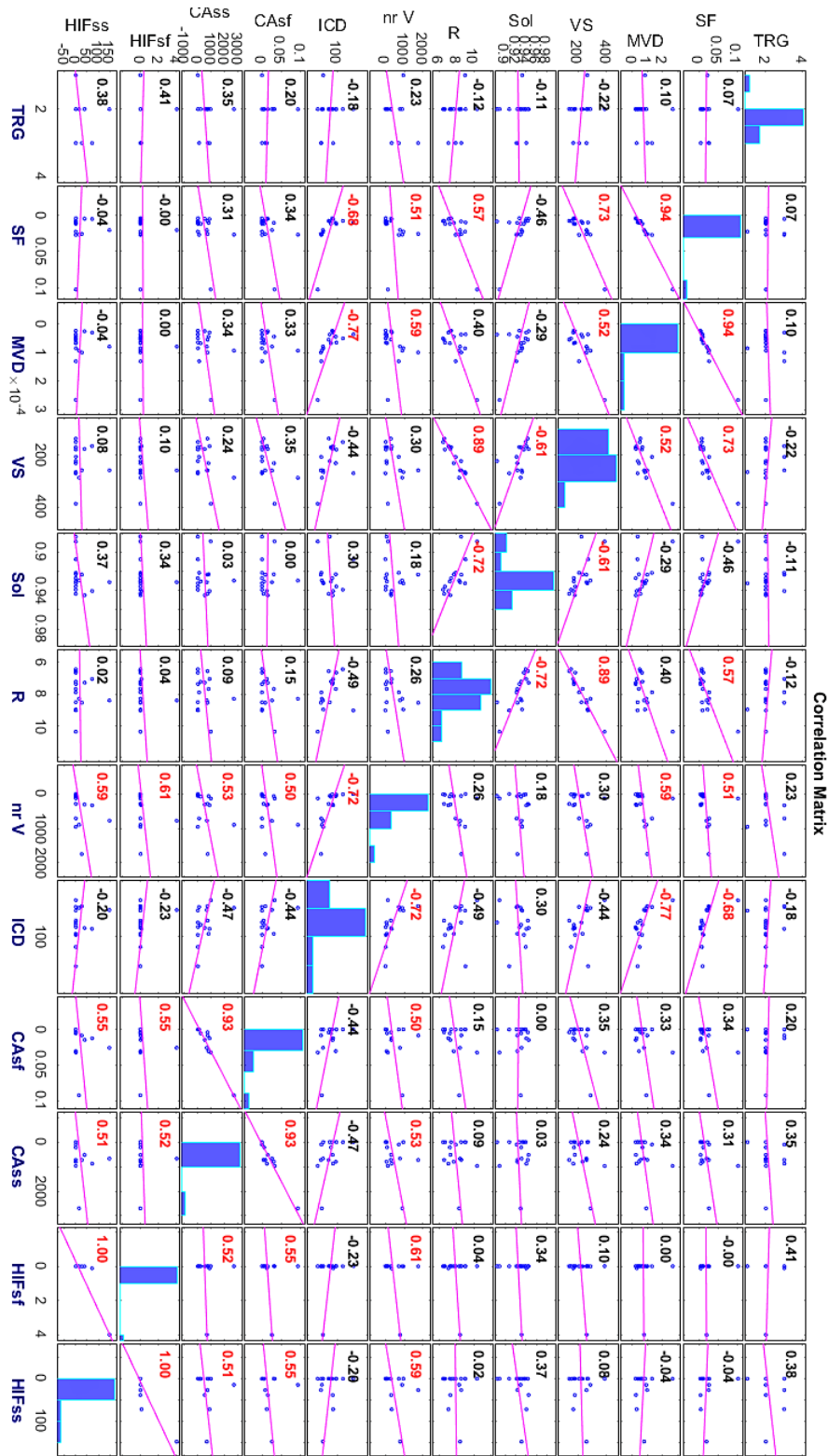


Figure 16: Correlation matrix for IHC features and TRG. Entries above and below the diagonal are identical. The number in each window represents the correlation between the two parameters and the scatter-plot is shown in the same window. Values in red reflects Spearman correlations where the correlation value is > 0.50 or < 0.50 .

5 Discussion

In this chapter the methods results are discussed in separate sections. The first part is on the MRI alone and then the IHC alone, before the associations between MRI and IHC are

| HIF-1 α Endpoint | Stained Fraction, in $X \cdot 10^{-5}$ | | p-value |
|--------------------------------|--|------------------|---------|
| | Group 1 | Group 2 | |
| TRG0-2 vs. TRG3 | 0.60 (0.60-400) | 0.65 (0.61-12.5) | 0.800 |
| ypT0-2 vs. ypT3-4 | 0.69 (0.60-400) | 0.73 (0.47-37.7) | 0.717 |
| ypN0 vs. ypN1-2 | 1.78 (0.60-36.7) | 11.6 (0.47-400) | 0.129 |
| Δ N0 vs. Δ N1-2 | 0.75 (0.47-37.7) | 0.42 (0.60-400) | 0.967 |
| Downstaging vs. No-downstaging | 0.69 (0.60-400) | 0.72 (0.47-37.7) | 0.966 |
| HIF-1 α | Stain Size, in μm | | |
| TRG0-2 vs. TRG3 | 77.0 (30-296) | 98.8 (54-144) | 1.000 |
| ypT0-2 vs. ypT3-4 | 163.2 (30-296) | 173.2 (54-302) | 0.500 |
| ypN0 vs. ypN1-2 | 115.6 (30-274) | 200.8 (78-302) | 0.091 |
| Δ N0 vs. Δ N1-2 | 190.6 (44-302) | 139.8 (30-296) | 0.416 |
| Downstaging vs. No-downstaging | 163.2 (30-296) | 173.2 (44-302) | 0.898 |

Table 16: Results from the quantitative IHC analysis of the HIF-1 α -images. Stain fraction is the fraction of coloured pixels versus number of pixels in the tumour mask. Median number of pixels for each vessel in the tumour mask. The Results are given as median values and the range (min-max) given in parenthesis. The full dataset can be found in the appendix 26

| | TRG | SF | MVD | VS | Sol | R | nr V | ICD | CAsf | CAss | HIFsf | HIFss |
|-------|-------|-------|-------|-------|-------|-------|-------|-------|-------|-------|-------|-------|
| TRG | 1.000 | 0.791 | 0.710 | 0.423 | 0.694 | 0.647 | 0.393 | 0.494 | 0.448 | 0.179 | 0.112 | 0.149 |
| SF | 0.791 | 1.000 | 0.000 | 0.001 | 0.070 | 0.022 | 0.044 | 0.004 | 0.202 | 0.243 | 0.990 | 0.875 |
| MVD | 0.710 | 0.000 | 1.000 | 0.037 | 0.284 | 0.128 | 0.017 | 0.001 | 0.218 | 0.192 | 0.990 | 0.885 |
| VS | 0.423 | 0.001 | 0.037 | 1.000 | 0.013 | 0.000 | 0.254 | 0.092 | 0.185 | 0.364 | 0.722 | 0.772 |
| Sol | 0.694 | 0.070 | 0.284 | 0.013 | 1.000 | 0.002 | 0.499 | 0.259 | 0.987 | 0.925 | 0.203 | 0.156 |
| R | 0.647 | 0.022 | 0.128 | 0.000 | 0.002 | 1.000 | 0.322 | 0.052 | 0.569 | 0.730 | 0.875 | 0.948 |
| nr V | 0.393 | 0.044 | 0.017 | 0.254 | 0.499 | 0.322 | 1.000 | 0.002 | 0.048 | 0.034 | 0.012 | 0.016 |
| ICD | 0.494 | 0.004 | 0.001 | 0.092 | 0.259 | 0.052 | 0.002 | 1.000 | 0.086 | 0.066 | 0.386 | 0.457 |
| CAsf | 0.448 | 0.202 | 0.218 | 0.185 | 0.987 | 0.569 | 0.048 | 0.086 | 1.000 | 0.000 | 0.028 | 0.026 |
| CAss | 0.179 | 0.243 | 0.192 | 0.364 | 0.925 | 0.730 | 0.034 | 0.066 | 0.000 | 1.000 | 0.040 | 0.045 |
| HIFsf | 0.112 | 0.990 | 0.990 | 0.722 | 0.203 | 0.875 | 0.012 | 0.386 | 0.028 | 0.040 | 1.000 | 0.000 |
| HIFss | 0.149 | 0.875 | 0.885 | 0.772 | 0.156 | 0.948 | 0.016 | 0.457 | 0.026 | 0.045 | 0.000 | 1.000 |

Table 17: P-value for the pathological data. The p-value for the correlation of each feature with all other features as well as TRG. Each side of the diagonal, represented by the ones, are identical. Values in bold are significant values, as long as they do not represent the same thing (like CAIX and HIF-1 α).

discussed. The last part is topics for further work.

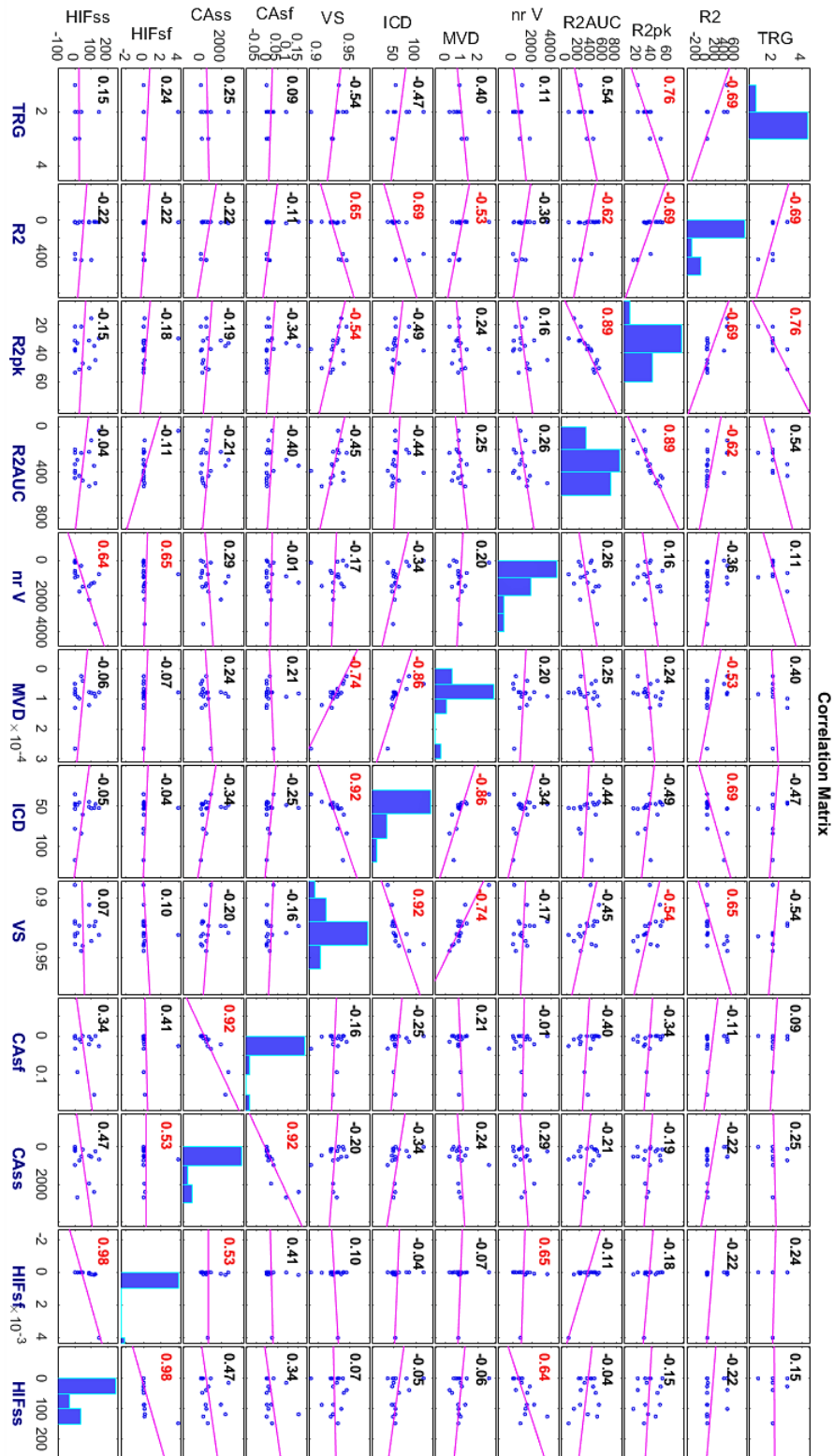
5.1 Discussion of MRI

5.1.1 Discussion of Materials

The MRI images from the T2-weighted sequence had good resolution, contrast and no artefacts.

The images for the DSC data are hard to interpret visually as they are not purely anatomical, but are used for the quantitative analysis and estimation of dynamic parameters.

Figure 17: Correlation matrix for MR and IHC data. Entries above and below the diagonal are identical. R2 is the parameter R_2^* , R2pk is R_2^* -peak_{enh} and R2AUC is R_2^* -AUC for the time point 525second. The number in each window represents the correlation between the two parameters and the scatter-plot is shown in the same window. Values in red reflects Spearman correlations where the correlation value is > 0.50 or < -0.50 .



The images from the static R_2^* sequence had a relatively high rate of artefacts. This can be attributed to movements of the bowel. Although measures were taken to reduce bowel move-

| | TRG | R2 | R2-peak | R2-AUC | Nr V | MVD | ICD | VS | CAsf | CAss | HIFsf | HIFss |
|---------|--------------|--------------|--------------|--------|--------------|-------|-------|-------|-------|-------|-------|-------|
| TRG | 1.000 | 0.040 | 0.024 | 0.135 | 0.778 | 0.302 | 0.206 | 0.135 | 0.841 | 0.532 | 0.603 | 0.778 |
| R2 | 0.040 | 1.000 | 0.004 | 0.012 | 0.176 | 0.037 | 0.004 | 0.008 | 0.676 | 0.415 | 0.415 | 0.402 |
| R2-peak | 0.024 | 0.004 | 1.000 | 0.000 | 0.564 | 0.379 | 0.054 | 0.034 | 0.202 | 0.474 | 0.495 | 0.584 |
| R2-AUC | 0.135 | 0.012 | 0.000 | 1.000 | 0.321 | 0.355 | 0.091 | 0.082 | 0.121 | 0.424 | 0.672 | 0.885 |
| Nr V | 0.778 | 0.176 | 0.564 | 0.321 | 1.000 | 0.463 | 0.200 | 0.527 | 0.965 | 0.268 | 0.006 | 0.007 |
| MVD | 0.302 | 0.037 | 0.379 | 0.355 | 0.463 | 1.000 | 0.000 | 0.001 | 0.441 | 0.365 | 0.807 | 0.824 |
| ICD | 0.206 | 0.004 | 0.054 | 0.091 | 0.200 | 0.000 | 1.000 | 0.000 | 0.356 | 0.200 | 0.890 | 0.855 |
| VS | 0.135 | 0.008 | 0.034 | 0.082 | 0.527 | 0.001 | 0.000 | 1.000 | 0.564 | 0.451 | 0.718 | 0.785 |
| CAsf | 0.841 | 0.676 | 0.202 | 0.121 | 0.965 | 0.441 | 0.356 | 0.564 | 1.000 | 0.000 | 0.117 | 0.191 |
| CAss | 0.532 | 0.415 | 0.474 | 0.424 | 0.268 | 0.365 | 0.200 | 0.451 | 0.000 | 1.000 | 0.035 | 0.066 |
| HIFsf | 0.603 | 0.415 | 0.495 | 0.672 | 0.006 | 0.807 | 0.890 | 0.718 | 0.117 | 0.035 | 1.000 | 0.000 |
| HIFss | 0.778 | 0.402 | 0.584 | 0.885 | 0.007 | 0.824 | 0.855 | 0.785 | 0.191 | 0.066 | 0.000 | 1.000 |

Table 18: P-value matrix for MR and Histological data. The p-value for the correlation of each feature with all other features as well as TRG. Each side of the diagonal, represented by the ones, are identical. R2 is the parameter R_2^* , R2pk is R_2^* -peak_{enh} and R2AUC is R_2^* -AUC for the time point 525second. Values in bold are significant values, as long as they do not represent the same thing (like CAIX and HIF-1 α).

ments, they are difficult to remove entirely. MRI acquisition of the rectum is difficult because the presence of air cavities often induces susceptibility effects, this gives signal loss because of increased R_2^* . These artefacts are difficult to remove entirely and therefore CA is often avoided for MRI of the rectum. In this project glucagon and Buscopan injection was able to remove a high amount of the bowel movements. Some cases were not used due to these problems in total 13 patients were excluded from the static results.

5.1.2 Discussion of Methods

In DSC-MRI the first pass of the contrast agent is what is usually imaged. In cancer, especially rectal cancer, the vessel walls are especially permeable leading to contrast agent leaking out. This means that the signal measured will be different from that of normal DSC-MRI and must be corrected. Since kinetic parameters were not calculated the correction was not necessary. In this project R_2^* was found using a multi-echo sequence and calculated from 9, which should remove most R_1 effects from R_2^* values. Since the relaxation of the CA is weaker when it is not in contact with blood, R_2^* will scale down with the amount of CA leakage. As a consequence R_2^* may be lower in more aggressive tumours as they generally have more leaky vessels.

The time of arrival of CA into the tumour volume is important in the calculation of R_2^* -peak_{enh} as the value depends on the baseline of R_2^* before the CA injection. The number of baseline images varied between patients because the timing of CA injection was done manually and timed by simple counting. Counting is very subjective and can vary a lot for each instance. An automated system would have been preferable to achieve the same timing for all patients. As a consequence of this variation the number of baseline images had to be found, in this project it was done manually by looking at the curve of the signal and finding the point where the curve starts to rise towards the peak. This was not trivial to find as it varies to some extent from pixel to pixel and the exact start of the rise is not always straight forward to determine.

Most patients did not have image acquisition at the same time points for the R_2^* -AUC, because of this the time interval for the R_2^* -AUC had slight variations. The interval for R_2^* -AUC could not stop in-between images, it had to end on an acquired image. This gives rise to small

differences in the R_2^* -AUC values. This could have been corrected by performing a regression between the two last data points to have all patients end at the same time or using a conventional sequence. The images were acquired before this thesis started, so this would not have been possible. The regression was not done for two reasons, the time frame did not allow it and the error is likely to not have a large impact on results.

For some patients a rise in the R_2^* -AUC curve could be seen towards the end of the longer time intervals. This is probably caused by the accumulation of CA in the bladder which increases R_2^* of nearby tissue [16]. Patients with a very large rise ($Rise \approx Peak$) in the R_2^* -AUC at late times were excluded from the results. This exclusion was only based on a visual inspection of the curve and not any specific cut-off value. This might provide some uncertainty into the results. For shorter time intervals this effect should be greatly diminished.

Some patients also had very unnatural curves before the initial rise to the peak. These include values deviating from the apparent baseline by rising before the observed peak or dipping far below the baseline. This might be due to the contrast agent reaching some pixels much earlier than others or artefacts in the image. Patients with large deviations were also excluded.

In total 14 patients were excluded from the dynamic results.

5.1.3 Additional Methodological Factors

The patients included in this project were also included in another project, therefore patients had many sequences taken and stayed in the MRI scanner for a long time. MRI acquisition for rectal cancer is a long process (≈ 45 minutes) and the additional sequences added $\approx 15 - 20$ minutes to the acquisition. It is therefore quite likely that patients had some movement and created motion artefacts.

The delineation of the tumour mask is also exposed to human errors and intra-observer variability [31]. As well when the tumour mask is adapted to the image some small error is introduced because of the different resolution of the images.

The number of patients with MRI data that were also treated with CRT is low so some endpoints have few patients, in addition some patients were not included in either the static or dynamic results, giving a lower number for each modality than the number of patients with CRT. As a consequence of the low number of patients the Mann-Whitney U test was used for the statistical analysis. The exact treatment of the CRT varies between patients and it is uncertain what effect this had on the result.

5.1.4 Discussion of Results

The static R_2^* had no significant results for the different endpoints, the endpoint group that had the lowest p-value was TRG0-2 vs. TRG3 ($p = 0.135$). This might be connected to the large semi-overlapping range of values for the different groups and to some extent the amount of artefacts and movement errors. There were some differences in the median values between some endpoints. Especially for the change in T stage ($\Delta T0-1$ vs. $\Delta T2-4$, and $\Delta T0-2$ vs. $\Delta T3-4$), but high p-value ($p = 0.578$ and $p = 0.869$). In general we see higher R_2^* -values for patients in the groups with favourable responses. It was assumed that patients with more aggressive tumours and most likely more hypoxia and therefore poorer treatment response should show higher R_2^*

values. It is not possible to give any conclusive result on this theory from these results, the p-value for the TRG groups looks promising but is not significant. Studies with larger patient groups should be performed.

Other studies have found results that were more promising. For instance Sun and colleagues investigated the role of static R_2^* in differentiating malignant from benign lesions in the liver [40]. In the study it was found that malignant lesions had R_2^* values that were higher than benign lesions with a p-value of < 0.001 . In another study by Li and colleagues, R_2^* was investigated in cervical cancer [21] patients who received CRT. After treatment the follow-up examinations were done and it was found that patients with poor response had significantly higher R_2^* than patients with better response and had a p-value of 0.02. In both studies the explanation for the differences in response was the presence of hypoxia.

The R_2^* value is not only affected by oxygen in the blood, the amount of haemoglobin in the blood as well as the amount of red blood cells are factors and both vary individually. In the rectum the it is of high importance to consider the interface between air and tissue. They can increase the R_2^* value in an interface region and should not be included. The artefacts in some images can have affected this and lead to some air-cavities being included in the tumour mask. The most sever cases were removed, but some milder cases of artefacts were included to not further lower the amount of patients in the study, however this probably introduced more variance in the values.

It might be that the expected correlation with tumour hypoxia is not manifested as the CA is not able to reach chronically hypoxic cells, since the supply of blood to these cells is, by virtue of being chronically hypoxic, very low.

The dynamic R_2^* -peak_{enh} had one significant result. This result was found in the patients without CRT in the group pN0 vs. pN1-2 ($p = 0.024$). The endpoint ypN0 vs. ypN1-2 had a p-value of 0.065 represents a strong trend. It showed a difference in median values that suggests a lower values for patients without malignant lymph nodes. This has been seen in other studies where a significant association was found between both K_{trans} and R_2^* -peak_{enh} in the primary tumour and histological nodal status of the surgical specimen [11]. It was suggested that both R_2^* -peak_{enh} and nodal status were connected to tumour aggressiveness that was caused by hypoxia, and that a low R_2^* -peak_{enh} may be an indicator of poor blood flow. A similar result was found in this study between R_2^* -peak_{enh} and the pN stage. This supports the case that R_2^* -peak_{enh} may be associated with poorer blood flow and as a consequence a more aggressive phenotype. In general the patients with better outcomes have slightly lower values.

R_2^* -peak_{enh} is affected by many factors. Blood flow should affect the rate at which CA is transported through the tumour and thereby affect the maximum R_2^* . More blood flow would give faster enhancement of R_2^* and therefore a higher peak value. In contrast hypoxic areas should have higher R_2^* because of de-oxygenated haemoglobin, but it might be that CA agent does not reach these areas because of the poor blood flow or diffusion that is associated with hypoxia. It is likely that in reality the truth lies somewhere in the middle and they both contribute.

The dynamic R_2^* -AUC did have some significant results, but only for the longer time intervals, this might mean that there is some accumulation or temporal aspect to these results. For the 525 ± 25 s both TRG0-2 vs. TRG3 and $\Delta T0-1$ vs. $\Delta T2-4$ were found to be significant with p-values of 0.008 and 0.014. It can be seen that in both groupings the patients with poorer response had higher values, indicating higher values for more aggressive tumours, except for

the TRG group where the patients with a better response had a lower value. Grøvik and colleagues also looked at R_2^* -AUC and found that patients with nodal metastasis as well as patients with T3-4 tumours had lower values for the R_2^* -AUC, these results were not significant though ($p = 0.07 - 0.20$). This might further indicate that this result has to be seen in contrast to the time interval used, which again might be associated with the CA having more time to leak into the tissue. In addition the TN stage of a tumour is not necessarily connected with tumour aggressiveness, whereas the tumour response to treatment is usually considered to be fairly well correlated with aggressiveness.

In DSC-MRI one usually looks at the first-pass of CA, therefore looking at R_2^* -AUC for the whole acquisition time is an uncommon approach. As a consequence there had not been found any literature on how to analyse these findings. R_2^* -AUC generally reflects the amount of CA transitioning the vasculature and is proportional to the blood volume as long as the first-pass is the only part being considered and one assumes no leakage [38]. The high vascular permeability of rectal cancer changes this and the general principles cannot be followed. A possible explanation of the differences in first-pass results is that all the CA does not leave the tumour volume after the first-pass of aggressive tumours. It is this effect that can be observed with the full time interval approach.

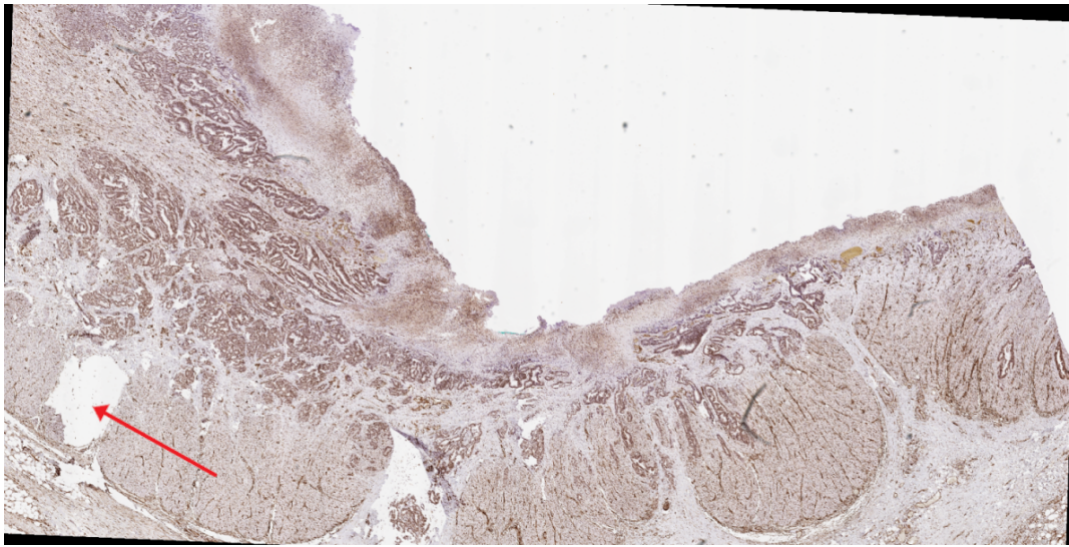
There are several reasons why the CA might linger longer in more aggressive tumours. The first being that aggressive tumours have more leaky vessels leading to more CA leaking into the tissue, the enhancement of the signal when CA leaks into tissue is small, but with increasing concentrations the effect should increase. Second the abnormal and torturous vasculature of more aggressive tumours could be less effective at clearing the CA from the tissue. Third the irregular blood flow of aggressive tumours could cause CA that leaks into tissue to remain much longer than in less aggressive cases. Fourth the vasculature could have dead-ends and sections where blood pools up without being drained and causing blood lakes. It is also not known how VM plays into the specific dynamics of CA transportation.

5.2 Discussion of Quantitative Immunohistochemistry

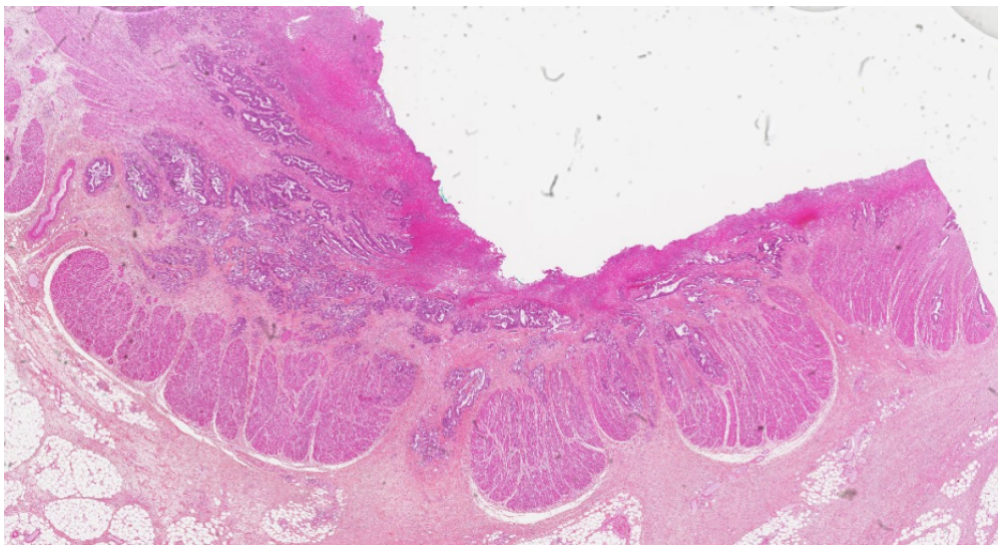
5.2.1 Discussion of Materials

The staining for the H&E, CD34, CAIX all had good staining with sufficient contrast. The HIF-1 α stain had poor staining, why this was the case is unsure, but it might have been a result of issues in the thinning process of the staining procedure or the time from operation to being paraffin embedded. Other reasons could be that primary antibodies generally lose affinity for the target antigen over time, either due to protein degradation or denaturation caused by long-term storage, microbial contamination, changes in pH or harsh treatments. The CAIX did not have this issue which shows that the issue was not a lack of hypoxia within the sections.

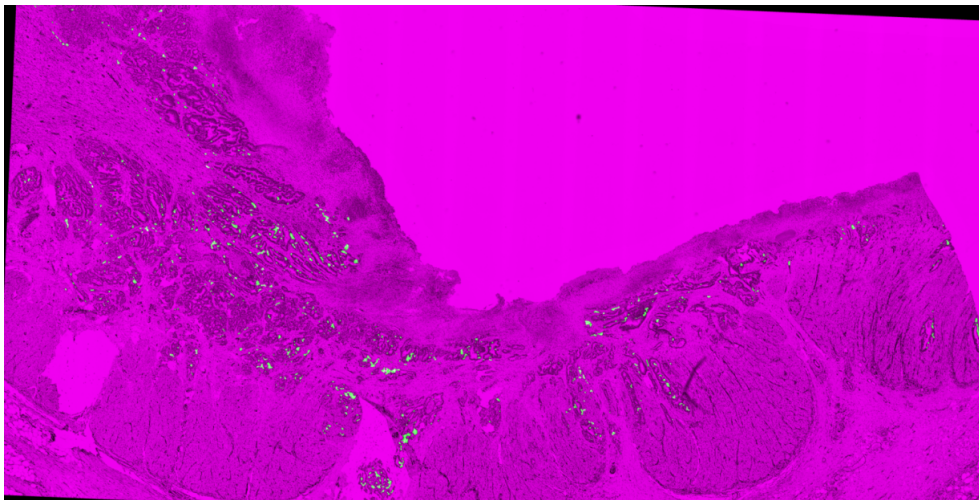
Some slides had tearing, this could have happened when the slides were mounted on the microscope or when the slice was mounted on the slide. The latter is the most probable. Since the slices are very thin it takes very little for them to tear. This was a minor issue and generally the tears were small. There were however three cases with large tears, in these cases the results were checked to see that no data was gathered in these regions. Only one of the three tears had enough staining to be visible after thresholding. An example of tearing is shown in figure 18a. In this case the tearing is outside the data-area as seen in figure 18c, therefore there are no consequences.



(a) Example of tearing form a CAIX image



(b) The H&E image in the same area as the tear on the CAIX image



(c) Image showing the included pixels (green) in the teared image

The images used in the pathological results were digitized at $\times 20$ and $\times 40$ magnification. The first downsampled layer (1:4) of the $\times 20$ images were used to run the analysis, this yielded good results and all features were sufficiently resolved. The $\times 40$ images and the full resolution $\times 20$ images were not used as the first downsampled layer of the $\times 20$ images provided enough

detail to find the outline of vessels, in addition higher resolutions would require substantially more computing power or time for computation. However for the feature 'Solidity' it might have been beneficial to use higher resolution to accurately determine the vessel branches.

5.2.2 Discussion of Methods

Many steps in the processing was evaluated by visual inspection, this naturally has a inherent flaws. There is however no clear and easy alternative in assessing image quality in the different steps that do not also require a lot more time investment, complexity and restriction of flexibility. With this in mind most parts of the processing seem to have generated good results.

Image registration was vital to the processing of the images since only one mask was drawn for each case, on the H&E stain. The registration had to correctly align tumour areas in the other stains with the original mask. Failure to do so would either introduce undesired data from outside the tumour region or lose tissue data from areas not covered. The image registration was largely successful, the most troublesome cases were the ones that had many small tumour areas. For these cases tiled image-registration could have helped, but with the current program this was not possible. The other option for the bad cases would have been to draw masks for all stains.

An alternative to image registration would have been to draw masks for all stains. This would have been a time consuming endeavour and was not guaranteed to give better results, because it is not always possible to identify the correct tumour regions on the non-H&E stains.

The standard procedure for determining vessel parameters in IHC stained tumours use manual determination of which cells are stained sufficiently and correspond to vessels. The general method uses a "hot spot" approach were a few regions with high vessel density are studied. A certain number of regions are selected and the number cells or vessels marked with a given marker are counted. In this project a more straight forward and "honest" approach was used, were the whole tumour area was analysed. In addition this project employs an automated approach to vessel identification by using color thresholds, thus removing the subjective perspective from this process.

The thresholding was not highly investigated. It was based on visual inspection and no inspection of the false negative rates or false positive rates with respect to the threshold values were performed. Threshold values were selected with the idea in mind that false positives were considered worse than false negatives. As a consequence some weaker stains were most likely lost. However false positives could give wrong results whereas false negatives would only give no conclusive results.

The post-processing kept the smallest stains out of the feature extraction. Minuscule stains in the features could cloud the data and might give some false positives. To counteract the weak staining in the HIF1- α a weaker erosion was used for these slides. No further inspection was performed into the effects of the threshold process.

5.2.3 Discussion of Histology Results

The data for each feature will be discussed, followed by an overall look at how the data can be interpreted and finally how they relate to the MRI data.

Number of vessels. The only feature that showed some tendency toward significance for any endpoint was the number of vessels for TRG0-2 vs TRG3 where the p-value was $p = 0.101$. The values show that for patients with better response had tumours with fewer vessels. This seems to be contradicted by the fact that it is the other way around in the TRG0-1 vs. TRG2-3 group, but there was only one patient in the TRG0-1 group so this data should not be considered. This is a result of many of the patients in the TRG0-1 group having no cancer left in the image slice and therefore were not included. The TRG2-3 group however had more patients (15) and had a higher value than the TRG0-2 group, but a lot lower than the TRG3 group which had three patients. The endpoint ypN0 vs ypN1-2 had quite a difference in the values for the two groups, but very high p-value ($p = 0.785$), this could be due to overlapping groups. Downstaging vs no-downstaging also had some difference in the median values but a p-value of 0.367.

In VM the vessel-like channels do not contain endothelial cells, therefore they would not be stained by CD34 and would not show up on the results. The amount of VM in the sections is therefore unknown and the impact they have on the tumour environment is unclear, it might be that areas of low vessel density rely more on VM to supply blood.

Median average vessel size is closely related to average vessel radius. Looking at the values from these two features, the values for the groups align to some extent. Meaning that when the values for one group are higher than the other for one feature this is also true of the other feature. This makes sense as both features measure the magnitude of a vessel. The p-values also match up to some extent. For both features the ypN0 vs. ypN1-2 endpoint gave the best p-value around 0.23.

MVD also gave a lower value for patients with better response to the treatment (TRG0-2) compared to patients with poor response (TRG3), but showed no statistical significance ($p = 0.448$). It would be very beneficial to compare with the TRG0-1 vs TRG2-3 group data. We can not use TRG0-1 as discussed earlier, but we can use the TRG2-3 value. This group gives a higher median value than the TRG3 group, showing that there might be some connection between number of vessels in an area and its response to treatment. This is what has been found in many other studies. MVD has been linked with treatment response and metastasis [45], but the varying methods used to evaluate MVD has complicated comparisons and a lack satisfactory methods in a clinical environment has limited its use [Myiata] [6]. MVD was a significant although weak prognostic factor in women with breast cancer. Standardization of MVD assessment is needed. This project used a method not widely used in other studies. The method uses the entire tumour volume, within the central slice instead of using specific hot spots. The method in this project provides a larger perspective of the tumour and considers all parts of the tumour, instead of only investigating the most dense vessel areas. It also avoids subjective biases and should be easily reproducible.

Although different results has been found for some types of cancer, colorectal cancer seems to show good correlation between MVD and prognosis. 2014 meta-analysis by Wang and colleges found that patients with colorectal cancer showed an increase in MVD-levels and this correlated with tumour aggressiveness, poor differentiation and higher frequencies of vascular-lymphatic invasion, lymph node invasion, and distant metastases [45]. Another study stated that angiogenesis, as assessed by MVD, in colorectal cancer is an important prognostic factor for tumour growth at the primary site [48]. A study from 2017 indicated that MVD, regional lymph node metastasis and tumour size were independent risk factors for distant metastases in colorectal cancer [42].

None of the other groups for MVD showed any statistical significance. In addition the ΔN_0 vs. ΔN_{1-2} as well as the downstaging vs no-downstaging had only a very small difference in median values.

ICD had very small differences between most endpoints except the TRG grouping where there was a lower value for TRG0-1 than for TRG2-3, but also a lower value for TRG3 than for TRG0-2. We might see a trend toward lower values for poorer treatment outcomes, but a low patient number in the TRG0-1 group most likely prohibits this trend becoming significant. This would make intuitive sense as we saw a tendency for higher vessel numbers in higher regression grades, which should decrease vessel distance. Once again there are no significant results.

Solidity. From the solidity data there seems to be a decline in solidity for increasing tumour grade, meaning that for tumours with poorer response the vessels are more branched and irregular in shape. This is seen in the difference between TRG0-1 and TRG2-3 as well as in the difference between TRG0-2 and TRG3. This is in line with the general tendency for tumour vasculature to be poorly regulated and forming tortuous networks. The downstaging vs. no-downstaging group did not show this tendency. Whether the post-processing affected this value is uncertain.

The stained fraction is a combination of vessel number and vessel size, and the stained fraction increases from TRG0-2 to TRG3 as expected, but in the TRG0-1 vs. TRG2-3 case we once again see exceptions presumably due to the low patient number. In ypT0-2 vs. ypT3-4 we see higher values for the ypT0-2 group than for the ypT3-4 group. In ypN0 vs. ypN1-2 we also see higher values for ypN0 than for ypN1-2. For the difference in downstaging we see that patients with downstaging had higher fractions.

Correlation data: The first thing to note is that stained fraction correlates quite strongly with vessel size and MVD. This makes sense as the larger the vessels the more staining would be observed and if they were tightly packed we would also likely have a higher stain fraction. In the same way MVD and ICD are highly inversely correlated with each other. Continuing with this idea vessel size and vessel radius are very strongly correlated as well for obvious reasons. Stained fraction correlates, although not as much as vessel size and MVD, with number of vessels, vessel radius and ICD. The p-value for all these features is below 0.05. Number of vessels, vessel radius and ICD will be discussed in their own sections.

The correlation p-value for the TRG was > 0.110 for all variables. The two HIF1- α variables and CAIX stain size were the closest to being significant ($CA_{s,s} = 0.179$, $HIF_{s,f} = 0.112$, $HIF_{s,s} = 0.149$) all other variables had p-values > 0.20 .

ICD had p-values for both CAIX features of $p = 0.086$ and 0.066 . The correlation coefficients were $\rho = -0.44$ and $\rho = -0.47$ showing a decrease in CAIX staining fraction and stain size for increasing ICD.

Number of vessels is correlated with seven parameters. The most strongly correlated parameter is ICD with an inverse relationship. Increasing the number of vessels decreases their spacing, but the number of vessels is also correlated with stained fraction and MVD so the area of the tumour does not seem to increase at the same rate as the number of vessels. If that was the case, the stained fraction would remain the same for increasing vessel number, however this might be because the sections only represent a two-dimensional image of the three-dimensional tumour. Number of vessels was the only feature to have a correlation with CAIX and HIF1- α

features and had a p-value > 0.05 for all pairs. As the grouping data showed, the number of vessels seemed to have a connection with treatment-response and hypoxia is known to limit treatment effectiveness. It is therefore interesting to see that the number of vessels has some correlation with the hypoxia markers in this project. The correlation is moderate with values between $0.50 - 0.61$.

5.2.4 Discussion of Correlation between MRI and Quantitative Immunohistochemistry

The correlation matrix for the MRI and IHC data can be seen in figure 17. The corresponding p-values can be seen in figure 18.

Looking at the correlation matrix one can see that MVD is quite strongly correlated with R_2^* with an inverse relationship. A lower correlation with R_2^* -peak_{enh} and R_2^* -AUC is seen and not with the inverse relationship. P-values are 0.037, 0.379 and 0.355 for R_2^* , R_2^* -peak_{enh} and R_2^* -AUC respectively. Meaning that R_2^* is the only one that is considered significant

Looking at the MRI parameters of the static R_2^* , dynamic R_2^* -peak_{enh} and dynamic R_2^* -AUC we see that they have very low p-values for both ICD and vessel size ($p = 0.004 - 0.091$). For R_2^* -peak_{enh} and R_2^* -AUC the correlation values with ICD and vessel size are in the range -0.45 to -0.54 . For R_2^* the correlation values are 0.65 and 0.69. This shows that there is a difference in how the tumour vasculature is represented by R_2^* -peak_{enh} and R_2^* -AUC compared to R_2^* . The correlation of R_2^* -peak_{enh} and R_2^* -AUC with ICD distance might be because when the distance between the vessels increase there is more tissue that is unaffected by the contrast agent. The correlation with vessel size might be explained by the increased blood flow, so that the CA washes out of the volume faster. The difference in the sign of the correlation of R_2^* -peak_{enh} and R_2^* -AUC versus R_2^* is hard to explain and more research might be needed to fully explain it.

Interestingly R_2^* is strongly correlated with ICD and as seen earlier ICD had a low correlation but also a very low p-value for CAIX. We also see that the p-value for R_2^* and CAIX features are 0,676 0,415 and a low correlation -0.11 and -0.22 .

The feature with the lowest p-value for the MRI parameter R_2^* -AUC other than ICD and vessel size was CA stain fraction with a value of 0.121. The correlation value is -0.44 . This is also the MRI parameter with the lowest p-value for both CAIX features and HIF1- α features. Thereafter the second lowest p-value for CAIX features and HIF1- α features when compared to the MRI parameters is 0.202 for R_2^* -peak_{enh} and CAIX stain fraction. For these there is a correlation value of -0.34 . All other p-values for MRI parameters with CAIX or HIF1- α are > 0.400 .

If we look at the overall correlation of MRI parameters with CAIX and HIF1- α features, we have in general a low correlation. Except for the CAIX stain fraction correlation with R_2^* -peak_{enh} and R_2^* -AUC, all correlation values for CAIX and HIF1- α features are in the range from -0.04 to -0.22 . This generally low correlation value probably reflects the multiple interactions and variables that affect of both tumour hypoxia and MRI parameter values. In addition the low amount of patients in this analysis ($n = 20$) makes it difficult to make any clear conclusions about the relationship between these parameters.

It should be noted that the MRI data is based on a large volume, while the IHC parameters are only based on a single slice of the tumour.

5.3 Suggestions for Further Work

- The process of segmentation in the IHC images could be investigated to see how the choice of erosion and dilation thresholds affects the rate of false-positives and false-negatives.
- A study into different features should be done as there is a large array of features to look at.
- A study with a larger number of patients.
- Studying a larger portion of the tumour were more than a single slice is made for each stain would be very interesting. in that way close to the entire tumour volume could be analysed.
- The mask creation has a large affect on what features can and should be extracted as well as having a role in feature results, how these masks are drawn and the margins applied was not investigated in this project. It would be enlightening to see how it affects the outcome of the study.

6 Conclusion

This thesis used MRI as well as histological and IHC images from a total of 113 patients to quantitatively investigate the vascular function of malignant tumours.

The parameter R_2^* was calculated from static T_2^* -weighted images and from dynamic R_2^* time curves derived from DSC data, R_2^* -peak_{enh} and R_2^* -AUC were calculated. Correlation between the MRI parameters and various endpoints representing tumour response to CRT was investigated. Four significant results were found for the parameter R_2^* -AUC. Two significant results were found for the longest time points one for the second longest and one for the second shortest, while the shortest had one group verging on significance.

Using an automated computer program a wide array of features were calculated from IHC images stained with CD34, CAIX and HIF-1 α . These features were correlated with various endpoints representing tumour response to CRT and further correlated to the previously found MRI parameters.

The IHC data gave many features which differed between long-term endpoints, but no significant results were found. Further, drawing any clear conclusions from these data are difficult as there are not enough patients in most groups to consider the values as well distributed. The correlation results for IHC and MRI data had a couple of significant results. Vessel size was significant for correlation with static R_2^* and dynamic R_2^* -peak_{enh}. R_2^* was also significantly correlated with MVD and ICD. There seemed to be indicators in the results that the IHC features studied were relevant for the purpose of studying tumour vascularization and their connections to MRI. Additionally, features that have been purposed in the literature to be of prognostic value did have strong trends in this study, but were not found to be significant. As such, the connection between the number of vessels, MVD and hypoxia, as indirectly assessed by MRI, is interesting and overlaps to some extent with what is theorised as the reason for poor treatment response.

The main weakness of the thesis is the small number of patients in total and especially patients with CRT, MRI and IHC. In spite of these problems this thesis gives a good example of how the analysis of vascular function in IHC images can be automatised and streamlined. A standardization of the methods in vascular IHC analysis is much needed to make comparisons of results across studies possible.

In conclusion the analysis provided good reasons for being optimistic about the possible use of these parameters. Based on these results of this thesis, it is recommended that a larger study is performed as this is the only way the real usefulness of the parameters can be identified and expanded upon.

References

- [1] Maniotis AJ et al. “Vascular channel formation by human melanoma cells in vivo and in vitro. vasculogenic mimicry.” In: *The american journal of pathology* (1999).
- [2] *AJCC, Cancer Staging, Manual*. 2009.
- [3] Warren BA et al. “The microcirculation in two transplantable melanomas of the hamster. II. Scanning electron microscopy.” In: *Cancer letters* (1978).
- [4] EM. Caspani et al. “Glioblastoma. a pathogenic crosstalk between tumor cells and pericytes.” In: *PLoS One* (2014).
- [5] Wykoff CC et al. “Hypoxia-inducible expression of tumor-associated carbonic anhydrases.” In: *Cancer research* (2000).
- [6] SH. Cheng et al. “Prognostic role of microvessel density in patients with renal cell carcinoma. a meta-analysis”. In: *International Journal of Clinical and Experimental Pathology* (2014).
- [7] Massimo Cristofanilli, Chusilp Charansangavej, and Gabriel N. Hortobagyi. “Angiogenesis modulation in cancer research. novel clinical approaches”. In: *Nature Reviews, Drug Discovery* (2002).
- [8] Brizel DM et al. “Tumor oxygenation predicts for the likelihood of distant metastases in human soft tissue sarcoma.” In: *Cancer research* (1996).
- [9] Tom Donnem et al. “Non-angiogenic tumours and their influence on cancer biology”. In: *NATURE REVIEWS. CANCER* (2018).
- [10] A. Dudley. “Tumor Endothelial Cells”. In: *Cold Spring Harbor Perspectives in Medicine* (2012).
- [11] Grovik E et al. “Dynamic multi-echo DCE- and DSC-MRI in rectal cancer. Low primary tumor Ktrans and delta R2star peak are significantly associated with lymph node metastasis.” In: *Journal of Magnetic Resonance Imaging* (2017).
- [12] Kyrre E. Emblem et al. “Vessel calibre—a potential MRI biomarker of tumour response in clinical trials”. In: *Nature Reviews Clinical Oncology* (2014).
- [13] Bray F et al. “Global cancer statistics 2018. GLOBOCAN estimates of incidence and mortality worldwide for 36 cancers in 185 countries”. In: *CA: A Cancer Journal for Clinicians* (2018).
- [14] Yuan G et al. “Ca²⁺-calmodulin kinase-dependent activation of hypoxia inducible factor 1 transcriptional activity in cells subjected to intermittent hypoxia.” In: *The journal of biological chemistry* (2005).
- [15] L. Gerlowski and R. Jain. “Microvascular Permeability of Normal and Neoplastic Tissues”. In: *Microvascular research* (1986).
- [16] E. Grovik et al. “Dynamic multi-echo DCE- and DSC-MRI in rectal cancer. Low primary tumor Ktrans and R2star peak are significantly associated with lymph node metastasis”. In: *Journal of Magnetic Resonance Imaging* (2017).
- [17] Michael R. Horsman et al. “Imaging hypoxia to improve radiotherapy outcome.” In: *Nature Reviews, Clinical Oncology* (2012).
- [18] Holash J et al. “Vessel cooption, regression, and growth in tumors mediated by angiopoietins and VEGF.” English. In: *Science* 284 (June 1999), pp. 1994–8.
- [19] Kreftregisteret. *CANCER STATISTICS*. Tech. rep. Cancer Registry of Norway, 2018.

- [20] Chen-Ting Lee, Mary-Keara Boss, and Mark W. Dewhirst. “Imaging Tumor Hypoxia to Advance Radiation Oncology”. In: *Antioxidants and Redox Signaling* (2014).
- [21] X. S. Li et al. “Value of R2star obtained from T2star-weighted imaging in predicting the prognosis of advanced cervical squamous carcinoma treated with concurrent chemoradiotherapy”. In: *Journal of Magnetic Resonance Imaging* (2015).
- [22] Hockel M et al. “Intratumoral pO2 predicts survival in advanced cancer of the uterine cervix.” In: *Radiotherapy and oncology. journal of the European Society of therapeutic radiology and oncology* (1993).
- [23] Konerding MA et al. “Evidence for characteristic vascular patterns in solid tumours. quantitative studies using corrosion casts.” English. In: *British journal of cancer* 80 (May 1999), pp. 724–32.
- [24] Lars Tore Gyland Mikalsen. “Quantification of Angiogenesis in Breast Cancer by Automated Vessel Identification in CD34 Immunohistochemical Sections”. In: *Anticancer Research* (2011).
- [25] Lars Tore Gyland Mikalsen. “The Clinical Impact of Mean Vessel Size and Solidity in Breast Carcinoma Patients”. In: *PLOS One* (2013).
- [26] V. Montana and H. Sontheimer. “Bradykinin promotes the chemotactic invasion of primary brain tumors.” In: *The journal of neuroscience* (2011).
- [27] Pusztaszeri MP, Seelentag W, and Bosman FT. “Immunohistochemical expression of endothelial markers CD31, CD34, von Willebrand factor, and Fli-1 in normal human tissues.” In: *The journal of histochemistry and cytochemistry* (2006).
- [28] Dewhirst MW. “Relationships between cycling hypoxia, HIF-1, angiogenesis and oxidative stress.” In: *Radiation research* (2009).
- [29] Dewhirst MW, Cao Y, and Moeller B. “Relationships between cycling hypoxia, HIF-1, angiogenesis and oxidative stress.” In: *Nature reviews. Cancer.* (2008).
- [30] Dewhirst MW et al. “Microvascular studies on the origins of perfusion-limited hypoxia.” In: *British journal of cancer* (1996).
- [31] Jackson PC et al. “The reduction of inter- and intra-observer variability for defining regions of interest in nuclear medicine.” In: *European Journal of Nuclear Medicine* (1985).
- [32] Olive PL, Vikse C, and Trotter MJ. “Measurement of oxygen diffusion distance in tumor cubes using a fluorescent hypoxia probe.” In: *International journal of radiation oncology, biology and physics* (1992).
- [33] Sakariassen PØ et al. “Angiogenesis-independent tumor growth mediated by stem-like cancer cells.” In: *Proceedings of the National Academy of Sciences of the United States of America* (2006).
- [34] L. Qiao et al. “Advanced research on vasculogenic mimicry in cancer.” In: *Journal of cellular and molecular medicine* (2015).
- [35] Kathrine Roe Redalen. *Functional MRI of Hypoxia-mediated Rectal Cancer Aggressiveness (OxyTarget)*. 2013. URL: <https://clinicaltrials.gov/ct2/show/NCT01816607>.
- [36] Riccardo Ridolf. “Study of the track reconstruction in the FOOT experiment for Hadrontherapy”. MA thesis. University of Bologna, 2017.
- [37] Micheal H. Ross and Wojciech Pawlina. *Histology: A Text and Atlas*. 6th ed. Lippincott Williams and Wilkins, 2011.
- [38] M. Shiroishi et al. “Principles of T2star-Weighted Dynamic Susceptibility Contrast MRI Technique in Brain Tumor Imaging”. In: *Journal of Magnetic Resonance Imaging* (2015).

- [39] J. J. Smith and J. Garcia-Aguilar. “Advances and challenges in treatment of locally advanced rectal cancer”. In: *Journal of Clinical Oncology* (2015).
- [40] M. Sun et al. “Utility of R2star obtained from T2star-weighted imaging in differentiating hepatocellular carcinomas from cavernous hemangiomas of the liver”. In: *PLoS ONE* (2014).
- [41] Ingrid Frammaas Syversen. “Prediction of chemoradiotherapy response in rectal cancer using static and dynamic R2star MRI measurements”. Project paper. NTNU, 2017.
- [42] Cho T et al. “The role of microvessel density, lymph node metastasis, and tumor size as prognostic factors of distant metastasis in colorectal cancer.” In: *Oncology Letters* (2014).
- [43] Mary M. Vaughan et al. “Double Immunohistochemical Staining Method for HIF-1A and its Regulators PHD2 and PHD3 in Formalin Fixed Paraffin Embedded Tissues”. In: *Applied Immunohistochemistry and Molecular Morphology*. (2016).
- [44] Joseph C. Walsh et al. “The Clinical Importance of Assessing Tumor Hypoxia. Relationship of Tumor Hypoxia to Prognosis and Therapeutic Opportunities”. In: *Antioxidants and Redox Signaling* (2014).
- [45] Yibaina Wang et al. “Can Vascular Endothelial Growth Factor and Microvessel Density Be Used as Prognostic Biomarkers for Colorectal Cancer. A Systematic Review and Meta-Analysis”. In: *Thee Scientific World Journal* (2014).
- [46] G. F. Weber et al. “Multi-modal treatment strategies for locally advanced rectal cancer”. In: *Expert Review of Anticancer Therapy* (2012).
- [47] J. Wiig, KE Giercksky, and K. Tveit. “Intraoperative radiotherapy for locally advanced or locally recurrent rectal cancer. Does it work at all.” In: *Acta Oncologica* (2014).
- [48] Kimura Y et al. “Clinicopathological significance of vascular endothelial growth factor, thymidine phosphorylase and microvessel density in colorectal cancer.” In: *Molecular Medicine Reports* (2016).
- [49] G. Yancopoulos et al. “Vascular-specific growth factors and blood vessel formation”. In: *Nature* (2000).
- [50] Peng YJ et al. “Heterozygous HIF-1alpha deficiency impairs carotid body-mediated systemic responses and reactive oxygen species generation in mice exposed to intermittent hypoxia.” In: *The journal of physiology* (2006).
- [51] M. Yoshimura et al. “Microenvironment and Radiation Therapy”. In: *BioMed Research International* (2013).

A Appendix

Figure 19: Kaplan-Meier plot for stained fraction of CD34

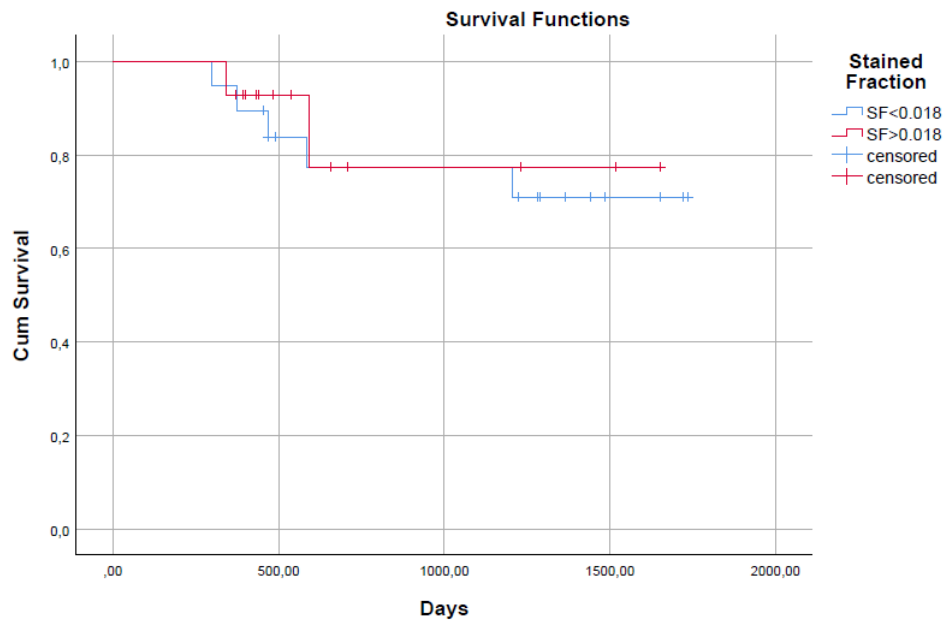
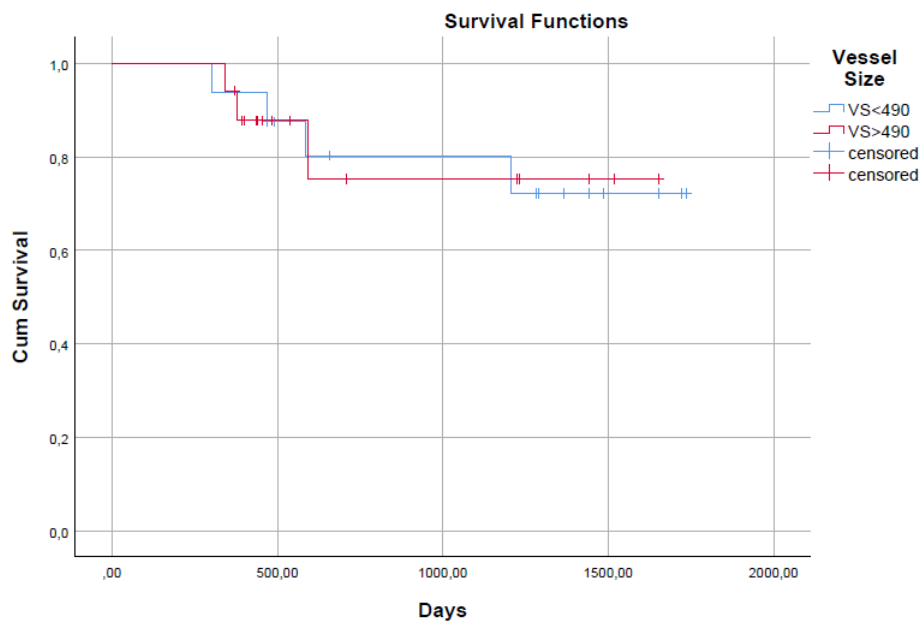


Figure 20: Kaplan-Meier plot for the vessel size



B Matlab Code

B.1 Code for MRI Analysis

```

%This program uploads dicomfiles and sorts them. This is for images in
the
%T2 folder (anatomical images), and the images are sorted by slice
%position.

clear all
filePath = 'C:\Users\Vidar\Downloads\Master\Patients\';

%patientNR = [1 2 3 4 5 6 7 8 9 10 11 12 13 14 15 16 17 18
19 20 21 22 23 24 25 26 27 28 29 30 31 32 33 34 35 36 37 38 39 40 41
42 43 44 45 46 47 48 49
patientList = [24 25 27 29 30 31 32 34 39 40 41 43 44 45 46 47 48 49
50 51 52 54 55 56 57 58 60 64 65 67 68 69 72 73 74 75 76 77 78 79 80
83 85 87 88 89 90 92 94 ...
...50 51 52 53 54 55 56 57 58 59 60 61 62 63
64 65 66 67 68 69 70 71 72 73 74 75 76 77 78 79 80
81 82 83 84
95 96 102 103 106 107 108 110 111 112 113 114 115 116
118 119 120 121 123 125 126 127 128 131 133 134 138 142 143 144 146
147 148 149 150 ...
... 85 86 87 88 89 90 91 92 93 94 95 96 97 98
99 100 101 102 103]
151 152 153 154 155 156 157 158 159 160 161 162 163 164
165 166 169 170 171];

n = length(patientList);

%Loop that goes over all patients that are going to be analysed
for patient = 1:n

    clear imInfo

    patientNr = patientList(patient); %Draw out the number of the
patient

    %Make a list over all the image files and count how many there are
imList = dir([filePath2 'Oxytarget_' int2str(patientNr) ' PRE/T2/
*#*']);
nImT2 = length(imList);

    %Acquire z value from the info file
zValueT2 = ones(nImT2,1);

    %Create a matrix with room for all the images (resolution 512x512)
if (patientNr==68) || (patientNr==126)
    imT2 = zeros(528,528,nImT2);
elseif(patientNr==75)
    imT2 = zeros(560,560,nImT2);
else
    imT2 = zeros(512,512,nImT2);
end

```

```

    %This loop goes over all the images in the folder and reads them
in
    for imageNr = 1:nImT2

        %Reads all the images into a matrix, plus the associated info
file
        info = dicominfo([filePath2 'Oxytarget_' int2str(patientNr) '
PRE/T2/' imList(imageNr).name]);
        imT2(:, :, imageNr) = dicomread([filePath2 'Oxytarget_'
int2str(patientNr) ' PRE/T2/' imList(imageNr).name]);

        %Puts slice position into a long vector
        zValueT2(imageNr) = info.ImagePositionPatient(3);

    end %All images are read

    %%Sorts the slices into order
    [zValueT2, indzSort] = sort(zValueT2);
    imT2 = imT2(:, :, indzSort);

    nSlicesT2 = nImT2;

    %Saving variables to a .mat-file in the patient's T2 folder
    save([filePath 'Oxytarget_' int2str(patientNr) '
PRE/3Dmatrix.mat'], 'imT2', 'zValueT2', 'nSlicesT2', 'nImT2')
end

```

Published with MATLAB® R2016b

```

%This program uploads dicomfiles and sorts them. This is for images in
the
%FFE folder (static sequence), and the images are sorted by slice
position
%and echo time.

clear all
filePath = 'C:\Users\Vidar\Downloads\Master\Patients\';

%patientNR = [1 2 3 4 5 6 7 8 9 10 11 12 13 14 15 16 17 18
19 20 21 22 23 24 25 26 27 28 29 30 31 32 33 34 35 36 37 38 39 40 41
42 43 44 45 46 47 48 49
patientList = [24 25 27 29 30 32 31 34 39 40 41 43 44 45 46 47 48 49
50 51 52 54 55 56 57 58 60 64 65 67 68 69 72 73 74 75 76 77 78 79 80
83 85 87 88 89 90 92 94 ...
...50 51 52 53 54 55 56 57 58 59 60 61 62 63
64 65 66 67 68 69 70 71 72 73 74 75 76 77 78 79 80
81 82 83 84
95 96 102 103 106 107 108 110 111 112 113 114 115 116
118 119 120 121 123 125 126 127 128 131 133 134 138 142 143 144 146
147 148 149 150 ...
... 85 86 87 88 89 90 91 92 93 94 95 96 97 98
99 100 101 102 103]
151 152 153 154 155 156 157 158 159 160 161 162 163 164
165 166 169 170 171];

n = length(patientList);

%Loop that goes over all patients that are going to be analysed
for patient = 1:n

    clear imInfo

    patientNr = patientList(patient); %Draw out the number of the
patient

    %Make a list over all the image files and count how many there are
    if(patientNr==97) || (patientNr==102) ||(patientNr==128)
    || (patientNr==130) || (patientNr==131) || (patientNr==132) ||
(patientNr==133) || (patientNr==134) || (patientNr==142)
        imList = dir([filePath2 'Oxytarget_' int2str(patientNr) ' PRE/
FFE/*Im*']);
    else
        imList = dir([filePath2 'Oxytarget_' int2str(patientNr) ' PRE/
FFE/*Image*']);
    end
    nIm = length(imList);

    %Acquire echo time value and z value from the info file
    echoTimeValue = zeros(nIm,1);
    zValue = ones(nIm,1);

```

```

%Create a matrix with room for all the images (resolution 256x256)
im = zeros(256,256,nIm);

%This loop goes over all the images in the folder and reads them
in
for imageNr = 1:nIm

    %Reads all the images into a matrix, plus the associated info
file
    info = dicominfo([filePath2 'Oxytarget_' int2str(patientNr) '
PRE/FFE/' imList(imageNr).name]);
    im(:,:,imageNr) = dicomread([filePath2 'Oxytarget_'
int2str(patientNr) ' PRE/FFE/' imList(imageNr).name]);

    %Puts echo time value and slice position into a long vector
    echoTimeValue(imageNr) = info.EchoTime;
    zValue(imageNr) = info.ImagePositionPatient(3);

end %All images are read

%Sorts the slices into order
[zValue, indzSort] = sort(zValue);
im = im(:,:,indzSort);
echoTimeValue = echoTimeValue(indzSort);

%Sorts the echo time values into order
[echoTimeValue, indEtSort] = sort(echoTimeValue);
im = im(:,:,indEtSort);

nEt = length(unique(echoTimeValue)); %Counts number of echo time
values
nSlices = nIm/nEt; %Number of slices is (number of images)/(number
of echo time values)

%Here the matrix is reshaped into 4D where the first two
dimensions are
%x and y directions, dimension three is z direction and dimension
four
%is the echo time values.
im = reshape(im, [256, 256, nSlices, nEt]);
echoTimeValue = reshape(echoTimeValue, [nSlices, nEt]);
zValue = reshape(zValue, [nEt, nSlices]);

%Saving variables to a .mat-file in the patient's FFE folder
save([filePath 'Oxytarget_' int2str(patientNr) ' PRE/
FFE/4Dmatrix.mat'],'im','echoTimeValue','zValue','nEt','nSlices','nIm')
end

```

Published with MATLAB® R2016b

```

%This program uploads dicomfiles and sorts them. This is for images in
the
%R2Star folder (dynamic sequence), and the images are sorted by slice
position
%and acquisition time.

clear all
filePath = 'C:\Users\Vidar\Downloads\Master\Patients\';

%patientNR = [1 2 3 4 5 6 7 8 9 10 11 12 13 14 15 16 17 18
19 20 21 22 23 24 25 26 27 28 29 30 31 32 33 34 35 36 37 38 39 40 41
42 43 44 45 46 47 48 49
patientList = [24 25 27 29 30 32 31 34 39 40 41 43 44 45 46 47 48 49
50 51 52 54 55 56 57 58 60 64 65 67 68 69 72 73 74 75 76 77 78 79 80
83 85 87 88 89 90 92 94 ...
...50 51 52 53 54 55 56 57 58 59 60 61 62 63
64 65 66 67 68 69 70 71 72 73 74 75 76 77 78 79 80
81 82 83 84
95 96 102 103 106 107 108 110 111 112 113 114 115 116
118 119 120 121 123 125 126 127 128 131 133 134 138 142 143 144 146
147 148 149 150 ...
... 85 86 87 88 89 90 91 92 93 94 95 96 97 98
99 100 101 102 103]
151 152 153 154 155 156 157 158 159 160 161 162 163 164
165 166 169 170 171];

n = length(patientList);

%Loop that goes over all patients that are going to be analysed
for patient = 1:n
    clear imInfo

    patientNr = patientList(patient); %Draw out the number of the
patient

    %Make a list over all the image files and count how many there are
imList = dir([filePath2 'Oxytarget_' int2str(patientNr) ' PRE/
R2Star/*#*']);

    nIm = length(imList);

    %Acquire echo time value and z value from the info file
acqTimeValue = zeros(nIm,1);
zValue = ones(nIm,1);

    %Create a matrix with room for all the images (resolution 256x256)
im = zeros(256,256,nIm);

    %This loop goes over all the images in the folder and reads them
in
for imageNr = 1:nIm

```

```

        %Reads all the images into a matrix, plus the associated info
file
        info = dicominfo([filePath2 'Oxytarget_' int2str(patientNr) '
PRE/R2Star/' imList(imageNr).name], 'UseDictionaryVR', true);
        im(:,:,imageNr) = dicomread([filePath2 'Oxytarget_'
int2str(patientNr) ' PRE/R2Star/' imList(imageNr).name]);

        %Puts echo time value and slice position into a long vector
acqTimeValue(imageNr) = str2double(info.AcquisitionTime);
zValue(imageNr) = info.ImagePositionPatient(3);

        %Image needs to be multiplied with a scaling factor to get the
%correct R2* value
scalingFactor = info.Private_0077_1001;
im(:,:,imageNr) = scalingFactor.*im(:,:,imageNr);

end %All images are read

%Sorts the slices into order
[zValue, indzSort] = sort(zValue);
im = im(:,:,indzSort);
acqTimeValue = acqTimeValue(indzSort);

%Sorts the echo time values into order
[acqTimeValue, indAtSort] = sort(acqTimeValue);
im = im(:,:,indAtSort);

nAt = length(unique(acqTimeValue)); %Counts number of echo time
values
nSlices = nIm/nAt; %Number of slices is (number of images)/(number
of echo time values)

%Here the matrix is reshaped into 4D where the first two
dimensions are
%x and y directions, dimension three is z direction and dimension
four
%is the echo time values.
im = reshape(im, [256, 256, nSlices, nAt]);
acqTimeValue = reshape(acqTimeValue, [nSlices, nAt]);
zValue = reshape(zValue, [nAt, nSlices]);

%Saving variables to a .mat-file in the patient's R2Star folder
save([filePath2 'Oxytarget_' int2str(patientNr) '
PRE/4Dmatrix.mat'], 'im', 'acqTimeValue', 'zValue', 'nAt', 'nSlices', 'nIm')
end

```

Published with MATLAB® R2016b

```

%This program imports and adapts the ROIs to fit the FFE images.

clear all
filePath = 'C:\Users\Vidar\Downloads\Master\Patients\';
addpath('C:\Users\Vidar\Downloads\Master\Matlab prosjektoppgave
\ekstra');
addpath('C:\Users\Vidar\Downloads\Master\Matlab prosjektoppgave\ekstra
\imshow3D')

%patientNR = [1 2 3 4 5 6 7 8 9 10 11 12 13 14 15 16 17 18
19 20 21 22 23 24 25 26 27 28 29 30 31 32 33 34 35 36 37 38 39 40 41
42 43 44 45 46 47 48
patientList = [24 25 27 29 30 32 31 34 39 40 41 43 44 45 46 47 48 49
50 51 52 54 55 56 57 58 60 64 65 67 68 69 72 73 74 75 76 77 78 79 80
83 85 87 88 89 90 92 ...
...49 50 51 52 53 54 55 56 57 58 59 60 61 62 63
64 65 66 67 68 69 70 71 72 73 74 75 76 77 78 79 80
81 82 83
94 95 96 102 103 106 107 108 110 111 112 113 114 115
116 118 119 120 121 123 125 126 127 128 131 133 134 138 142 143 144
146 147 148 149 ...
... 84 85 86 87 88 89 90 91 92 93 94 95 96 97
98 99 100 101 102 103]
150 151 152 153 154 155 156 157 158 159 160 161 162 163
164 165 166 169 170 171];

n = length(patientList);

%Loop that goes over all patients that are going to be analysed
for patient = 1:n

    patientNr = patientList(patient);

    %Loading the sorted FFE and T2 images
    load([filePath 'Oxytarget_' int2str(patientNr) ' PRE/
FFE/4Dmatrix.mat']);
    load([filePath 'Oxytarget_' int2str(patientNr) ' PRE/
T2/3Dmatrix.mat']);

    %Loading the ROI from the NIfTI file
    if patientNr == 28 || patientNr==118 || patientNr == 75 ||
patientNr == 102 || patientNr==156 || patientNr == 172
        nii = load_untouch_nii([filePath 'Oxytarget_'
int2str(patientNr) ' PRE/binary/shh/tumour.nii']);
    else
        nii = load_untouch_nii([filePath 'Oxytarget_'
int2str(patientNr) ' PRE/binary/an/tumour.nii']);
    end

    %Getting the right dimensions and scaling
    unscaledROI = nii.img;
    unscaledROI = permute(unscaledROI, [2 1 3]);

```

```

unscaledROI = unscaledROI./(nii.hdr.dime.glmax);

[xPixels,yPixels,zSlices] = size(unscaledROI);

if (patientNr == 32) || (patientNr == 74) || (patientNr == 79)
|| (patientNr == 96) || (patientNr == 40) || (patientNr == 46) ||
(patientNr == 65) ...
    || (patientNr == 69) || (patientNr == 77) || (patientNr ==
85) || (patientNr == 103) || (patientNr == 106) || (patientNr == 113)
|| (patientNr == 134) ...
    || (patientNr == 133) || (patientNr == 141) || (patientNr
== 151) || (patientNr == 152) || (patientNr == 155) || (patientNr ==
160) ...
    || (patientNr == 163) || (patientNr == 169) %for these
patients, the ROI slices are in the opposite order!
    copy = unscaledROI;
    index = 1;
    for s = zSlices:(-1):1
        unscaledROI(:,:,index) = copy(:,:,s);
        index = index + 1;
    end
end

staticROI = zeros(256,256,nSlices);

%Adapting the ROI to fit the FFE image
for z = 1:nSlices
    slice = 1;
    min = 10;
    if zSlices > size(zValueT2,1)
        zSlices=size(zValueT2,1);
    end
    for i = 1:zSlices
        if abs(zValue(1,z) - zValueT2(i,1)) < min
            min = abs(zValue(1,z) - zValueT2(i,1));
            slice = i;
        end
    end
    if min < 4 %if the T2 and FFE sequences have very different z
range
        if (patientNr == 28) %if the image has different
dimensions
            for x = 1:64
                for y = 1:64
                    if ( unscaledROI(2*x,2*y,slice) == 1) ||
(unscaledROI(2*x-1,2*y,slice) == 1) || (unscaledROI(2*x,2*y-1,slice)
== 1) || (unscaledROI(2*x-1,2*y-1,slice) == 1) )
                        staticROI(x,y,z) = 1;
                    end
                end
            end
        else
            for x = 1:256
                for y = 1:256

```

```

                                if ( (unscaledROI(2*x,2*y,slice) == 1) ||
(unscaledROI(2*x-1,2*y,slice) == 1) || (unscaledROI(2*x,2*y-1,slice)
== 1) || (unscaledROI(2*x-1,2*y-1,slice) == 1) )
                                    staticROI(x,y,z) = 1;
                                end
                            end
                        end
                    end
                end
            end

%Plotting to check that the ROIs look alright

%     figure;
%     imshow3D(im(:,:, :,2)+250.*staticROI)
%     figure;
%     imshow3D(imT2+250.*double(unscaledROI))
%     figure;
%     imshow3D(staticROI)

%Saving variables to a .mat-file in the patient's folder
save([filePath 'Oxytarget_' int2str(patientNr) ' PRE/
staticROI.mat'], 'staticROI', 'xPixels', 'yPixels', 'zSlices')

end

```

Published with MATLAB® R2016b

```

%This program imports and adapts the ROIs to fit the DSC data.
clear all
filePath = 'C:\Users\Vidar\Downloads\Master\Patients\';
addpath('C:\Users\Vidar\Downloads\Master\Matlab prosjektoppgave\ekstra');
addpath('C:\Users\Vidar\Downloads\Master\Matlab prosjektoppgave\ekstra\imshow3d');

%patientNR = [1 2 3 4 5 6 7 8 9 10 11 12 13 14 15 16 17 18
19 20 21 22 23 24 25 26 27 28 29 30 31 32 33 34 35 36 37 38 39 40 41
42 43 44 45 46 47 48 49
patientList = [24 25 27 29 30 32 31 34 39 40 41 43 44 45 46 47 48 49
50 51 52 54 55 56 57 58 60 64 65 67 68 69 72 73 74 75 76 77 78 79 80
83 85 87 88 89 90 92 94 ...
...50 51 52 53 54 55 56 57 58 59 60 61 62 63
64 65 66 67 68 69 70 71 72 73 74 75 76 77 78 79 80
81 82 83 84
95 96 102 103 106 107 108 110 111 112 113 114 115 116
118 119 120 121 123 125 126 127 128 131 133 134 138 142 143 144 146
147 148 149 150 ...
... 85 86 87 88 89 90 91 92 93 94 95 96 97 98
99 100 101 102 103]
151 152 153 154 155 156 157 158 159 160 161 162 163 164
165 166 169 170 171];

n = length(patientList);

%Loop that goes over all patients that are going to be analysed
for patient = 1:n
    patientNr = patientList(patient);

    %Loading the sorted DSC and T2 images
    load([filePath 'Oxytarget_' int2str(patientNr) ' PRE/
R2Star/4Dmatrix.mat']);
    load([filePath 'Oxytarget_' int2str(patientNr) ' PRE/
T2/3Dmatrix.mat']);

    %Loading the ROI from the NIfTI file
    if patientNr==28 || patientNr==156 || (patientNr == 102)
        nii = load_untouch_nii([filePath 'Oxytarget_'
int2str(patientNr) ' PRE/binary/shh/tumour.nii']);
    else
        nii = load_untouch_nii([filePath 'Oxytarget_'
int2str(patientNr) ' PRE/binary/an/tumour.nii']);
    end

    %Getting the right dimensions and scaling
    unscaledROI = nii.img;
    unscaledROI = permute(unscaledROI, [2 1 3]);
    unscaledROI = unscaledROI./1000;

    [xPixels,yPixels,zSlices] = size(unscaledROI);

```

```

        if (patientNr == 32) || (patientNr == 74) || (patientNr == 79)
        || (patientNr == 96) || (patientNr == 40) || (patientNr == 46) ||
(patientNr == 65) || (patientNr == 69) ...
        || (patientNr == 77) || (patientNr == 85) || (patientNr == 103)
        || (patientNr == 106) || (patientNr == 113) || (patientNr == 132) ||
(patientNr == 133) || (patientNr == 134) ...
        || (patientNr == 151) || (patientNr == 152) || (patientNr == 155)
        || (patientNr == 160) || (patientNr == 163) %for these patients, the
ROI slices are in the opposite order!
        copy = unscaledROI;
        index = 1;
        for snitt = zSlices:(-1):1
            unscaledROI(:,:,index) = copy(:,:,snitt);
            index = index + 1;
        end
    end

dynamicROI = zeros(256,256,nSlices);

%Adapting the ROI to fit the DSC data
for z = 1:nSlices
    slice = 1;
    min = 10;
    for i = 1:zSlices
        if abs(zValue(1,z) - zValueT2(i,1)) < min
            min = abs(zValue(1,z) - zValueT2(i,1));
            slice = i;
        end
    end
    if min < 4 %if the T2 and FFE sequences have very different z
range
        for x = 1:256
            for y = 1:256
                if ( (unscaledROI(2*x,2*y,slice) == 1) ||
(unscaledROI(2*x-1,2*y,slice) == 1) || (unscaledROI(2*x,2*y-1,slice)
== 1) || (unscaledROI(2*x-1,2*y-1,slice) == 1) )
                    dynamicROI(x,y,z) = 1;
                end
            end
        end
    end
end

%Plotting to check that the ROIs look alright
%figure, imshow3D(im(:,:, :,1)+200.*dynamicROI)
%figure, imshow3D(imT2+250.*double(unscaledROI))
%figure, imshow3D(dynamicROI*1000)

%Saving variables to a .mat-file in the patient's folder
save([filePath 'Oxytarget_' int2str(patientNr) ' PRE/
dynamicROI.mat'],'dynamicROI','xPixels','yPixels','zSlices')

end

```

Published with MATLAB® R2016b

```

%staticR2Star Vidar
%This program calculates the static R2* for the images in the FFE
  folder
%(based on the 4D image matrices made in sortStatic).

clear all
filePath = 'C:\Users\Vidar\Downloads\Master\Patients\';
addpath('C:\Users\Vidar\Downloads\Master\Matlab prosjektoppgave\ekstra
\imshow3d');

%patientNR = [1 2 3 4 5 6 7 8 9 10 11 12 13 14 15 16 17 18
19 20 21 22 23 24 25 26 27 28 29 30 31 32 33 34 35 36 37 38 39 40 41
42 43 44 45 46 47 48
patientList = [24 25 27 29 30 32 31 34 39 40 41 43 44 45 46 47 48 49
50 51 52 54 55 56 57 58 60 64 65 67 68 69 72 73 74 75 76 77 78 79 80
83 85 87 88 89 90 92 ...
...49 50 51 52 53 54 55 56 57 58 59 60 61 62 63
64 65 66 67 68 69 70 71 72 73 74 75 76 77 78 79 80
81 82 83
94 95 96 102 103 106 107 108 110 111 112 113 114 115
116 118 119 120 121 123 125 126 127 128 131 133 134 138 142 143 144
146 147 148 149 ...
... 84 85 86 87 88 89 90 91 92 93 94 95 96 97
98 99 100 101 102 103]
150 151 152 153 154 155 156 157 158 159 160 161 162 163
164 165 166 169 170 171];

n = length(patientList);

%Loop that goes over all patients that are going to be analysed
for patient = 1:n

    patientNr = patientList(patient); %Draw out the number of the
    patient

    %Load the 4D image matrix and other variables, and the ROI
    load([filePath 'Oxytarget_' int2str(patientNr) ' PRE/
FFE/4Dmatrix.mat']);
    load([filePath 'Oxytarget_' int2str(patientNr) ' PRE/
staticROI.mat']);

    staticR2StarMap = zeros(256,256,nSlices);

    staticR2StarValues = zeros(1,1);

    index = 1;
    negativeValuesStatic = 0;

    lnIm = log(im);

    for sliceNumber = 1:nSlices

```

```

        t = 1E-3.*(echoTimeValue(sliceNumber,:))'; %scale from
milliseconds to seconds

        imMatrix = permute(squeeze(im(:,:,sliceNumber,:)),[3 1
2]); %to get convenient matrix dimensions for exponential fit

        for x = 1:256
            for y = 1:256
                if staticROI(x,y,sliceNumber) == 1 %only looking at
pixels inside ROI
                    f = fit(t,imMatrix(:,x,y),'expl'); %exponential
fit to find R2*
                    if -f.b > 0 %negative values are considered
"unphysical" and are therefore excluded
                        staticR2StarMap(x,y,sliceNumber) = -f.b;
                        staticR2StarValues(index) = -f.b;
                        index = index + 1;
                    elseif -f.b < 0 %negative R2* are considered
"unphysical" and are excluded
                        negativeValuesStatic = negativeValuesStatic +
1;
                    end
                end
            end
        end

        %Plotting to check the R2* maps
        % figure, imagesc(staticR2StarMap(:,:,sliceNumber)),
colormap('gray')

    end
    figure, imshow3D(staticR2StarMap)
    staticR2StarValues = sort(staticR2StarValues);

    staticMedian = median(staticR2StarValues);
    staticMean = mean(staticR2StarValues);
    staticStd = std(staticR2StarValues);
    staticIqr = iqr(staticR2StarValues);
    staticMax = max(staticR2StarValues);
    staticMin = min(staticR2StarValues);
    staticRange = range(staticR2StarValues);

    %Saving variables to a .mat-file in the patient's FFE folder
    save([filePath 'Oxytarget_' int2str(patientNr) ' PRE/FFE/
staticR2StarMap.mat'],'staticR2StarMap','staticR2StarValues','staticMedian','stati
end

```

Published with MATLAB® R2016b

```

%This program calculates the dynamic R2* for the images in the R2Star
%folder (based on the 4D image matrices made in sortDynamic).

clear all
filePath = 'C:\Users\Vidar\Downloads\Master\Patients\';
addpath('C:\Users\Vidar\Downloads\Master\Matlab prosjektoppgave\ekstra
\imshow3d');

%patientNR = [1 2 3 4 5 6 7 8 9 10 11 12 13 14 15 16 17 18
19 20 21 22 23 24 25 26 27 28 29 30 31 32 33 34 35 36 37 38 39 40 41
42 43 44 45 46 47 48
patientList = [24 25 27 29 30 32 31 34 39 40 41 43 44 45 46 47 48 49
50 51 52 54 55 56 57 58 60 64 65 67 68 69 72 73 74 75 76 77 78 79 80
83 85 87 88 89 90 92 ...
...49 50 51 52 53 54 55 56 57 58 59 60 61 62 63
64 65 66 67 68 69 70 71 72 73 74 75 76 77 78 79 80
81 82 83
94 95 96 102 103 106 107 108 110 111 112 113 114 115
116 118 119 120 121 123 125 126 127 128 131 133 134 138 142 143 144
146 147 148 149 ...
... 84 85 86 87 88 89 90 91 92 93 94 95 96 97
98 99 100 101 102 103]
150 151 152 153 154 155 156 157 158 159 160 161 162 163
164 165 166 169 170 171];

n = length(patientList);
%patientNR = [1 2 3 4 5 6 7 8 9 10 11 12 13 14 15 16 17
18 19 20 21 22 23 24 25 26 27 28 29 30 31 32 33 34 35 36 37 38 39 40
41 42]
nBaselineImages = [11 15 12 14 08 11 10 12 05 12 11 10 17 12 14 10 13
09 06 07 11 15 11 15 14 14 14 14 17 14 18 18 14 18 16 17 15 19 18 16
17 18 ...
...[43 44 45 46 47 48 49 50 51 52 53 54 55 56 57 58 59 60 61 62 63 64
65 66 67 68 69 70 71 72 73 74 75 76 77 78 79 80 81 82 83 84 85 86 87
88 89]
15 14 18 16 15 14 16 16 14 15 12 15 15 13 19 15 13 16 16 18 14 14
21 19 14 23 15 22 13 16 13 14 14 20 13 19 12 16 20 13 13 20 19 14 14
20 17 ...
...[90 91 92 93 94 95 96 97 98 99 00 01 02 03]
14 16 20 14 16 16 18 16 16 16 23 15 21 17];

%Loop that goes over all patients that are going to be analysed
for patient = 1:n

for x = 1:10
disp(x)
end

patientNr = patientList(patient); %Draw out the number of the
patient

```

```

    %Load the 4D image matrix and other variables, and the ROI
    load([filePath 'Oxytarget_' int2str(patientNr) ' PRE/
R2Star/4Dmatrix.mat']);
    load([filePath 'Oxytarget_' int2str(patientNr) ' PRE/
dynamicROI.mat']);

    R2StarPeakEnhancedMap = zeros(256,256,nSlices);
    AUCmap = zeros(256,256,nSlices);

    R2StarPeakEnhancedValues = zeros(1,1);
    AUCvalues = zeros(1,1);

    if patientNr == 159 || patientNr == 160 || patientNr == 162 ||
patientNr == 163 || patientNr == 164 || patientNr == 166 || patientNr
== 169 || patientNr == 171
        curveAverage = zeros(1,70);
    else
        curveAverage = zeros(1,60);
    end

    index = 1;
    negativeValuesDynamic = 0;

    for sliceNumber = 1:nSlices
        t = acqTimeValue(sliceNumber,:);

        for it = 1:length(t) %change from acquisition time to seconds
            h = floor(t(it)*1E-4);
            m = floor((t(it)-h*1E4)*1E-2);
            s = floor(t(it)-h*1E4-m*1E2);
            t(it) = h*60*60 + m*60 + s + (t(it)-floor(t(it)));
        end

        t = t-t(1);

        tAUC = zeros(1,1);
        tVal = t(1);
        indexT = 1;

        AUCinterval = 525; %only finding AUC in this interval

        if max(t) < AUCinterval
            tAUC = t;
        else
            while tVal < AUCinterval
                tAUC(indexT) = t(indexT);
                indexT = indexT + 1;
                tVal = t(indexT);
            end
        end

        for x = 1:256
            for y = 1:256
                if dynamicROI(x,y,sliceNumber) == 1

```

```

        sum = 0;
        for i = 1:nBaselineImages(patient)
            sum = sum + im(x,y,sliceNumber,i);
        end
        baseline = sum/nBaselineImages(patient);
        pixelArray = squeeze(im(x,y,sliceNumber,:))-
baseline; %setting baseline to 0
        maximum = max(pixelArray); %finding the maximum
        value of delta-R2* (R2*-peak_enh)

        if maximum > 0 %only interested in positive R2*-
peak_enh
            R2StarPeakEnhancedMap(x,y,sliceNumber) =
maximum;

            R2StarPeakEnhancedValues(index) = maximum;
            pixelArrayAUC = zeros(1,length(tAUC));
            for it = 1:length(pixelArrayAUC)
                pixelArrayAUC(it) = pixelArray(it);
            end
            AUCvalues(index) =
trapz(tAUC,pixelArrayAUC); %finding R2*-AUC
            AUCmap(x,y,sliceNumber) = AUCvalues(index);
            curveAverage(index,:) = pixelArray;
            index = index + 1;
        elseif maximum < 0
            negativeValuesDynamic = negativeValuesDynamic
+ 1;
        end
    end
end
end

    %Plotting to check the R2*-peak-enh and R2*-AUC maps
    %figure, imagesc(R2StarPeakEnhancedMap(:,:,sliceNumber)),
colormap('gray')
    %figure, imagesc(AUCmap(:,:,sliceNumber)), colormap('gray')
end

    %figure, plot(t,curveAverage)
    %figure, imshow3D(AUCmap)
    %figure, imshow3D(R2StarPeakEnhancedMap)

    %Plotting the average of all delta-R2* curves to see how it looks
    for j = 1:60
        sum = 0;
        for k = 1:length(R2StarPeakEnhancedValues)
            sum = sum + curveAverage(k,j);
            %disp(curveAverage(k,j))
        end
        curveAverage((length(R2StarPeakEnhancedValues)+1),j) = sum/
(length(R2StarPeakEnhancedValues));
    end
    figure,
    plot(t,curveAverage((length(R2StarPeakEnhancedValues)+1),:))

```

```
R2StarPeakEnhancedValues = sort(R2StarPeakEnhancedValues);
AUCvalues = sort(AUCvalues);

dynamicMedian = median(R2StarPeakEnhancedValues);
dynamicMean = mean(R2StarPeakEnhancedValues);
dynamicStd = std(R2StarPeakEnhancedValues);
dynamicIqr = iqr(R2StarPeakEnhancedValues);
dynamicMax = max(R2StarPeakEnhancedValues);
dynamicMin = min(R2StarPeakEnhancedValues);
dynamicRange = range(R2StarPeakEnhancedValues);

AUCmedian = median(AUCvalues);
AUCmean = mean(AUCvalues);
AUCstd = std(AUCvalues);
AUCiqr = iqr(AUCvalues);
AUCmax = max(AUCvalues);
AUCmin = min(AUCvalues);
AUCrange = range(AUCvalues);

%Saving variables to a .mat-file in the patient's FFE folder
save([filePath 'Oxytarget_' int2str(patientNr) ' PRE/R2Star/
R2StarPeakEnhancedMap.mat'], 'R2StarPeakEnhancedMap', 'R2StarPeakEnhancedValues', 'dy
end
```

Published with MATLAB® R2016b

```

%This program does a statistical analysis (with the Mann-Whitney U
test) on
%the correlation between the parameters and the endpoints.

clear all
filePath = 'C:\Users\Vidar\Downloads\Master\Patients\';

resultsMatrixStatic = zeros(8,4);
resultsMatrixDynamic = zeros(8,4);
resultsMatrixAUC = zeros(8,4);

%Making vectors with the patients within each endpoint, then doing the
%Mann-Whitney U test (ranksum function)

%Endpoint: Tumour regression grade (TRG), TRG0-1 vs. TRG2-3

TRG01patients = [41 43 50 51 55 56 67 87 107 119 120 121 131 150 156
169];
index = 0;

for patient = 1:length(TRG01patients)

    patientNr = TRG01patients(patient);

    %Loading the calculated values for the patients in the group
    if (patientNr ~= 156) && (patientNr ~= 169) %these patients had no
FFE sequence
        load([filePath 'Oxytarget_' int2str(patientNr) ' PRE/
staticR2StarMap.mat']);
        index = index + 1;
        TRG01staticValues(index) = staticMedian;
    end
    if (patientNr ~= 119) %these patients had no R2Star sequence or
couldn't run some part of the program
        load([filePath 'Oxytarget_' int2str(patientNr) ' PRE/
R2StarPeakEnhancedMap_135.mat']);

        TRG01dynamicValues(patient) = dynamicMedian;
        TRG01AUCValues(patient) = AUCmedian;
    end
end

TRG01staticMean = mean(TRG01staticValues);
TRG01staticMedian = median(TRG01staticValues);
TRG01staticStd = std(TRG01staticValues);
TRG01staticIqr = iqr(TRG01staticValues);
TRG01staticMax = max(TRG01staticValues);
TRG01staticMin = min(TRG01staticValues);
TRG01dynamicMean = mean(TRG01dynamicValues);
TRG01dynamicMedian = median(TRG01dynamicValues);
TRG01dynamicStd = std(TRG01dynamicValues);
TRG01dynamicIqr = iqr(TRG01dynamicValues);

```

```

TRG01dynamicMax = max(TRG01dynamicValues);
TRG01dynamicMin = min(TRG01dynamicValues);
TRG01AUCMean = mean(TRG01AUCValues);
TRG01AUCMedian = median(TRG01AUCValues);
TRG01AUCStd = std(TRG01AUCValues);
TRG01AUCIqr = iqr(TRG01AUCValues);
TRG01AUCMax = max(TRG01AUCValues);
TRG01AUCMin = min(TRG01AUCValues);

TRG23patients = [24 27 32 44 47 49 52 74 79 80 89 90 96 113 116 125
 126 128 138 146 153 162 166 170];
index = 0;

for patient = 1:length(TRG23patients)

    patientNr = TRG23patients(patient);

    %Loading the calculated values for the patients in the group
    if (patientNr ~= 58) %these patients had no FFE sequence
        load([filePath 'Oxytarget_' int2str(patientNr) ' PRE/
staticR2StarMap.mat']);
        index = index + 1;
        TRG23staticValues(index) = staticMedian;
    end
    load([filePath 'Oxytarget_' int2str(patientNr) ' PRE/
R2StarPeakEnhancedMap_135.mat']);

    if (patientNr ~= 97) && (patientNr ~= 28) %these patients had no
R2Star sequence or couldn't run some part of the program
        load([filePath 'Oxytarget_' int2str(patientNr) ' PRE/
R2StarPeakEnhancedMap_135.mat']);

        TRG23dynamicValues(patient) = dynamicMedian;
        TRG23AUCValues(patient) = AUCmedian;
    end
end

TRG23staticMean = mean(TRG23staticValues);
TRG23staticMedian = median(TRG23staticValues);
TRG23staticStd = std(TRG23staticValues);
TRG23staticIqr = iqr(TRG23staticValues);
TRG23staticMax = max(TRG23staticValues);
TRG23staticMin = min(TRG23staticValues);
TRG23dynamicMean = mean(TRG23dynamicValues);
TRG23dynamicMedian = median(TRG23dynamicValues);
TRG23dynamicStd = std(TRG23dynamicValues);
TRG23dynamicIqr = iqr(TRG23dynamicValues);
TRG23dynamicMax = max(TRG23dynamicValues);
TRG23dynamicMin = min(TRG23dynamicValues);
TRG23AUCMean = mean(TRG23AUCValues);
TRG23AUCMedian = median(TRG23AUCValues);
TRG23AUCStd = std(TRG23AUCValues);
TRG23AUCIqr = iqr(TRG23AUCValues);

```

```
TRG23AUCMax = max(TRG23AUCValues);  
TRG23AUCMin = min(TRG23AUCValues);
```

```
%Mann-Whitney U test
```

```
[p_TRG01vsTRG23static,h_TRG01vsTRG23static] =  
    ranksum(TRG01staticValues,TRG23staticValues)  
[p_TRG01vsTRG23dynamic,h_TRG01vsTRG23dynamic] =  
    ranksum(TRG01dynamicValues,TRG23dynamicValues)  
[p_TRG01vsTRG23AUC,h_TRG01vsTRG23AUC] =  
    ranksum(TRG01AUCValues,TRG23AUCValues)
```

```
%Saving the results in matrices
```

```
resultsMatrixStatic(1,:) = [TRG01staticMedian, TRG23staticMedian,  
    p_TRG01vsTRG23static, h_TRG01vsTRG23static];  
resultsMatrixDynamic(1,:) = [TRG01dynamicMedian, TRG23dynamicMedian,  
    p_TRG01vsTRG23dynamic, h_TRG01vsTRG23dynamic];  
resultsMatrixAUC(1,:) = [TRG01AUCMedian, TRG23AUCMedian,  
    p_TRG01vsTRG23AUC, h_TRG01vsTRG23AUC];
```

Published with MATLAB® R2016b

B.2 Code for the IHC Analysis

Table of Contents

| | |
|---|---|
| Main | 1 |
| Extract masks | 1 |
| Check mask in original image | 2 |
| Analyse higher resolution IHC -- CD34 example | 2 |
| SEGMENT IHC | 4 |

Main

```
clear,
format compact

%Load excel sheet med all the filename and storage positions and
stores
%them in an array
filename='C:\Users\Vidar\Downloads\Master\Pathology\patients.xlsx';
[num,txt,row] = xlsread(filename);

%Number of patients to run the program for
nrPatients=length(row)-1;

for patient = 1:nrPatients

data_path = {'D:\Oxytarget Pathology\' char(txt(patient+1,23)) '\'
char(txt(patient+1,2)) ' ' num2str(num(patient,1))}];

p = {};
for dp = data_path(:)'
    fn = dir([dp{1},filesep,'*.svs']);
    fn = fullfile(dp, {fn.name});
    p(end+(1:length(fn))) = fn;
end

%Check how many slides there are
nr_slides=[0 0 0 0 0 0];
for i=1:numel(nr_slides)
    if ~isnan(num(patient,i+12))
        nr_slides(i)=1;
    end
end

FN = (1:sum(nr_slides(:) == 1)); % full set for case patient

key = {'HPS', 'CD3', 'CD8', 'CD34', 'CA9', 'HIF-1@'};
```

Extract masks

```
for i = 1:numel(FN)
    cp = p(FN(i));
```

```

    [currentpath,casename] = fileparts(cp{:});
    pattern = sprintf('%s%s%s-*mask*',currentpath,filesep,casename);
    mask_fn = dir(pattern);
    if ~isempty(mask_fn)
        MaskFN{i} = strcat(currentpath, filesep, {mask_fn.name});
        mask = [];
    end
end

[currentpath,casename] = fileparts(p{FN(1)});

hasMask = ~cellfun(@isempty,MaskFN);
MaskS =
    struct('referenceSlide',key(hasMask), 'propagateMask',true,'BW',mask);

maskPreProcess = @(mask)imfill(~mask(:,:,1),'holes'); % invert and
    fill holes.
maskBehaviour =
    struct('propagateMask',true,'invertMask',false,'mergeFunction',@and, 'processFunc
    maskPreProcess);

CC = PICase(casename,key, p(FN)); % CC = current case
CC.addMasks(key(hasMask), MaskFN(hasMask), maskBehaviour); %Add masks
    to image
CC.initialRegistration(); % register all to first slide using full
    image.

```

Check mask in original image

```

illustrateMaskByEdge = @(im, mask)im.*cast((repmat(imerode(~bwperim(mask),strel('disk',7)),1,1,3)),class(im)); [im0, ref0, mask0] = CC.extractMaskedSlide('HPS'); % load
    same image size as mask matrix by default figure(1), clf, imshow(illustrateMaskByEdge(im0, mask0),
    ref0)

```

Analyse higher resolution IHC -- CD34 example

```

% PE = [8, 8]; % Second downscaled image.
% PE = [16,16]; % Third downscaled image. Good size for initial tests

PE = [4 4]; %

[imcropHPS, imrefHPS, mask] = CC.extractMaskedSlide('HPS',PE);
[imcropCD, imrefCD, maskCD] = CC.extractMaskedSlide('CD34',PE);
[imcropCA, imrefCA, maskCA] = CC.extractMaskedSlide('CA9',PE);
[imcropHIF, imrefHIF, maskHIF] = CC.extractMaskedSlide('HIF_1A',PE);

% figure('Name','imcropHPS, mask'), imshowpair(mask, imcropHPS)
% figure('Name','imcropCD, original mask'), imshowpair(maskCD,
    imcropCD)
% figure('Name','imcropCA, original mask'), imshowpair(maskCA,
    imcropCA)
% figure('Name','imcropHIF, original mask'), imshowpair(maskHIF,
    imcropHIF)

```

```

% imwrite(imcropCD,[char(data_path),'\\','imcropCD.png'])
% imwrite(imcropCA,[char(data_path),'\\','imcropCA.png'])
% imwrite(imcropHIF,[char(data_path),'\\','imcropHIF.png'])
%
% imwrite(imrefCD,[char(data_path),'\\','imrefCD.png'])
% imwrite(imrefCA,[char(data_path),'\\','imrefCA.png'])
% imwrite(imrefHIF,[char(data_path),'\\','imrefHIF.png'])

% CC.maskedRegistration(); % register all to first slide using only
  data
% in the mask of the reference slide (full bounding box or mask out
% non-true pixels).

if exist([currentpath,'\\','registeredCA.png'], 'file') &&
  exist([currentpath,'\\','registeredCD.png'], 'file') &&
  exist([currentpath,'\\','registeredHIF.png'], 'file')
    registeredCD=imread([char(data_path),'\\','registeredCD.png']);
    registeredCA=imread([char(data_path),'\\','registeredCA.png']);
    registeredHIF=imread([char(data_path),'\\','registeredHIF.png']);
else

  registeredCD=CC.maskedRegistration(imcropHPS,imcropCD,'CD34',data_path);

  registeredCA=CC.maskedRegistration(imcropHPS,imcropCA,'CA9',data_path);

  registeredHIF=CC.maskedRegistration(imcropHPS,imcropHIF,'HIF-1A',data_path);

  imwrite(registeredCD,[char(data_path),'\\','registeredCDe.png'])
  imwrite(registeredCA,[char(data_path),'\\','registeredCA.png'])
  imwrite(registeredHIF,[char(data_path),'\\','registeredHIF.png'])

%   figure('Name','HPS, mask'), imshowpair(mask, imcropHPS),
%   title('Mask, imcropHPS')
%
%   figure('Name','Original CD, original mask'), subplot(1,2,1),
%   imshowpair(maskCD, imcropCD), title('MaskCD, imcropCD')
%   subplot(1,2,2), imshowpair(mask, registeredCD), title('mask,
%   registeredCD')
%
%   figure('Name','Original CA, original mask'), subplot(1,2,1),
%   imshowpair(maskCA, imcropCA), title('MaskCA, imcropCA')
%   subplot(1,2,2), imshowpair(mask, registeredCA), title('mask,
%   registeredCA')
%
%   figure('Name','Original HIF, original mask'), subplot(1,2,1),
%   imshowpair(maskHIF, imcropHIF), title('MaskHIF, imcropHIF')
%   subplot(1,2,2), imshowpair(mask, registeredHIF), title('mask,
%   registeredHIF')

end

T=load([char(data_path) '\\tformCD34'], 'tform');
tform_cd=T.('tform');

```

```

T=load([char(data_path) '\tformCA9'], 'tform');
tform_ca=T.('tform');

T=load([char(data_path) '\tformHIF-1A'], 'tform');
tform_hif=T.('tform');

registeredCD_large=imwarp(imcropCD,tform_cd);
registeredCA_large=imwarp(imcropCD,tform_ca);
registeredHIF_large=imwarp(imcropCD,tform_hif);

imwrite(registeredCD_large,
[char(data_path), '\', 'registeredCD_large.png'])
imwrite(registeredCA_large,
[char(data_path), '\', 'registeredCA_large.png'])
imwrite(registeredHIF_large,
[char(data_path), '\', 'registeredHIF_large.png'])

```

SEGMENT IHC

```

registeredCD=imread([char(data_path), '\', 'registeredCD.png']);
registeredCA=imread([char(data_path), '\', 'registeredCA.png']);
registeredHIF=imread([char(data_path), '\', 'registeredHIF.png']);

imref_reg_CD=imrefHPS;
imref_reg_CA=imrefHPS;
imref_reg_HIF=imrefHPS;

%Segment IHC (CD34)

ihc_mask = segmentIHC(registeredCD, imref_reg_CD, mask);

hlink = comparisonPlot(registeredCD, imref_reg_CD, ihc_mask, 'col',
[1,0,1]);

% POSTPROCESS IHC (CD34)

ihc_mask_post = postprocessIHC(ihc_mask, imref_reg_CD, 'CD34');

hlink = comparisonPlot(registeredCD, imref_reg_CD,
ihc_mask_post, 'col', [1,0,1]);

save([char(data_path) '\ihc_mask_post_CD'], 'ihc_mask_post')

% SEGMENT IHC (CA9)

ihc_mask = segmentIHC(registeredCA, imref_reg_CA, mask);

hlink = comparisonPlot(registeredCA, imref_reg_CA, ihc_mask, 'col',
[1,0,1]);

% POSTPROCESS IHC (CA9)

```

```
ihc_mask_post = postprocessIHC(ihc_mask, imrefCA, 'CA9');

hlink = comparisonPlot(registeredCA, imref_reg_CA,
    ihc_mask_post, 'col', [1,0,1]);

save([char(data_path) '\ihc_mask_post_CA'], 'ihc_mask_post')

% SEGMENT IHC (HIF-1A)

ihc_mask = segmentIHC(registeredHIF, imref_reg_HIF, mask);

hlink = comparisonPlot(registeredHIF, imref_reg_HIF, ihc_mask, 'col',
    [1,0,1]);

% POSTPROCESS IHC (HIF-1A)

ihc_mask_post = postprocessIHC(ihc_mask, imref_reg_HIF, 'CD34');

hlink = comparisonPlot(registeredHIF, imref_reg_HIF,
    ihc_mask_post, 'col', [1,0,1]);

save([char(data_path) '\ihc_mask_post_HIF'], 'ihc_mask_post')

end
```

Published with MATLAB® R2016b

Table of Contents

| | |
|---|---|
| | 1 |
| Dependents | 1 |
| Main method block | 2 |
| Mask methods | 2 |
| Parse input | 3 |
| Parse input | 6 |
| Loop input masks | 6 |
| Mask postprocessing may be added here. | 8 |
| Coregistration methods | 8 |

```
classdef PICase < handle % handle class -> copy by reference

    properties

        name;
        slideNames = {};
        Slides = struct();
        Masks = struct();

        % Registration properties
        Registration = struct('name',[],'type',[],'T',[],'outputRef',
[]); % T = affine3d or displacement field; outputRef = imref2d to
crop.
        Settings = struct('Registration',struct('optimizer',
[],'metric',[]));
    end
    properties (Hidden, SetAccess = private)
        % ReferenceSystem: Use ReferenceSystemName when accessing this
        % property externally.
        ReferenceSystem = 1; % first provided by default. Hidden
because it does not provide information that is useful externally.
    end
end
```

Dependents

```
properties (Dependent)
    ReferenceSystemName % loaded using ReferenceSystem property
from get.ReferenceSystemName()
end
methods % get/set methods
    function name = get.ReferenceSystemName(obj)
        name = obj.slideNames{obj.ReferenceSystem};
    end
    function obj = set.ReferenceSystemName(obj,s)
        obj.ReferenceSystem = find(strcmp(s, obj.slideNames));
    end
end
```

Main method block

methods

```
function [obj, slideNameList] = PICase(caseName,
slideNameList, fileList, varargin)
%         ip = inputParser();
%         ip.AddParameter('Mask',[]);
%         ip.Parse(varargin{:});

% Constructor
obj.name = caseName;
% Load slides
for i=1:numel(slideNameList)
    sn = slideNameList{i};
    sn = obj.fieldnameCleaner(sn);
    fn = fileList{i};
    slide = PISlide(sn,fn);
    obj.Slides.(sn) = slide;
    obj.slideNames = [obj.slideNames, sn];
end
% Default settings
[optimizer, metric] = imregconfig('multimodal');
obj.Settings.Registration =
struct('optimizer',optimizer,'metric',metric);

% Override default properties
for i=1:2:length(varargin)
    obj.(varargin{i}) = obj.(varargin{i+1});
end
end

function slide = Slide(obj, ind)
% index Slides using numeric or non-clean field name (e.g.
% "HIF-1@".
if isnumeric(ind)
    slide = obj.Slides.(obj.slideNames{ind});
elseif ischar(ind)
    slide = obj.Slides.(obj.fieldnameCleaner(ind));
else
    error('Invalid class ("%s") for first
input',class(ind))
end
end

function ind = ind(obj, name)
ind = find(strcmp(obj.slideNames, name));
end
```

Mask methods

```
function [imcrop, imref, mask] = extractMaskedSlide(obj,
slide, outref)
```

```

combines      % Warps alle propagating masks to the selected slide,
of            % them according to the obj.Masks.(slide).combineFunction
combined     % each Mask, extracts the bounding box of the warped,
             % masks and the resulting mask in the slides own reference
             % system.

```

Parse input

```

if isnumeric(slide) && isscalar(slide)
    slide = slideNames{slide};
elseif ischar(slide)
    %pass
else
    error('Expected input to be a scalar integer or a
character array. Instead %s was passed.',mat2str(slide));
end

Slide = obj.Slides.(slide);

for fn = fieldnames(obj.Masks)
    % Extract each mask in native reference system
    Mask = obj.Masks.(fn{1});
    combinedRef = [];
    combinedBW = [];
    if strcmp(fn, obj.ReferenceSystemName) ||
Mask.propagateMask % same system or propagate
        imref = Mask.imref;

        bw = Mask.BW;
        % Obtain natives mask's registration to reference
system

        if ~strcmp(fn, obj.ReferenceSystemName)
            % propagate from different registration
            T0 = obj.Registration(obj.ind(fn)); %maskref ->
referenceSystem
        else
            T0 = affine2d(); % identity transform
        end

        % Obtain slides registration compared to reference
        % system.
        if ~strcmp(slide, obj.ReferenceSystemName)
            % Convert to the reference system of the
specified slide.

            T1 = obj.Registration(obj.ind(slide)).T;
        else
            T1 = affine2d(); % identity transform
        end

        % Combined transform: Mask->Reference->Slide

```

```

        T = affine2d(T0.T * T1.invert.T); % reverse
transform (ref -> slide).
        [bw2, regref] = imwarp(bw, imref, T, 'nearest');
        if(regref.YWorldLimits(2)>Slide.WorldLimits{1,2}(2))
            regref.YWorldLimits(2)=Slide.WorldLimits{1,2}
(2)-1;
        end
        if(regref.XWorldLimits(2)>Slide.WorldLimits{1,1}(2))
            regref.XWorldLimits(2)=Slide.WorldLimits{1,1}
(2)-1;
        end

        if~(mod(regref.YWorldLimits(1),1)==0 ||
mod(regref.XWorldLimits(1),1)==0 || (mod(regref.YWorldLimits(2),1)==0
|| mod(regref.XWorldLimits(2),1)==0))
            regref.YWorldLimits=fix(regref.YWorldLimits);
            regref.XWorldLimits=fix(regref.XWorldLimits);
            warning('Round off occured in extractMaskedSlide,
regref.')
```

```

        end

        if isempty(combinedBW)
            % first mask.
            combinedRef = regref;
            combinedBW = bw2;
        else
            % Combined imrefs:
            combinedRef = imrefUnion(combinedRef,regref);
            % Use imwarp with affine2d() to change imrefs.
(TODO: Cheaper
to be
correct
            % to do in dedicated function, the matrix needs
            % copy pasted into a larger/different matrix at
            % indices.)
            bw3 = imwarp(bw2, regref,
affine2d(), 'nearest', 'OutputView', combinedRef);
            combinedBW = imwarp(combinedBW, regref,
affine2d(), 'nearest', 'OutputView', combinedRef);
            combinedBW = Mask.mergeFunction(combinedBW,
bw3);
        end
    else
        % pass, mask not to be used on specified slide.
    end

    % output data

    % Extract crop of image according to mask bounding box.
    if nargin<3 % outref not specified
        incrop = Slide.data(combinedRef);
        imref = combinedRef;
        mask = combinedBW;
    else

```

```

        % alter crop to specified outref.
        if isnumeric(outref)&&numel(outref)==2
            % Interpret outref as pixel extent. Use
specified PE
            % along with combinedRef.WorldLimits.
            PE = outref;
            WL = {combinedRef.XWorldLimits,
combinedRef.YWorldLimits};
            if (~(mod(WL{1,1}(1),1)==0) || ~(mod(WL{1,1}
(2),1)==0) || ~(mod(WL{1,2}(1),1)==0) || ~(mod(WL{1,2}(2),1)==0)))
                WL{1,1}=round(WL{1,1});
                WL{1,2}=round(WL{1,2});
                warning('Round off occurred in
extractMaskedSlide, WL.')
            end
            siz =
[diff(combinedRef.YWorldLimits),diff(combinedRef.XWorldLimits)] ./
PE;
            if ~all(siz==fix(siz)) % noninteger
                warning('TODO: round off matrix size and
adapt world limits to fit the specified pixel element size');
            end

            imref = imref2d(fix(siz), WL{:});
        elseif isa(outref,'imref2d')
            imref = outref;
        else
            error('Unrecognized image reference
specification format. Use imref2d object or [pixelExtentInWorldX,
pixelExtentInWorldY]-format.');
```

```

        end
        imcrop = Slide.data(imref);

        imcrop = imwarp(imcrop, imref,
affine2d(), 'nearest');
        mask = imwarp(combinedBW, combinedRef,
affine2d(), 'nearest', 'OutputView', imref);
    end

end

function imref = imrefUnion(ref1, ref2)
    % merge world views of ref1 and ref2.
    % Keep pixel size of ref1.
    if isempty(ref1)
        imref=ref2;
    elseif isempty(ref2)
        imref=ref1;
    else
        WL1 = [ref1.XWorldLimits, ref1.YWorldLimits];
        WL2 = [ref2.XWorldLimits, ref2.YWorldLimits];
        WLu = [min(WL1(1),WL2(1)), max(WL1(2),WL2(2)),
min(WL1(3),WL2(3)), max(WL1(4),WL2(4))];

```

```

        imsiz = [WLu(4)-WLu(3), WLu(2)-WLu(1)];
        imref = imref2d(imsiz, WLu(1:2), WLu(3:4));
    end
end

end
function addMasks(obj, varargin)

    % Add one or more mask files to one or more slides.

```

Parse input

```

    default_settings =
    struct('propagateMask',true,'invertMask',false,'mergeFunction',@and, 'processFunc
[]);
    ip = inputParser();
    ip.addRequired('referenceSlide', @(s)(iscell(s) &&
isvector(s)));
    ip.addRequired('mask', @(s)(iscell(s) && isvector(s)); %
filenames or array, wrapped in cell if mutliple.
    ip.addOptional('settings', default_settings);
    ip.addOptional('tag',[]); % may be used to locate
appropriate mask for a given operation later.
    ip.StructExpand = false;
    ip.parse(varargin{:});
    input = ip.Results;
    % add default values for partially specified settings.
    for fn = fieldnames(default_settings)'
        if ~isfield(input.settings, fn{1}), input.settings.
(fn{1}) = default_settings.(fn{1}); end
    end

```

Loop input masks

```

for sname = input.referenceSlide
    %             imref = obj.Slides.(sname{:}).imref
    slide = obj.Slides.(sname{1});
    WorldLimits = slide.WorldLimits;

    for fn = input.mask

        fn = fn{1}; % fn is scalar cell with this for
syntax.

        if iscell(fn)
            % multiple input masks for this entry
            for n = 1:numel(fn)
                if n==1
                    mask = loadMask(fn{n});
                else
                    % Combine with previous masks as
specified.

                    % All masks should be same size.

```

```

                                mask =
input.settings.mergeFunction(mask, loadMask(fn{n}));
                                end
                                end
                                else
                                mask = loadMask(fn);
                                end
                                mask = processMask(mask,
input.settings.processFunction);
                                % search for image layer matching mask matrix
slice.
                                s = slide.find('image');
                                matrices = [[slide.info(s).Height]',
[slide.info(s).Width]'];
                                ind =
find(all(repmat(size(mask),size(matrices,1),1)==matrices,2));
                                if ~isempty(ind)
                                imref = slide.imref(s(ind));
                                else
                                % otherwise, assume same field of view, but
different
                                % scale.
                                imref = imref2d(size(mask), WorldLimits{:});
                                end

                                if(imref.YWorldLimits(2)>obj.Slides.HPS.info(1).Height)
                                imref.YWorldLimits(2)=imref.YWorldLimits(2)-
(imref.YWorldLimits(2)-obj.Slides.HPS.info(1).Height);
                                end
                                [m,n] = ind2sub(size(mask), find(mask));
                                mnr = [min(m) max(m) min(n) max(n)]; %mn range
                                if ~(mnr(1)-100<=0 || mnr(2)+100>=size(mask,1) ||
mnr(3)-100<=0 || mnr(4)+100>=size(mask,2))
                                mnr = round(mnr+[-100 100 -100 100]); % adding
some frames outside the mask for registration as long as it is
smaller than image size
                                end
                                mask = mask(mnr(1):mnr(2), mnr(3):mnr(4));
                                [WL{1},WL{2}] =
imref.intrinsicToWorld(mnr(3:4)+[-1,1]./2,mnr(1:2)+[-1,1]./2); % +/-
1/2 to move coordinate from pixel center to outer corner.
                                imref = imref2d(size(mask),WL{:});

                                obj.Masks.(sname{1}) = struct('BW',mask, 'imref',
imref,'tag', input.tag,...
                                'propagateMask',
input.settings.propagateMask,...
                                'mergeFunction',
input.settings.mergeFunction);

                                end
                                end

```

```

function mask = loadMask(fn)
    % returns numeric matrix if a preloaded mask was
passed,
    % and reads the input matrix if a filename was
provided.
    if isnumeric(fn)
        mask = fn;
    else
        mask = imread(fn);
        if size(mask,3)>1 % color image
            if ~isequal(mask(:,:,1), mask(:,:,2),
mask(:,:,3))
                warning('mask files with different
information stored in each layer, currently not supported');
            end
            mask = mask(:,:,1);
            max_val = max(mask(:));
            if ~isequal(mask>0 , ~(mask<max_val))
                warning('mask with multiple non-zero
values encountered. All non-zero values will be merged.');
```

Mask postprocessing may be added here.

```

function mask = processMask(mask, processing)
    if ~isempty(processing)
        switch class(processing)
            case 'function_handle'
                mask = processing(mask);
            otherwise
                processFunction
        end
        %
        %         case 'filter1'
        %             % do filter 1
        %         case 'filter2'
        %             % do filter 2
        %
    end
end
end
end
```

Coregistration methods

```

function initialRegistration(obj, Ind)
    % Perform initial coregistration for all slices against
    % reference system. Initial registration is used done
using
```

```

        % thumbnail images for improved performance.

        % Reference system : fixed
        flatOutput = true;
        [fix,fixref] = obj.Slides.
(obj.ReferenceSystemName).layer('thumbnail',flatOutput);

        if ~exist('Ind','var')
            SlideNames = setdiff(obj.slideNames,
obj.ReferenceSystemName);
        end
        % Perform registration
        for slidename = SlideNames
            if iscell(slidename) && isscalar(slidename), slidename
= slidename{1}; end
            if isequal(slidename, obj.ReferenceSystemName)
                obj.Registration(obj.ind(slidename)) =
struct('name', slidename,...

                'type','reference','T',affine3d,'outputRef',fixref);
            else
                [mov,movref] =
obj.Slide(slidename).layer('thumbnail',flatOutput);

                tform = imregtform(mov, movref, fix,
fixref, 'similarity',...
                obj.Settings.Registration.optimizer,
obj.Settings.Registration.metric);
                % [movreg] = imwarp(moving, moving_ref, tform);
            end
            obj.Registration(obj.ind(slidename)) = struct('name',
slidename,...
                'type','initial','T',tform,'outputRef',fixref);
        end
    end

    function registered = maskedRegistration(obj, IM1, IM2, key,
path)
        % redo initial registration with only the masked part of
the
        % image active. This is done to ignore non-affine morphing
        % outside of the region to be analysed.

        fixed=rgb2gray(IM1);
        moving=rgb2gray(IM2);

        [optimizer, metric] = imregconfig('multimodal');

        optimizer.InitialRadius = 1.5e-3;
        optimizer.Epsilon = 1.5e-1;
        optimizer.GrowthFactor = 1.05;
        optimizer.MaximumIterations = 300;

        metric.NumberOfSpatialSamples = 500;

```

```
metric.NumberOfHistogramBins = 50;
metric.UseAllPixels = 1;

tform = imregtform(moving, fixed, 'affine', optimizer,
metric);

save([char(path) '\tform' key], 'tform')

registered=imwarp(IM2, tform, 'OutputView',
imref2d(size(fixed)));

end

end

methods (Hidden)
function s = fieldnameCleaner(obj, s)
    s = regexp(s, {'-', '\\', '/'}, '_');
    s = regexp(s, {'@'}, 'A');
end

end

end
```

Published with MATLAB® R2016b

```

classdef PISlide < handle
    % PISlide is a wrapper class for handling Pathology Images in the
    % Aperio format (.svs).

    % Matrix sizes and aperios 1:1, 1:4, 1:16, 1:32 etc. format does
    not
    % match exactly between layers. Assume integer pixels sizes with
    round
    % off affecting matrix size (slight cropping).
    properties
        name
        info

        WorldLimits;

        Flatten = @rgb2gray; % use standard grayscale transform when
        converting layer to grayscale
        Resolution = [1,1]; % pixel size in layer 1
    end

    methods
        function obj = PISlide(name, info, varargin)
            % Constructor
            obj.name = name;
            if isstruct(info)
                % info struct
                obj.info = info;
            elseif ischar(info)
                % path
                obj.info = imfinfo(info);
            end
            % dependent defaults
            obj.WorldLimits = {[1, obj.info(1).Width]+[-1,1]./2, [1,
            obj.info(1).Height]+[-1,1]./2]; % +/- 1/2 to move coordinate from
            pixel center to outer corner.
            % use override of defaults
            for i=1:2:length(varargin)
                obj.(varargin{i}) = obj.(varargin{i+1});
            end

        end

        function ind = find(obj, s)
            % return ind of info for specified layer
            if ~isnumeric(s)
                switch s
                    case 'thumbnail'
                        ind = 2;
                    case {'1','main','full','fullsize'}
                        ind = 1;
                    case 'identifier'
                        ind = length(obj.info)-1;
                    case 'slideregion'

```

```

        ind = length(obj.info);
        case 'image'
            ind = [1,3:(length(obj.info)-2)];
        case '1:4'
            if length(obj.info)>4, ind = 3; else ind =
[]; end
        case {'2','1:16'}
            if length(obj.info)>5, ind = 4; else ind =
[]; end
        case {'3','1:32'}
            if length(obj.info)>6, ind = 5; else ind =
[]; end
        case {'4','1:64'}
            if length(obj.info)>7, ind = 6; else ind =
[]; end
        case {'5','1:128'} % likely larger than relevant.
            if length(obj.info)>8, ind = 7; else ind =
[]; end
    end
    else
        error('numeric specification recieved in
PISlide.find(). Input should be a character array');
    end
end

function [PE,s] = PixelExtent(obj, s)
% Report PixelExtent for all image layers, or for
requested
% layer if 's' is specified.
if nargin==1
    % Default: all image layers
    s = obj.find('image');
end
iPEall = 2.^([0:2,4:numel(obj.info)]');
PE = iPEall(s) .* obj.Resolution;
end

function [im, imref] = data(obj, outref, doRescale)
% Read data in region imref in the first layer with equal
or
% resolution for the image region specified.
if nargin<3, doRescale = true; end
WL = [outref.XWorldLimits, outref.YWorldLimits];
PE = [outref.PixelExtentInWorldX,
outref.PixelExtentInWorldY];
% Determine which slide layer to read. Use smallest layer
with
% pixel sizes smaller or equal to the mask.
[PEi,s] = obj.PixelExtent();
use_layer = s(find(all(PEi <= PE, 2),1,'last'));

[im, imref] = obj.layerRegion(use_layer, outref);

```

```

        if doRescale && ~all([imref.PixelExtentInWorldX ==
outref.PixelExtentInWorldX, ...
            imref.PixelExtentInWorldY ==
outref.PixelExtentInWorldY])
            [im,imref] = imwarp(im, imref,
affine2d(), 'linear', 'OutputView', outref);
        end
    end

    function [im, imref] = layer(obj, s, doFlatten)
        % read and return specified layer (specify using numeric
indice
        % or character name
        if ischar(s)
            ind = obj.find(s);
        elseif isnumeric(s)
            ind = s;
        end
        if length(ind)>1
            error('non-specific layer requested');
        end
        im = imread(obj.info(ind).Filename, 'Index', ind, 'Info',
obj.info);
        imref = imref2d([size(im,1),size(im,2)],
obj.WorldLimits{:});
        if exist('doFlatten','var') && doFlatten
            im = obj.Flatten(im);
        end
    end

    function [im, imref] = layerRegion(obj, s, outref, doFlatten)
        % read and return specified layer (specify using numeric
indice
        % or character name
        if ischar(s)
            ind = obj.find(s);
        elseif isnumeric(s)
            ind = s;
        end
        if length(ind)>1
            error('non-specific layer requested');
        end

        imref = obj.imref(ind);

        [pixelRegion{1},pixelRegion{2}] =
imref.worldToSubscript(outref.XWorldLimits, outref.YWorldLimits);

        pixelRegion = {pixelRegion{1}-[0,1], pixelRegion{2}-
[0,1]};

        if ~mod(outref.PixelExtentInWorldX,
imref.PixelExtentInWorldX) &&...

```

```

        ~mod(outref.PixelExtentInWorldY,
imref.PixelExtentInWorldY)
        step = [outref.PixelExtentInWorldX,
outref.PixelExtentInWorldY]./[imref.PixelExtentInWorldX,
imref.PixelExtentInWorldY];
        if any(step~=1)
            % Extract only every other pixel from image file
            % instead of reading full matrix and interpolating
to
            % reduce matrix.
            pixelRegion = {[pixelRegion{1}
(1),step(1),pixelRegion{1}(2)],...
[pixelRegion{2}(1),step(2),pixelRegion{2}
(2)]};
        end
    end
    im = imread(obj.info(ind).Filename, 'Index', ind, 'Info',
obj.info, 'PixelRegion', pixelRegion);
    imref = imref2d(size(im), outref.XWorldLimits,
outref.YWorldLimits);
    if exist('doFlatten','var') && doFlatten
        im = obj.Flatten(im);
    end
end

function ref = imref(obj,s)
    if ischar(s)
        ind = obj.find(s);
    elseif isnumeric(s)
        ind = s;
    end
    if length(ind)>1
        error('non-specific layer requested');
    end
    info = obj.info(s);
    % ref = imref2d([info.Height, info.Width],
obj.WorldLimits{:});
    PE = obj.PixelExtent(s);
    ref = imref2d([info.Height, info.Width], PE(1), PE(2));
end
end
end

```

Published with MATLAB® R2016b

Table of Contents

| | |
|---|---|
| | 1 |
| Segmentation tool for peroxidase mediated IHC stains. | 1 |
| 2) Analyse color | 2 |
| Threshold | 2 |
| Combine intensity and saturation for segmentation, then mask with hue. | 3 |

```
function BW = segmentIHC( RGB, imref, varargin)
```

Segmentation tool for peroxidase mediated IHC stains.

Peroxidase mediated stains are dark, saturated and red. The function combines segmentation of each of these features using HSV transform and the B layer of RGB. The B layer is used because it has the greatest contrast of the three RGB layers for the red/brown color of the stain, and any mix of them (such as the perceptual transform made by `rgb2gray()`) will only serve to reduce the contrast.

There are two proposed algorithms that work OK. Either use `mode=='B&S&H'` to segment B, S and H independently and return their intersection, or use `mode=='BS&H'`, to combine Blue color channel (for intensity) and color saturation (according to HSV transform) prior to segmenting them, and then returning the intersection of the BS and H masks.

B is segmented using S is segmented using BS is segmented using H is segmented using fixed thresholds of $(H < 0.1)$ $(H > 0.9)$, which is equivalent to $-36 \text{ degrees} < H < 36 \text{ degrees}$.

```
ip = inputParser;
ip.addOptional('mask',true); % only pixels in mask will be considered
when segmenting
ip.addParameter('verbose',false); % plot figures of partial masks and
colorspaces
ip.addParameter('mode','B&S&H'); % Specifies segmentation algorithm
% Morphological (or other) processing between segmentation and merger
ip.addParameter('morphB',@(B)B); % Default value: no morphological
post processing (identity function).
ip.addParameter('morphS',@(S)S); % Default value: no morphological
post processing (identity function).
ip.addParameter('morphBS',@(BS)BS); % Default value: no morphological
post processing of BS (identity function).
ip.addParameter('morphH',@(H)H); % Default value: no morphological
post processing of H (identity function).
% Postprocessing of final mask
ip.addParameter('morphBW',@(BW)BW); % Default value: no morphological
post processing of final result (identity function).
ip.parse(varargin{:});
options = ip.Results;

options.mode = validatestring(options.mode,{'BS&H','B&S&H'});
mask = ip.Results.mask;
```

2) Analyse color

```
siz = size(RGB(:,:,1));

HSV = single(rgb2hsv(RGB));
H = HSV(:,:,1);
S = HSV(:,:,2);
B = RGB(:,:,3);
if strfind(options.mode, 'BS')
    if isa(RGB, 'uint8')
        BS = S - single(B)./255;
    elseif isfloat(RGB)
        BS = S - B;
    else % other numeric class
        error('TODO');
    end
end
```

Threshold

```
Hseg = @(H) H<0.1 | H>0.9; % fixed treshold

switch options.mode
    case 'B&S&H'

        % S
        if false
            S = HSV(:,:,2);
            [ind, N,X, order] =
thresholdKI(S(mask), 'mode','recursive');
            th = X( ind(find(order==2, 1, 'last')) ); % threshold
twice for higher values
            if false
                Smask = S > max(th,0.5); % threshold is at least 0.5
            else
                Smask = S > th;
            end
        else % fixed threshold
            Smask = S > 0.5;
        end
        % B
        % intensity = RGB(:,:,3); % use blue layer to identify dark
stains (red stain);
        [ind, N,X,order] = thresholdKI(B(mask), 'mode','recursive');
        cN = cumsum(N);
        th = X(ind(find(cN(ind) >= sum(Smask(:))/100,
1, 'first'))); % first threshold with at least 1 % of the pixels of
the saturation mask.
        th = 127; % looser fixed threshold.
        Bmask = B < th;
        % H
        BW = options.morphB(Bmask) & options.morphS(Smask) &
options.morphH(Hseg(H));
```

```

    if options.verbose

        figure(11),
        h = subplot(1,2,1), imshow(RGB)
        h(2) = subplot(1,2,2), imshow(1.5*single(Bmask) +
2*single(Smask) + single(Hseg(H)), [], colorbar; colormap('flag'));
title('Masks: H+1.5*B+2*S');
        hlink = linkprop(h, {'XLim','YLim'}); % NB! Gjør det mye
letter å sammenligne maske og RGB

    end

    case 'BS&H'

```

Combine intensity and saturation for segmentation, then mask with hue.

Currently gives a looser result than current B&S&H.

```

    if true
        [ind, N,X, order] =
thresholdKI(BS(mask), 'mode','recursive');
        th=X(ind(find(order==2,1,'last'))); % threshold twice
%         th=X(ind(find(X(ind)>0,1,'first')));
    else
        th = 0; % i.e. S > B;
    end
    BSmask = BS >= th;
    BW = options.morphBS(BSmask) & options.morphH(Hseg(H));

    if options.verbose, figure(11), imshow(BS, []), colorbar;
title('BS'); end
    % figure(12), imshowpair(CombMetric, BW, 'falsecolor');

    otherwise
        error('Unknown segmentation mode')
    end
end

```

Published with MATLAB® R2016b

Table of Contents

| | |
|--|---|
| | 1 |
| Threshold function by Kittler and Illingworths minimum error threshold algorithm. | 1 |
| Kittler an Illingworth minimum error thresholding v 2018 | 2 |
| Vectorized version of the kittler and illingworth minimum error thresholding algorithm. | 2 |

```
function [th, N, X, order] = thresholdKI(varargin)
```

Threshold function by Kittler and Illingworths minimum error threshold algorithm.

Parse input

```
[N,X, settings] = parseInput(varargin{:});
if strcmp(settings.mode, 'recursive')
    [~, ThInd, order] = kittler_and_illingworth(N, X); % ,
    settings.precision
    th = ThInd;
    % Note: th is now an indice and X(th) must be used to segment the
    data.
else %scalar
    th = kittler_and_illingworth(N, X); % , settings.precision
end
```

```
function [N,X, settings] = parseInput(varargin)
    ip = inputParser();
    ip.addRequired('data');
    ip.addOptional('histogram',[]);
    ip.addParameter('precision',12);
    ip.addParameter('mode','scalar');
    ip.parse(varargin{:});
    settings = ip.Results;
    if ~isempty(ip.Results.histogram)
        [N,X] = varargin{1:2};
    else
        A = varargin{1}(:);
        % matrix input
        if isinteger(A)
            [N,X] = hist(A,
double(intmin(class(A)):intmax(class(A))));
            % histcounts(A, 'integer');
            X = cast(X,class(A));
        elseif isfloat(A)
            [N,X] = hist(A, settings.precision);
        %
            [N,X] = histcounts(A);
        end
    end
end
```

```
end
```

```
end
```

Kittler and Illingworth minimum error thresholding v 2018

```
function [th, ThInd, order] = kittler_and_illingworth(im_h, im_v)
```

Vectorized version of the kittler and illingworth minimum error thresholding algorithm.

Variables M0-M2 are statistical moments.

```
% Mass (left hand side)
M0a = cumsum(im_h);

% a posteriori probability
P1 = M0a ./ M0a(end);
P2 = 1-P1;
% Standard deviations
% Left hand side of histogram
im_h = double(im_h);
vals = (0:numel(im_h)-1);
M1a = cumsum( vals.*im_h );
M2a = cumsum( vals.^2.*im_h );
STDEV1 = 1./M0a.*sqrt(M0a.*M2a - M1a.^2);
% Right hand side of histogram
% vals = vals(end:-1:1);
M0b = cumsum(im_h, 'reverse');
M1b = cumsum( vals.*im_h, 'reverse');
M2b = cumsum( vals.^2.*im_h, 'reverse' );
STDEV2 = 1./M0b.*sqrt(M0b.*M2b - M1b.^2);

% error function
J = 1 + 2*(P1.*log(STDEV1) + P2.*log(STDEV2)) - 2*(P1.*log(P1) +
  P2.*log(P2));
J(~isfinite(J)) = nan;
% figure(1002), plot(J);

[~, ind] = nanmin(J);
th = im_v(ind);

if nargin>1
    ThInd = ind;
    [ThInd, order, convergance] = ki_threshold_tree(M0a, M1a, M2a, M0b,
    M1b, M2b, {'<', '>'}, ThInd);
end
% th = ThInd;

end
```

```

function [ThTree, order, convergance] = ki_threshold_tree(M0a,M1a,M2a,
    M0b, M1b, M2b, operator, ThTree, order, convergance)
% Using the cumulative sum vectors of the vectorised ki_threshold
% method,
% it is possible to obtain the result of the algorithm applied again
% on
% only the pixels in a selected image rage (i.e. those left by the
% previous
% threshold) without recalculating histogram or cumulative vectors.
% Because
% this solution is cheap the function finds all thresholds in both
% direction by recursively calling itself.
if ~exist('convergance','var')
    convergance = false(1,numel(operator));
end
if ~exist('ThTree','var') || isempty(ThTree)
    ThTree = {0};
end
if ~exist('order','var')
    order = 1;
end

ThTree0 = ThTree;
if ~iscell(operator), operator = {operator}; end
for i=1:length(operator)%
    opr = operator{i};
    if convergance(i), continue, end
    if isa(opr, 'function_handle'), opr = func2str(opr); end
    switch opr
        case {'<', 'lt'} % keep values below threshold.
            % only include image data with th>Th, i.e. retreshold the
            % part of the
            % image on the specified side of the threshold.
            thind = ThTree0(1);
            Ind = 1:ThTree0(1)-1;
            Pa = M0a(Ind) ./ M0a(Ind(end));
            STDEV1 = 1./M0a(Ind).*sqrt(M0a(Ind).*M2a(Ind) -
M1a(Ind).^2);
            Pb = 1-Pa;
            M0b2 = M0b(Ind)-M0b(Ind(end)+1);
            M1b2 = M1b(Ind)-M1b(Ind(end)+1);
            M2b2 = M2b(Ind)-M2b(Ind(end)+1);
            STDEV2 = 1./M0b2.*sqrt(M0b2.*M2b2 - M1b2.^2);
        case {'>', 'gt'}
            % keep values above threshold
            thind = ThTree0(end);
            Ind = ThTree0(end)+1:numel(M0a);
            Pb = M0b(Ind) ./ M0b(Ind(1));
            STDEV2 = 1./M0b(Ind).*sqrt(M0b(Ind).*M2b(Ind) -
M1b(Ind).^2);
            Pa = 1-Pb;
            M0a2 = M0a(Ind)-M0a(Ind(1)-1);
            M1a2 = M1a(Ind)-M1a(Ind(1)-1);
    end
end

```

```

        M2a2 = M2a(Ind)-M2a(Ind(1)-1);
        STDEV1 = 1./M0a2.*sqrt(M0a2.*M2a2 - M1a2.^2);
    end
    J = 1 + 2*(Pa.*log(STDEV1) + Pb.*log(STDEV2)) - 2*(Pa.*log(Pa) +
Pb.*log(Pb));
    J(~isfinite(J)) = nan;
    [~, ind] = nanmin(J);
    % if ind is first or last non-nan, then the value is non-sensical.
    csJ = cumsum(isfinite(J));
    if csJ(ind)==1 || csJ(ind)==csJ(end)
        % minimum J is at edge. No true minimum found.
        convergence(i) = true;
    else
        ind = Ind(ind);
        % th = im_v(ind);
    % figure, plot(J)

        if any(ThTree == ind) ||... % already selected ind
%any( cellfun(@(C)C==ind, [ThTree]) )
            ind==1 || ind == numel(M0a) ||... % first or last
entry
                M0a(ind-1) == 0 || M0a(ind+1) == M0a(end) % all or no
data beyond this indice.
                convergence(i) = true;
        end
        if ind < thind
            ThTree = [ind, ThTree];
            order = [order(1)+1, order];
        elseif ind > thind
            ThTree = [ThTree, ind];
            order = [order, order(end)+1];
        end
    end
end
end
% Recursive
if ~all(convergence)
    [ThTree, order, convergence] = ki_threshold_tree(M0a,M1a,M2a, M0b,
M1b, M2b, operator, ThTree, order, convergence);
end
end

```

Published with MATLAB® R2016b

```
function BW = postprocessIHC(BW, imref, ihc_type)
% Morphological processing of BW mask.
% See "Morphological Operations" in help documentation, and in
% particular:
% imdilate(), imerode(), imopen(), imclose(), imreconstruct() and
% bwmorph().
PE = [imref.PixelExtentInWorldX, imref.PixelExtentInWorldY];

switch ihc_type
    % make individual adaptations.
    case {'CD3', 'CD34', 'CA9', }
        rad1 = ceil(2*16./PE(1)/2);
        rad2 = ceil(4*16./PE(1)/2);

        BW = imclose(BW, strel('disk',rad2));
        BW = imopen(BW, strel('disk',rad1));

    case {'HIF-1@'}
        rad1 = ceil(1*16./PE(1)/2);
        rad2 = ceil(4*16./PE(1)/2);

        BW = imclose(BW, strel('disk',rad2));
        BW = imopen(BW, strel('disk',rad1));
end
end
```

Published with MATLAB® R2016b

Table of Contents

| | |
|------------|---|
| | 1 |
| CD | 2 |
| CA | 3 |
| HIF | 3 |
| Save | 3 |

```
% Extract features from the registered images based on segmented and
post
% processed masks.
```

```
clear,
format compact
```

```
filename='C:\Users\Vidar\Downloads\Master\Pathology\patients.xlsx';
[numb,txt,row] = xlsread(filename);
nrPatients=length(row)-1;
```

```
for patient = 1:nrPatients
```

```
data_path = {'D:\Oxytarget Pathology\' char(txt(patient+1,23)) '\'
char(txt(patient+1,2)) ' ' num2str(numb(patient,1))}];
```

```
p = {};
for dp = data_path(:)
    fn = dir([dp{1},filesep,'*.svs']);
    fn = fullfile(dp, {fn.name});
    p(end+(1:length(fn))) = fn;
end
```

```
nr_slides=[0 0 0 0 0 0];
for i=1:numel(nr_slides)
    if ~isnan(numb(patient,i+12))
        nr_slides(i)=1;
    end
end
```

```
FN = (1:sum(nr_slides(:) == 1));
```

```
key = {'HPS', 'CD3', 'CD8', 'CD34', 'CA9', 'HIF-1@'};
```

```
for i = 1:numel(FN)
    cp = p(FN(i));
    [currentpath,casename] = fileparts(cp{:});
    pattern = sprintf('%s%s%s-*mask*',currentpath,filesep,casename);
    mask_fn = dir(pattern);
    if ~isempty(mask_fn)
        MaskFN{i} = strcat(currentpath, filesep, {mask_fn.name});
        mask = [];
    end
end
```

```

[currentpath,casename] = fileparts(p{FN(1)});

CC = PICase(casename,key, p(FN)); % CC = current case
CC.addMasks(key(hasMask), MaskFN(hasMask), maskBehaviour);

PE = [4 4];
[imcropHPS, imrefHPS, mask] = CC.extractMaskedSlide('HPS',PE);

```

CD

```

T=load([char(data_path) '\ihc_mask_post_CD'], 'ihc_mask_post');
ihc_mask_post_cd=T.('ihc_mask_post');

[Lbl,num] = bwlabel(ihc_mask_post_cd.*mask);
CD_statsP =
    regionprops(Lbl,ihc_mask_post_cd,'Area','Centroid','MajorAxisLength','MinorAxisLe
CD_stainedFraction = sum(ihc_mask_post_cd(mask))./sum(mask(:));
CD_microVesselDensity = num./(sum(mask(:)));
CD_averageStainSize = mean([CD_statsP.Area]);
CD_averageRadius = mean([CD_statsP.MajorAxisLength
    CD_statsP.MinorAxisLength],2)/2;
CD_MeanSolidity = mean([CD_statsP.Solidity]);
CD_NrVessels=num;
CD_VesselDensity=(num/sum([CD_statsP.Area])); % invers av vessel size
    (aka average stain size)

% Calculate intercapillary distance (ICD)
distance=zeros(num,1);
index_n=zeros(num,1);
vessels=zeros(num,2);

for i =1:length(CD_statsP)
    vessels(i,:)=CD_statsP(i).Centroid;
end
for i=1:length(CD_statsP)
    if i==1
        [index_n(i),distance(i)] =
dsearchn(vessels(2:end,:),CD_statsP(i).Centroid);
        index_n(i)=index_n(i)+1;
    elseif(i==110)
        [index_n(i),distance(i)] = dsearchn(vessels(1:
(length(CD_statsP)-1),:),CD_statsP(i).Centroid);
    else
        [index_n(i),distance(i)] = dsearchn(vessels([1:i-1,i
+1:end],:),CD_statsP(i).Centroid);
        if index_n(i)>=i
            index_n(i)=index_n(i)+1;
        end
    end
end
end

CD_meanICD=mean(distance);

```

CA

```
T=load([char(data_path) '\ihc_mask_post_CA'], 'ihc_mask_post');
ihc_mask_post_ca=T.('ihc_mask_post');

[Lbl,num] = bwlabel(ihc_mask_post_ca.*mask);
CA_statsP = regionprops(Lbl,ihc_mask_post_ca,'Area');
CA_stainedFraction = sum(ihc_mask_post_ca(mask))./sum(mask(:));
CA_averageStainSize = mean([CA_statsP.Area]);
```

HIF

```
if patient ~= 17 %no hif image
    T=load([char(data_path) '\ihc_mask_post_HIF'], 'ihc_mask_post');
    ihc_mask_post_hif=T.('ihc_mask_post');

    [Lbl,num] = bwlabel(ihc_mask_post_hif.*mask);
    HIF_statsP = regionprops(Lbl,ihc_mask_post_hif,'Area');
    HIF_stainedFraction = sum(ihc_mask_post_hif(mask))./sum(mask(:));
    HIF_averageStainSize = mean([HIF_statsP.Area]);

    [~,HPSfname] = fileparts(p{FN(1)});

    HIF_statTable(1,:) =
        table(string(HPSfname),HIF_stainedFraction,HIF_averageStainSize, 'VariableNames',
            {'HPS_filename', 'HIF_fraction', 'HIF_averageStainSize'});
end
```

Save

```
CD_statTable(1,:) =
    table(string(HPSfname),CD_stainedFraction,CD_microVesselDensity,CD_averageStainSi
        CD_meanICD, ...
        'VariableNames',
        {'HPS_filename', 'CD_StainedFraction', 'CD_microVesselDensity', 'CD_averageStainSize'});
CA_statTable(1,:) =
    table(string(HPSfname),CA_stainedFraction,CA_averageStainSize, 'VariableNames',
        {'HPS_filename', 'CA_fraction', 'CA_averageStainSize'});
if patient==17

    save([char(data_path) '\Path_data.mat'], 'CD_statTable', 'CA_statTable');
else

    save([char(data_path) '\Path_data.mat'], 'CD_statTable', 'CA_statTable', 'HIF_statTable');
end

end
```

Published with MATLAB® R2016b

Figure 21: Kaplan-Meier plot for the solidity

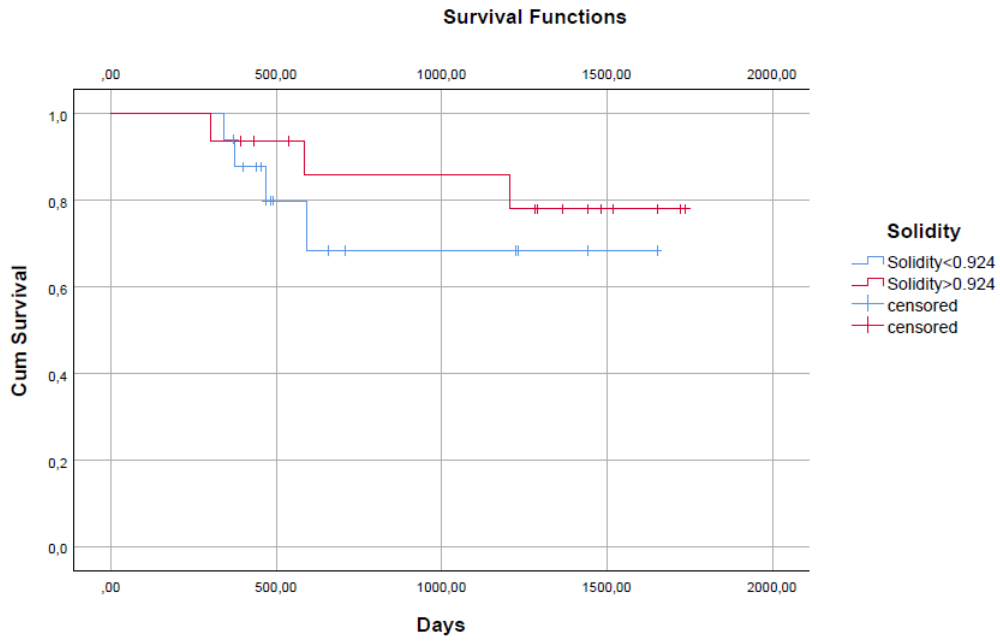


Figure 22: Kaplan-Meier plot vessel radius

Figure 23: Kaplan-Meier plot for the number of vessels

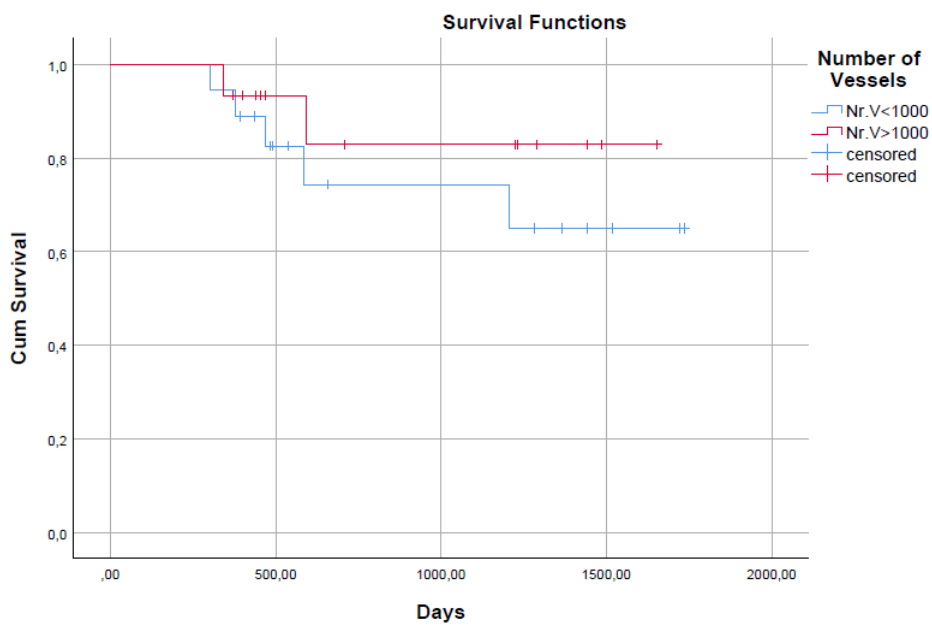


Figure 24: Kaplan-Meier plot for MVD

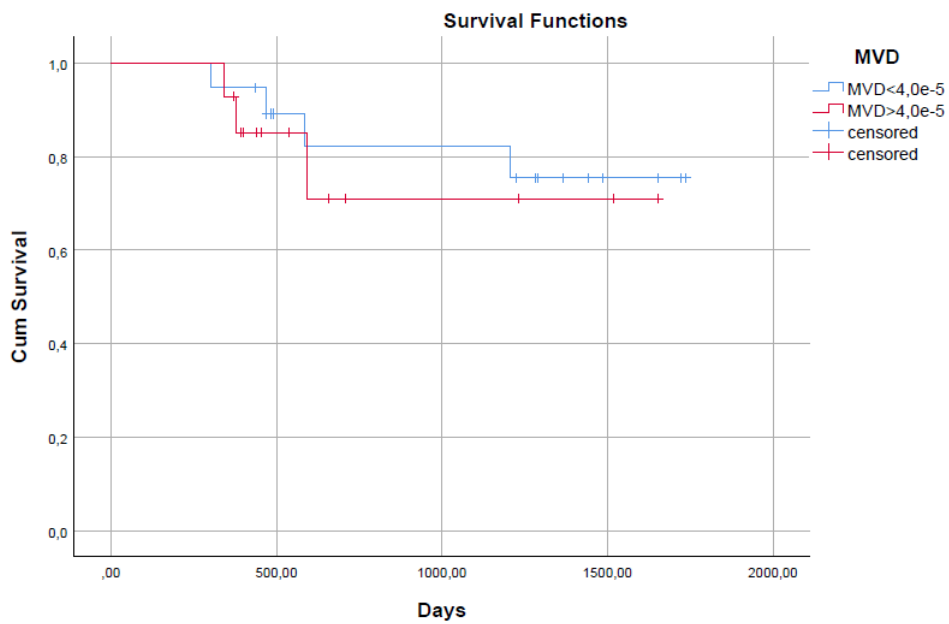


Figure 25: Kaplan-Meier plot for ICD

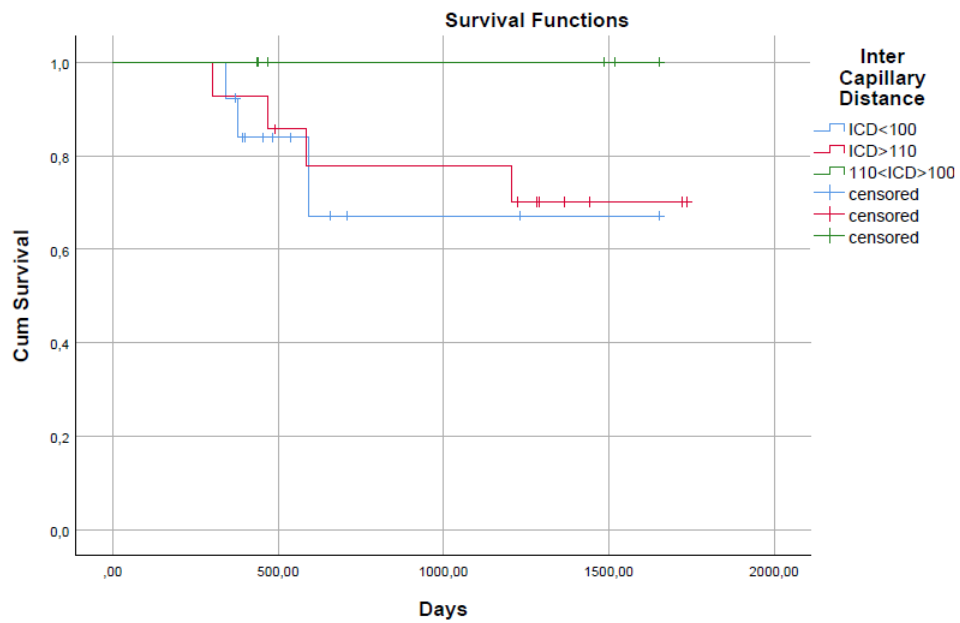


Figure 26: Kaplan-Meier plot

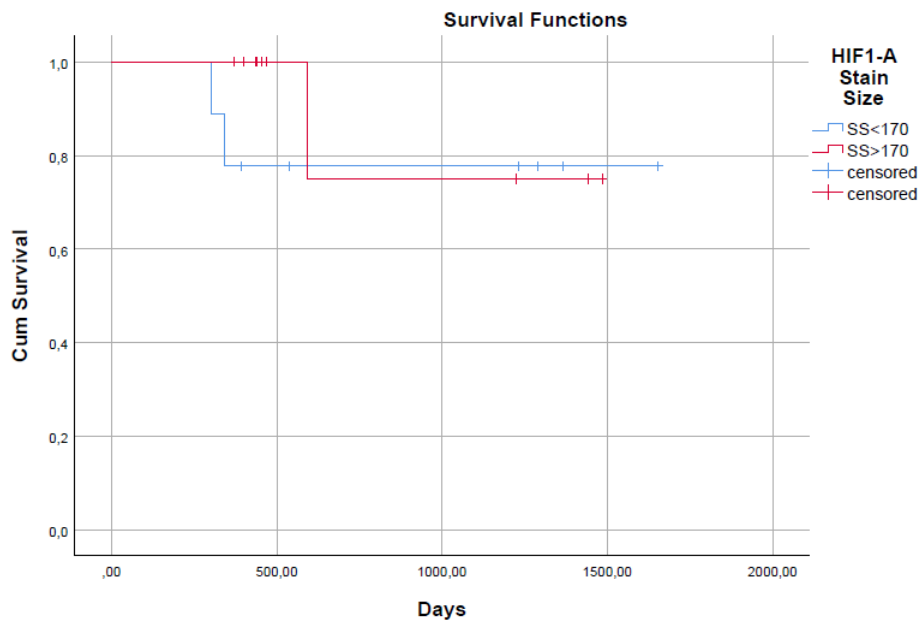


Figure 27: Kaplan-Meier plot for the stained fraction of HIF-1 α

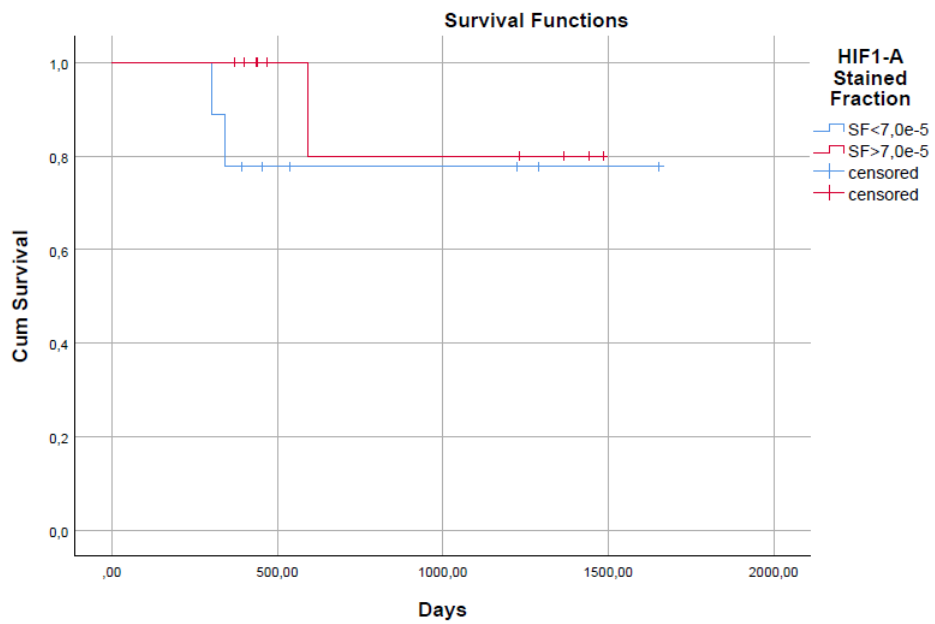


Figure 28: Kaplan-Meier plot for the stain size of HIF-1 α

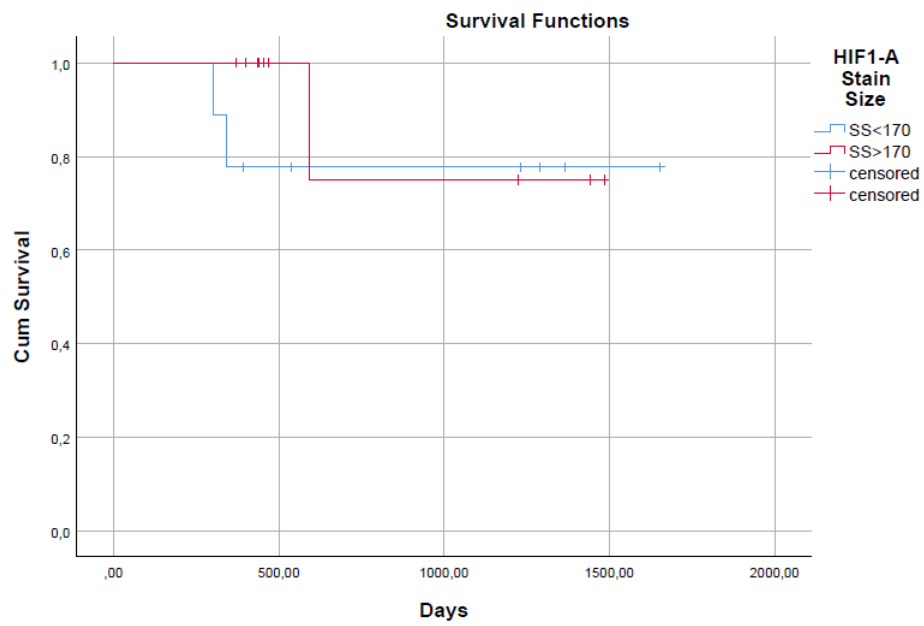


Figure 29: Kaplan-Meier plot for the stain size of CAIX

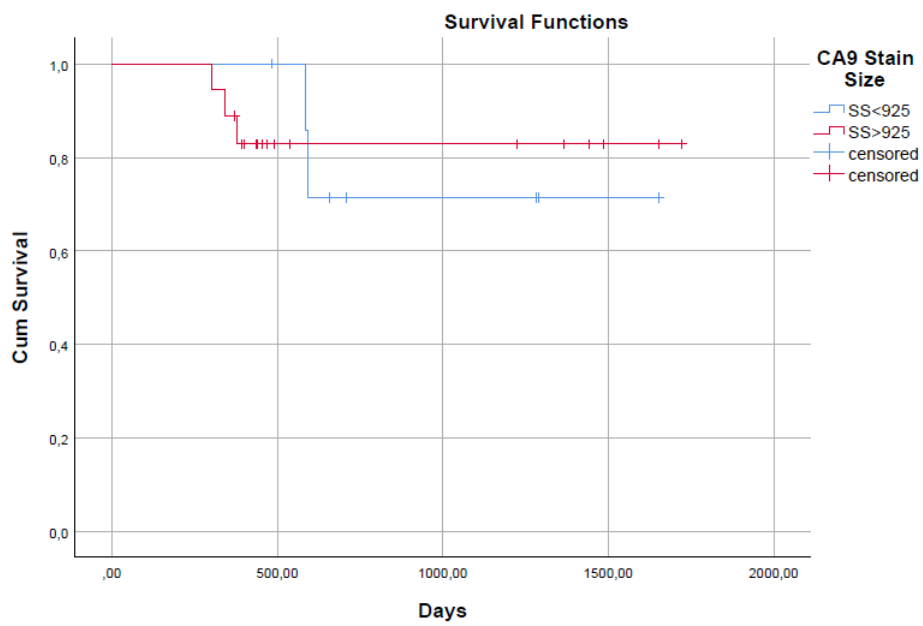


Figure 30: Kaplan-Meier plot for the stained fraction of CAIX

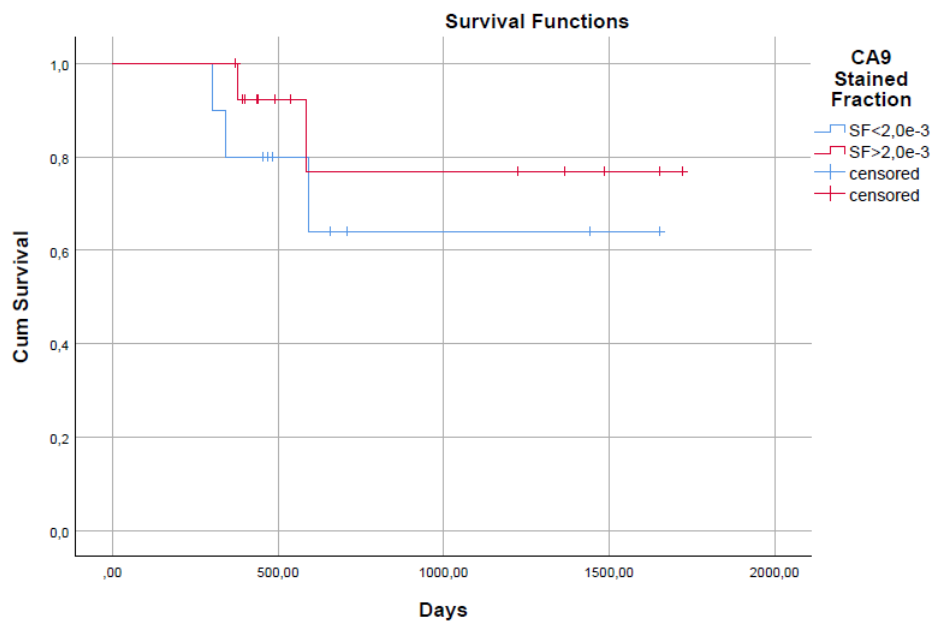


Table 19: MR values for all patients. Part 1/5.

| Patient | Static Median R_2^* | Dynamic Median R_2^* -peak _{enh} | R_2^* -AUC median for time point 49s |
|---------|-----------------------|---|--|
| 24 | 439,6 | 21,4 | 229,5 |
| 25 | 299,2 | 25,7 | 28,9 |
| 27 | 352,7 | 37,0 | 369,2 |
| 29 | 459,4 | 30,2 | 178,7 |
| 30 | 435,1 | 24,6 | 278,2 |
| 32 | 370,0 | 38,2 | 404,7 |
| 31 | 319,7 | 35,7 | 205,9 |
| 34 | 283,5 | 21,6 | 23,1 |
| 39 | 383,8 | 49,2 | 694,1 |
| 40 | 472,0 | 27,2 | 246,1 |
| 41 | 429,2 | 21,3 | 228,9 |
| 43 | 348,5 | 42,4 | 331,3 |
| 44 | 432,5 | 23,9 | 42,3 |
| 45 | 346,7 | 39,1 | 282,5 |
| 46 | 436,6 | 15,5 | 118,7 |
| 47 | 368,0 | 38,0 | 474,2 |
| 48 | 452,2 | 56,0 | 414,6 |
| 49 | 348,2 | 36,5 | 331,7 |
| 50 | 455,1 | 23,4 | 314,8 |
| 51 | 452,3 | 13,0 | 106,5 |
| 52 | 463,2 | 14,9 | 140,1 |
| 54 | 387,8 | 23,1 | 87,3 |
| 55 | 481,9 | 46,5 | 546,5 |
| 56 | 398,1 | 40,9 | 131,6 |
| 57 | 17,0 | 25,3 | 231,2 |
| 58 | 0,0 | 0,0 | 0,0 |
| 60 | 0,0 | 0,0 | 0,0 |
| 64 | 14,3 | 34,3 | 370,3 |
| 65 | 32,3 | 62,7 | 367,9 |
| 67 | 12,7 | 22,8 | 165,6 |
| 68 | 15,5 | 32,4 | 234,3 |
| 69 | 25,3 | 30,1 | 180,2 |
| 72 | 17,9 | 47,1 | 472,5 |
| 73 | 14,2 | 20,9 | 149,1 |
| 74 | 18,8 | 36,9 | 225,9 |
| 75 | 30,4 | 33,1 | 62,1 |
| 76 | 16,6 | 26,5 | 251,6 |
| 77 | 28,7 | 23,8 | 50,9 |
| 78 | 20,3 | 23,5 | 172,1 |
| 79 | 17,0 | 25,2 | 245,6 |
| 80 | 18,2 | 32,3 | 166,4 |
| 83 | 16,2 | 24,1 | 136,2 |
| 85 | 24,7 | 20,9 | 58,3 |

Table 20: MR values for all patients. Part 2/5.

| Patient | Static Median R_2^* | Dynamic Median R_2^* -peak _{enh} | R_2^* -AUC median for time point 49 s |
|---------|-----------------------|---|---|
| 87 | 39,6 | 75,2 | 105,3 |
| 88 | 24,2 | 33,0 | 154,7 |
| 89 | 24,2 | 39,1 | 248,1 |
| 90 | 23,1 | 31,2 | 199,6 |
| 92 | 56,5 | 49,9 | 213,6 |
| 94 | 13,8 | 38,0 | 395,3 |
| 95 | 16,4 | 42,1 | 459,9 |
| 96 | 16,1 | 34,7 | 363,1 |
| 102 | 16,2 | 37,4 | 310,8 |
| 103 | 18,5 | 44,8 | 496,4 |
| 106 | 26,6 | 25,6 | 76,6 |
| 107 | 22,1 | 25,0 | 181,2 |
| 108 | 25,5 | 32,6 | 179,2 |
| 110 | 41,4 | 39,3 | 202,0 |
| 111 | 20,1 | 29,9 | 171,7 |
| 112 | 34,8 | 27,2 | 39,0 |
| 113 | 20,8 | 29,1 | 128,4 |
| 114 | 16,8 | 16,1 | 98,8 |
| 115 | 33,3 | 43,9 | 226,5 |
| 116 | 18,8 | 43,0 | 268,3 |
| 118 | 0,0 | 0,0 | 0,0 |
| 119 | 42,4 | 100,3 | 153,4 |
| 120 | 17,7 | 30,8 | 192,8 |
| 121 | 15,3 | 28,9 | 280,5 |
| 123 | 19,4 | 31,8 | 65,0 |
| 125 | 33,3 | 40,6 | 311,3 |
| 126 | 20,5 | 21,4 | 125,7 |
| 127 | 14,1 | 53,3 | 593,5 |
| 128 | 18,9 | 37,4 | 329,6 |
| 131 | 18,2 | 29,1 | 323,8 |
| 133 | 19,1 | 38,8 | 343,4 |
| 134 | 17,1 | 61,4 | 616,9 |
| 138 | 13,1 | 24,7 | 83,2 |
| 142 | 14,5 | 14,3 | 126,4 |
| 143 | 32,4 | 47,1 | 162,8 |
| 144 | 17,5 | 36,9 | 359,6 |
| 146 | 31,0 | 32,9 | 291,2 |
| 147 | 44,6 | 47,3 | 66,8 |
| 148 | 16,7 | 36,9 | 121,8 |
| 149 | 34,3 | 42,4 | 2,7 |
| 150 | 13,6 | 25,0 | 170,0 |
| 151 | 20,4 | 51,9 | 338,7 |
| 152 | 19,5 | 56,8 | 103,5 |
| 153 | 17,4 | 37,1 | 387,1 |

Table 21: MR values for all patients. Part 3/5.

| Patient | Static Median R_2^* | Dynamic Median R_2^* -peak _{enh} | R_2^* -AUC median for time point 49 s |
|---------|-----------------------|---|---|
| 154 | 73,3 | 69,6 | -20,9 |
| 155 | 21,0 | 31,5 | 236,3 |
| 156 | 30,8 | 47,9 | 363,0 |
| 157 | 22,6 | 53,6 | 450,4 |
| 158 | 59,8 | 73,2 | 71,6 |
| 159 | 22,4 | 40,8 | 200,1 |
| 160 | 23,7 | 31,0 | 219,5 |
| 161 | 19,6 | 60,9 | 521,7 |
| 162 | 17,1 | 51,3 | 430,9 |
| 163 | 20,3 | 38,4 | 324,9 |
| 164 | 16,0 | 50,4 | 522,9 |
| 165 | 17,1 | 34,9 | 342,5 |
| 166 | 21,0 | 29,6 | 33,8 |
| 169 | 27,0 | 28,9 | 191,5 |
| 170 | 16,9 | 27,4 | 133,8 |
| 171 | 26,0 | 50,4 | 241,3 |

Table 22: MR values for all patients. Part 4/5.

| patient | R_2^* -AUC, time point 135 s | R_2^* -AUC, time point 222 s | R_2^* -AUC, time point 525 s |
|---------|--------------------------------|--------------------------------|--------------------------------|
| 24 | 438 | 1279 | 2335 |
| 25 | 28 | 21 | -15 |
| 27 | 934 | 2992 | 6015 |
| 29 | 596 | 1491 | 2202 |
| 30 | 533 | 890 | 1546 |
| 32 | 580 | 1395 | 2268 |
| 31 | 231 | 180 | -155 |
| 34 | 26 | -282 | -875 |
| 39 | 828 | 1124 | 1298 |
| 40 | 334 | 612 | 628 |
| 41 | 382 | 962 | 1616 |
| 43 | 423 | 597 | 520 |
| 44 | 361 | 1244 | 1820 |
| 45 | 285 | 162 | -294 |
| 46 | 222 | 523 | 591 |
| 47 | 767 | 1770 | 2981 |
| 48 | 1038 | 2287 | 6175 |
| 49 | 575 | 1399 | 3383 |
| 50 | 734 | 1099 | 1690 |
| 51 | 375 | 400 | 949 |
| 52 | 256 | 690 | 1129 |
| 54 | 366 | 1055 | 1891 |
| 55 | 779 | 1537 | 2417 |
| 56 | 430 | 864 | 247 |
| 57 | 553 | 696 | 1040 |
| 58 | 0 | 0 | 0 |
| 60 | 0 | 0 | 0 |
| 64 | 429 | 954 | 2384 |
| 65 | 623 | 649 | 194 |
| 67 | 423 | 578 | 966 |
| 68 | 884 | 1240 | 2226 |
| 69 | 622 | 792 | 883 |
| 72 | 984 | 1275 | 2022 |
| 73 | 654 | 936 | 1762 |
| 74 | 851 | 1277 | 3079 |
| 75 | 80 | 39 | -171 |
| 76 | 726 | 1024 | 1670 |
| 77 | -3 | -160 | -552 |
| 78 | 657 | 864 | 1284 |
| 79 | 787 | 1091 | 1869 |
| 80 | 505 | 725 | 2236 |
| 83 | 419 | 688 | 1431 |
| 85 | -19 | -161 | -2245 |
| 87 | 84 | -22 | 730 |
| 88 | 922 | 1339 | 2748 |
| 89 | 792 | 1290 | 2901 |
| 90 | 321 | 739 | 1444 |

Table 23: MR values for all patients. Part 5/5.

| patient | R_2^* -AUC, time point 135 s | R_2^* -AUC, time point 222 s | R_2^* -AUC, time point 525 s |
|---------|--------------------------------|--------------------------------|--------------------------------|
| 92 | 409 | 236 | 641 |
| 94 | 1261 | 1698 | 2662 |
| 95 | 1429 | 1977 | 3586 |
| 96 | 868 | 1121 | 1633 |
| 102 | 951 | 1333 | 2426 |
| 103 | 1250 | 1668 | 2772 |
| 106 | -19 | -225 | -958 |
| 107 | 496 | 662 | 959 |
| 108 | 274 | 649 | 1831 |
| 110 | 549 | 535 | 401 |
| 111 | 449 | 519 | 282 |
| 112 | 9 | -191 | -1308 |
| 113 | 264 | 382 | 867 |
| 114 | 414 | 603 | 1155 |
| 115 | 363 | 254 | -545 |
| 116 | 598 | 752 | 2215 |
| 118 | 0 | 0 | 0 |
| 119 | 532 | 712 | 1843 |
| 120 | 561 | 750 | 881 |
| 121 | 622 | 854 | 1592 |
| 123 | 898 | 1069 | 1386 |
| 125 | 678 | 758 | 1100 |
| 126 | 315 | 285 | -216 |
| 127 | 1292 | 1739 | 3013 |
| 128 | 1140 | 1593 | 3923 |
| 131 | 918 | 1322 | 2320 |
| 133 | 749 | 1024 | 1623 |
| 134 | 1334 | 1761 | 3028 |
| 138 | 686 | 886 | 1382 |
| 142 | 336 | 487 | 935 |
| 143 | 853 | 1083 | 1708 |
| 144 | 869 | 1197 | 2219 |
| 146 | 806 | 921 | 847 |
| 147 | 487 | 717 | 1021 |
| 148 | 261 | 915 | 3161 |
| 149 | -77 | -168 | -173 |
| 150 | 712 | 1016 | 2045 |
| 151 | 745 | 792 | 1984 |
| 152 | 271 | 648 | 3356 |
| 153 | 1073 | 1409 | 2333 |
| 154 | -1213 | -3383 | -10482 |
| 155 | 585 | 739 | 969 |
| 156 | 935 | 1290 | 2986 |
| 157 | 903 | 997 | 946 |
| 158 | -399 | -1751 | -5453 |
| 159 | 0 | 0 | 0 |
| 160 | 272 | 269 | -219 |
| 161 | 1735 | 2222 | 3259 |
| 162 | 747 | 1538 | 3553 |
| 163 | 451 | 939 | 1388 |
| 164 | 845 | 1656 | 3607 |
| 165 | 981 | 1333 | 2357 |

Table 24: Results from quantitative immunohistochemisrty of *CD34* stain. Part 1/2.

| Patient | Stain Fraction | MVD $\frac{1}{\mu\text{m}}$ | Vessel Size (μm) | Solidity |
|---------------|----------------|-----------------------------|-------------------------------|----------|
| Oxytarget 1 | 0,00375 | 2,23E-05 | 168,25 | 0,927 |
| Oxytarget 4 | 0,01141 | 6,42E-05 | 177,72 | 0,936 |
| Oxytarget 5 | 0,00730 | 5,38E-05 | 135,66 | 0,943 |
| Oxytarget 16 | 0,02301 | 1,03E-04 | 223,46 | 0,929 |
| Oxytarget 17 | 0,01742 | 7,06E-05 | 246,75 | 0,924 |
| Oxytarget 21 | 0 | 0 | 0 | 0 |
| Oxytarget 22 | 0,00796 | 3,58E-05 | 222,11 | 0,884 |
| Oxytarget 24 | 0,00422 | 2,41E-05 | 175,39 | 0,945 |
| Oxytarget 32 | 0,00736 | 4,94E-05 | 148,76 | 0,939 |
| Oxytarget 41 | 0,02225 | 8,41E-05 | 264,38 | 0,932 |
| Oxytarget 46 | 0,01637 | 7,95E-05 | 205,75 | 0,936 |
| Oxytarget 47 | 0,00945 | 3,51E-05 | 269,00 | 0,907 |
| Oxytarget 48 | 0,00560 | 3,40E-05 | 164,69 | 0,945 |
| Oxytarget 58 | 0,00474 | 2,88E-05 | 164,59 | 0,940 |
| Oxytarget 60 | 0 | 0 | 0 | 0 |
| Oxytarget 72 | 0,00750 | 3,94E-05 | 190,52 | 0,940 |
| Oxytarget 73 | 0,00463 | 2,44E-05 | 189,71 | 0,935 |
| Oxytarget 84 | 0,02501 | 9,00E-05 | 277,96 | 0,920 |
| Oxytarget 85 | 0,01783 | 5,03E-05 | 354,87 | 0,919 |
| Oxytarget 90 | 0,01122 | 6,64E-05 | 169,11 | 0,930 |
| Oxytarget 103 | 0,02777 | 9,13E-05 | 304,14 | 0,920 |
| Oxytarget 107 | 0 | 0 | 0 | 0 |
| Oxytarget 120 | 0 | 0 | 0 | 0 |
| Oxytarget 121 | 0 | 0 | 0 | 0 |
| Oxytarget 124 | 0,07899 | 1,62E-04 | 487,93 | 0,897 |
| Oxytarget 128 | 0,02668 | 1,30E-04 | 205,71 | 0,922 |
| Oxytarget 146 | 0,02643 | 9,24E-05 | 286,01 | 0,930 |
| Oxytarget 153 | 0,10268 | 2,66E-04 | 386,08 | 0,889 |
| Oxytarget 154 | 0,00998 | 4,34E-05 | 230,10 | 0,923 |
| Oxytarget 157 | 0,02038 | 7,73E-05 | 263,70 | 0,920 |
| Oxytarget 160 | 0,01793 | 7,72E-05 | 232,17 | 0,924 |
| Oxytarget 161 | 0 | 0 | 0 | 0 |
| Oxytarget 162 | 0,02547 | 9,89E-05 | 257,60 | 0,923 |
| Oxytarget 164 | 0,04150 | 1,20E-04 | 345,00 | 0,906 |
| Oxytarget 165 | 0,01999 | 8,15E-05 | 245,35 | 0,924 |
| Oxytarget 166 | 0,02011 | 7,80E-05 | 257,76 | 0,931 |
| Oxytarget 171 | 0,03618 | 8,74E-05 | 413,98 | 0,914 |
| Oxytarget 172 | 0,03369 | 9,61E-05 | 350,68 | 0,927 |
| Oxytarget 174 | 0,04330 | 1,43E-04 | 302,91 | 0,915 |

Table 25: Results from quantitative immunohistochemisrty of *CD34* stain. Part 2/2.

| Patient | Number Vessels | Vessel Radius (μm) | ICD (μm) |
|---------------|----------------|---------------------------------|-----------------------|
| Oxytarget 1 | 16 | 7,36 | 82,82 |
| Oxytarget 4 | 29 | 6,64 | 96,41 |
| Oxytarget 5 | 293 | 6,54 | 71,18 |
| Oxytarget 16 | 1240 | 8,19 | 45,94 |
| Oxytarget 17 | 1472 | 8,75 | 52,54 |
| Oxytarget 21 | 0 | 0 | 0 |
| Oxytarget 22 | 62 | 8,50 | 74,59 |
| Oxytarget 24 | 308 | 7,27 | 84,36 |
| Oxytarget 32 | 17 | 6,43 | 117,77 |
| Oxytarget 41 | 954 | 8,96 | 53,46 |
| Oxytarget 46 | 1305 | 7,97 | 52,87 |
| Oxytarget 47 | 8 | 9,02 | 151,83 |
| Oxytarget 48 | 1295 | 7,21 | 69,43 |
| Oxytarget 58 | 333 | 7,04 | 85,85 |
| Oxytarget 60 | 0 | 0 | 0 |
| Oxytarget 72 | 1481 | 7,57 | 60,74 |
| Oxytarget 73 | 201 | 7,55 | 88,91 |
| Oxytarget 84 | 1123 | 9,06 | 47,11 |
| Oxytarget 85 | 1745 | 9,34 | 63,06 |
| Oxytarget 90 | 83 | 7,21 | 78,53 |
| Oxytarget 103 | 3555 | 9,18 | 47,60 |
| Oxytarget 107 | 0 | 0 | 0 |
| Oxytarget 120 | 0 | 0 | 0 |
| Oxytarget 121 | 0 | 0 | 0 |
| Oxytarget 124 | 4048 | 11,03 | 39,25 |
| Oxytarget 128 | 714 | 7,88 | 47,11 |
| Oxytarget 146 | 897 | 8,28 | 48,72 |
| Oxytarget 153 | 135 | 10,36 | 35,24 |
| Oxytarget 154 | 68 | 7,67 | 94,49 |
| Oxytarget 157 | 599 | 8,90 | 48,45 |
| Oxytarget 160 | 2198 | 8,28 | 51,08 |
| Oxytarget 161 | 0 | 0 | 0 |
| Oxytarget 162 | 1742 | 8,53 | 45,67 |
| Oxytarget 164 | 1441 | 9,81 | 44,76 |
| Oxytarget 165 | 1250 | 8,60 | 52,35 |
| Oxytarget 166 | 781 | 8,39 | 52,45 |
| Oxytarget 171 | 2749 | 9,71 | 49,87 |
| Oxytarget 172 | 908 | 8,85 | 48,08 |
| Oxytarget 174 | 2853 | 9,32 | 43,15 |

Table 26: Results from quantitative immunohistochemisrty of CAIX and HIF1- α stains.

| Patient | CAIX: | | HIF1- α : | |
|---------------|----------------|------------------------------|------------------|------------------------------|
| | Stain Fraction | Stain Size (μm) | Stain Fraction | Stain Size (μm) |
| Oxytarget 1 | 0 | 0 | 0 | 0 |
| Oxytarget 4 | 0 | 0 | 0 | 0 |
| Oxytarget 5 | 0,00400 | 725,50 | 0 | 0 |
| Oxytarget 16 | 0 | 36,00 | 4,73E-06 | 57,00 |
| Oxytarget 17 | 0,00219 | 396,21 | 6,19E-05 | 67,89 |
| Oxytarget 21 | 0 | 0 | 0 | 0 |
| Oxytarget 22 | 0 | 0 | 0 | 0 |
| Oxytarget 24 | 0,01479 | 518,72 | 6,02E-06 | 38,50 |
| Oxytarget 32 | 0 | 0 | 0 | 0 |
| Oxytarget 41 | 0 | 0 | 0 | 0 |
| Oxytarget 46 | 0,00859 | 528,01 | 1,22E-04 | 100,40 |
| Oxytarget 47 | 0 | 0 | 0 | 0 |
| Oxytarget 48 | 0,00001 | 474,00 | 7,52E-05 | 136,38 |
| Oxytarget 58 | 0,01243 | 875,65 | 1,25E-04 | 71,95 |
| Oxytarget 60 | 0 | 0 | 0 | 0 |
| Oxytarget 72 | 0 | 141,00 | 1,02E-05 | 47,75 |
| Oxytarget 73 | 0 | 15,00 | 0 | 0 |
| Oxytarget 84 | 0 | 0 | 7,27E-05 | 47,79 |
| Oxytarget 85 | 0,05681 | 1360,44 | 5,12E-05 | 127,07 |
| Oxytarget 90 | 0,00547 | 213,75 | 0 | 0 |
| Oxytarget 103 | 0,00002 | 235,67 | 1,16E-04 | 125,69 |
| Oxytarget 107 | 0 | 0 | 0 | 0 |
| Oxytarget 120 | 0 | 0 | 0 | 0 |
| Oxytarget 121 | 0 | 0 | 0 | 0 |
| Oxytarget 124 | 0,00066 | 309,94 | 0 | 0 |
| Oxytarget 128 | 0,00005 | 98,33 | 0 | 0 |
| Oxytarget 146 | 0,09267 | 2701,83 | 5,97E-06 | 14,50 |
| Oxytarget 153 | 0,03248 | 969,94 | 0 | 0 |
| Oxytarget 154 | 0,03062 | 800,17 | 0 | 0 |
| Oxytarget 157 | 0,00003 | 135,50 | 0 | 0 |
| Oxytarget 160 | 0,02119 | 1964,26 | 8,52E-05 | 86,57 |
| Oxytarget 161 | 0 | 0 | 0 | 0 |
| Oxytarget 162 | 0,00840 | 725,70 | 6,07E-06 | 26,75 |
| Oxytarget 164 | 0,00135 | 462,94 | 2,18E-05 | 87,00 |
| Oxytarget 165 | 0,15088 | 2414,04 | 1,54E-04 | 118,00 |
| Oxytarget 166 | 0,02581 | 671,04 | 4,01E-03 | 147,99 |
| Oxytarget 171 | 0,12579 | 2043,78 | 3,61E-04 | 95,34 |
| Oxytarget 172 | 0,11802 | 3142,34 | 1,38E-05 | 21,67 |
| Oxytarget 174 | 0,00918 | 543,74 | 3,77E-04 | 150,58 |